RZESZOW UNIVERSITY OF TECHNOLOGY

Łukasiewicz IMBiGS

WSKAZÓWKI DOTYCZĄCE PRZYGOTOWANIA ARTYKUŁÓW

- Artykuły przeznaczone do opublikowania w kwartalniku „Technologia i Automatyzacja Montażu" powinny mieć oryginalny i naukowo--techniczny charakter i być zgodne z problematyką czasopisma. Redakcja przyjmuje artykuły w jęz. polskim, jęz. angielskim i jęz. rosyjskim.

- Artykuł o maksymalnej objętości 5 stron A4 wraz z ilustracjami powinien być napisany czcionką Times Roman lub Arial 11 pkt, z interlinią 12 pkt. Formatowany tekst nie powinien mieć podziału na kolumny.

- Tytuł artykułu należy podać w jęz. polskim i jęz. angielskim. Tytuł nieprzekraczający 10 słów powinien odzwierciedlać istotne elementy treści artykułu.

- Struktura artykułów naukowo-technicznych prezentujących prace autora(ów) powinna być następująca: wstęp (wprowadzenie); metodyka (badań, analiz, pracy z podaniem ewentualnie materiałów, założeń itp.); wyniki (badań, analiz); omówienie wyników; wnioski; spis literatury.

- Podpisy pod ilustracjami oraz tytuły tablic należy podać w jęz. artykułu i jęz. angielskim.

- Ilustracje należy dołączyć również jako osobne pliki w formacie: .jpg, .tiff, z rozdzielczością co najmniej 300 dpi. Wszystkie zamieszczane ilustracje powinny być własnością autora(ów) lub należy podać źródło pochodzenia rysunków.

- Wzory matematyczne pisane w edytorze równań Microsoft Equation i powinny być oznaczane kolejnym numerem w nawiasie okrągłym. Wszystkie symbole powinny być objaśnione. Należy stosować jednostki układu SI.

- Spis literatury należy podać w kolejności cytowania w tekście, a odnośniki w tekściepo winny być ponumerowane cyframi arabskimi i umieszczone w nawiasach kwadratowych. W przypadku korzystania z Internetu należy podać adres strony i datę odczytu. Liczbę autocytowań należy ograniczyć do niezbędnych.

- Do artykułu należy dołączyć streszczenie w jęz. artykułu i jęz. angielskim, zawierające minimum 200-250 słów.

- Pod streszczeniem należy podać 3-6 słów kluczowych w jęz. artykułu i jęz. angielskim, zwracając uwagę, by nie były one powtórzeniem tytułu pracy.

- Po spisie literatury zaleca się podanie źródła finansowania pracy.

- Na końcu artykułu należy podać: imiona i nazwiska autorów, tytuły naukowe lub zawodowe, telefon, faks, e-mail, miejsce zatrudnienia wraz z adresem do korespondencji.

PROCEDURA RECENZOWANIA

Procedura recenzowania artykułów w czasopiśmie jest zgodna z zaleceniami Ministerstwa Naukii Szkolnictwa Wyższego zawartymi w opracowaniu „Dobre praktyki w procedurach recenzyjnych w nauce", Warszawa 2011.

Wszystkie artykuły naukowo-techniczne publikowane w kwartalniku „Technologia i Automatyzacja Montażu" są recenzowane.

Nadesłane artykuły są poddawane redakcyjnej ocenie formalnej i otrzymują numer redakcyjny, identyfikujący je na dalszych etapach procesu wydawniczego, a redakcja wysyła do autorów informację o przyjęciu artykułu i wysłaniu go do recenzentów. Do oceny każdej publikacji powołuje się co najmniej dwóch niezależnych recenzentów. Redakcja dobiera recenzentów rzetelnych i kompetentnych w danej dziedzinie. Nadesłane artykuły nie są nigdy wysyłane do recenzentów z tej samej placówki, z której pochodzi autor. Prace recenzentów są poufne i anonimowe. Recenzja musi mieć formę pisemną i kończyć się jednoznacznym wnioskiem o dopuszczeniu artykułu do publikacji w czasopiśmie lub jego odrzuceniu. W przypadku pracy w języku obcym, co najmniej jeden z recenzentów jest afiliowany w instytucji zagranicznej innej niż narodowość autora pracy. Autorzy są informowani o wynikach recenzji oraz otrzymują je do wglądu. W sytuacjach spornych redakcja powołuje dodatkowych recenzentów.

Lista recenzentów publikowana jest w ostatnim zeszycie każdego rocznika.

Kwartalnik „Technologia i Automatyzacja Montażu" ukazuje się
w formie elektronicznej w otwartym dostępie (Open Access)
i jest dostępny na www.tiam.prz.edu.pl

CONTENTS / W NUMERZE

Iga Barca[1]

STRENGTH CALCULATIONS OF THE FORMULA 1 CAR SURVIVAL CELL

OBLICZENIA WYTRZYMAŁOŚCIOWE KOMORY PRZETRWANIA BOLIDU FORMUŁY 1

Abstract

The paper presents the results of calculations by the finite element method (FEM) of the monocoque survival cell of a Formula 1 car designed with the use of a sandwich structure in accordance with the Formula 1 Technical Regulations of 2020. The guidelines for the chamber geometry and the necessary certification tests were presented. Proposed solutions in the field of materials for the design of sandwich panels, including cladding made of carbon fiber reinforced laminates and honeycomb cores made of aluminum and titanium. The results of computer simulations were discussed. The analysis of the obtained results of numerical calculations shows that the height of the cell filler has the greatest impact on the strength of the analyzed structure.

Keywords: Formula 1, survival cell, sandwich structure, numerical strength analysis

Streszczenie

W pracy przedstawiono wyniki obliczeń metodą elementów skończonych (MES) komory przetrwania typu monocoque bolidu Formuły 1 projektowanej z wykorzystaniem struktury przekładkowej zgodnie z Regulaminem Technicznym Formuły 1 z 2020 roku. Przedstawiono wytyczne dotyczące geometrii komory oraz niezbędnych testów certyfikacyjnych. Zaproponowano rozwiązania w zakresie materiałów do projektowania płyt przekładkowych, w tym okładzin wykonanych z laminatów wzmacnianych włóknem węglowym oraz rdzeni typu honeycomb przygotowanych z aluminium i tytanu. Omówiono wyniki symulacji komputerowych, uwzględniając również koszty przyjętych rozwiązań. Analiza otrzymanych wyników obliczeń numerycznych wskazuje, że największy wpływ na wytrzymałość analizowanej struktury ma wysokość wypełniacza komórkowego.

Słowa kluczowe: Formuła 1, komora przetrwania, struktura przekładkowa, numeryczna analiza wytrzymałościowa

Introduction

The history of Formula 1 began on May 13, 1950 at the airport now called Silverstone in Great Britain. Motor racing was a very dangerous sport in which at least one driver was killed and injured every year [1]. This is why the International Automobile Federation at the beginning of the 1980s, in order to improve the safety of drivers, proposed the use of a technical solution in the construction of racing car bodies in the form of the so-called "survival cell" of the monocoque type [2]. The solutions adopted in these type of constructions, similar to those in aviation, were to be characterized by favorable strength parameters related to the weight of the structural elements. Hence, in the first solutions, aluminum alloys, known from aircraft structures, were used as construction material. Then,

car designers, similarly to aviation designers, began to use carbon fiber-reinforced polymer composite materials (CFRP), which account for up 85% of the structure [3]. In order to ensure favorable relative strength and stiffness parameters, as well as to construct vehicles with a high potential for absorbing impact energy, sandwich structures with a honeycomb core were used [4, 5].

Over the years, the regulations of the survival cell have been tightened to make the cell resistant to the most dangerous car collisions [6]. The existing solutions contributed to the reduction of the casualties to zero [7]. The last fatal accident in Formula 1 racing happened on October 5, 2014.

The provisions regarding the dimensions and strength of the survival cell are contained in the Technical Regulations [8] available on the official FIA

---

[1] M.Eng. Iga Barca, PhD student at the Military University of Technology, Sambora 11, Bydgoszcz 85-459, e-mail: iga.barca@wat.edu.pl, ORCID: 0000-0003-4687-4873.

website. The guidelines contained in the document concern: the geometrical dimensions of the vehicles and the survival cell, the materials used and the tests (static, dynamic and destructive) necessary for the certification of the solution.

The work presents structural analyses of the Formula 1 car survival cell in terms of its durability. It was proposed to use a sandwich structure with honeycomb core. A financial analysis of the adopted solution was also carried out. Modern design tools of the CAD type and calculation tools based on the finite element method were used in the considerations. The calculations and analysed were guided by the guidelines contained in the Formula 1 Technical Regulations of 2020.

Preparation of the calculation model

Survival cell geometry regulations

The Formula 1 technical regulations define the minimum dimensions of the survival cell [8]. Pic. 1 presents the shape and basic geometrical dimensions of the cell, which were adopted in the following considerations. The guidelines also present the requirements for performing static, dynamic and so-called crash tests. In order to certify the proposed solutions, the conducted experimental tests should be successful.
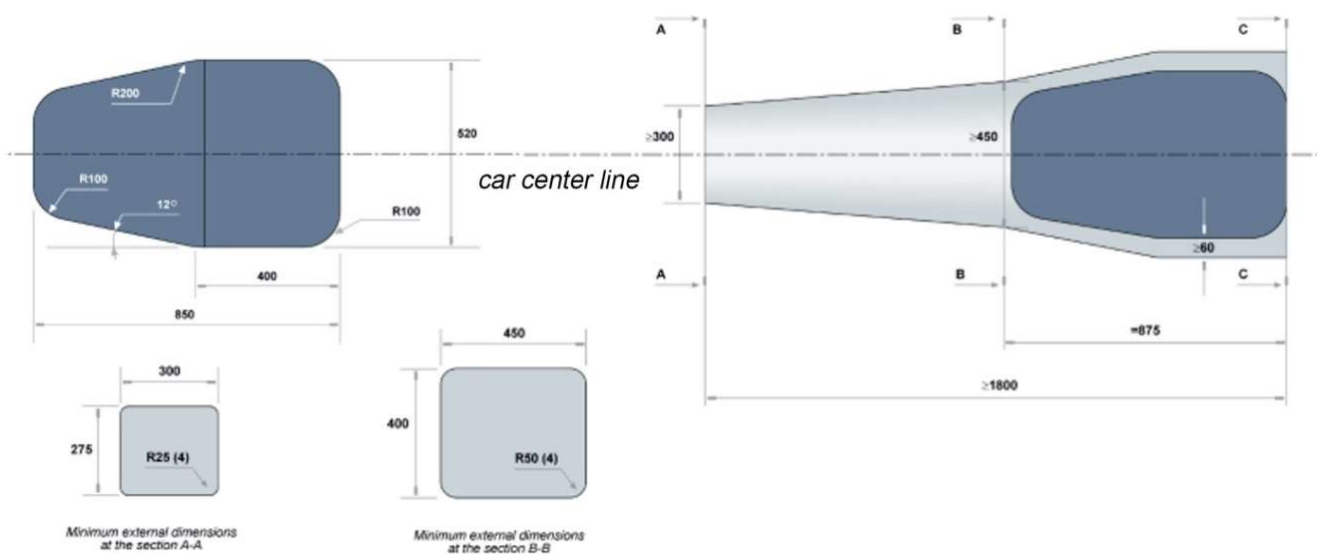
Pic. 1. Shape and minimum geometrical dimensions of the survival cell [8]

In the considerations presented in the article, the calculations defined for static tests were performed. Calculations performed with the finite element method are now a recommended and acceptable element of the methodology of planning and carrying out experimental research.

Types of analysed static tests

According to the regulations of the Formula 1 competition, the analysed cell should be checked, among others in five separate static load tests. The tests are based on loading selected surfaces of the chamber. Under no circumstances may there be any structural damage to the inner or outer wall of the sandwich structure.

The first two tests relate to the sidewall of the survival cell tests. During the first test, the load is carried out through a 100x300 mm shim. A load of 25 kN is set on the lateral outer surface of the chamber

structure at its end edge. The boundary conditions in the load range are presented in Pic. 2. The cell is fixed with the bottom part of the floor and the rear part of the cockpit.
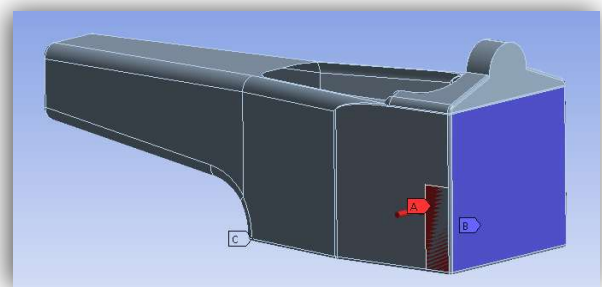
Pic. 2. View of the survival chamber with test load conditions no. 1 [own analysis]

During test no. 2, a load of 30 kN is released through a washer with a diameter of 200 mm (it was defined as a plane with given dimensions to which a given load value was applied). The washer is located on the outer surface of the chamber, the center of the washer is located in the middle of the chamber height and is 430 mm away from the C-C plane (see Pic. 1) – Pic. 3. The chamber is fixed on the same way as in test no. 1.
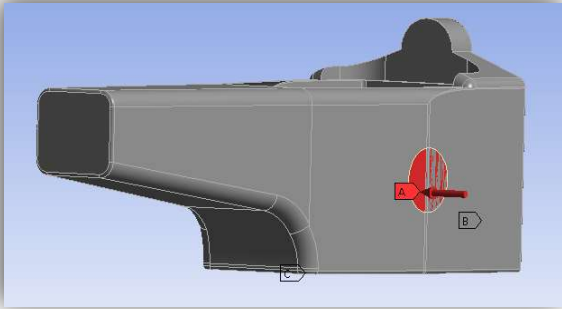
Pic. 3. View of the survival chamber with the load conditions of test no. 2

Test no. 3, is for the floor of the survival cell. A load of 12.5 kN, through a washer with a diameter of 200 mm, is carried out on the outer surface of the bottom of the survival cell in a position freely determined by the FIA technical delegate – Pic. 4. For the purposes of the calculations, it was assumed that the center of the spacer is located in the middle of the chamber width and 278 mm in front of the C-C plane (see Pic. 1). The cell is fixed by the upper part of the structure and the rear part of the cockpit.
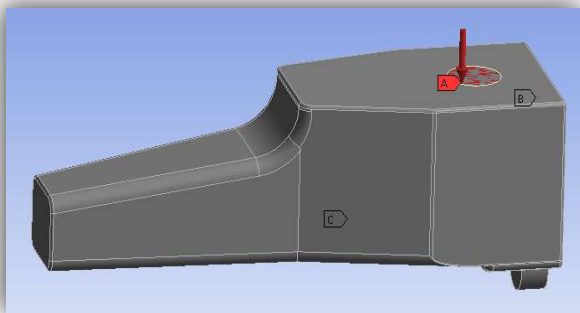
Pic. 4. View of the survival cell with the load conditions of test no. 3 [own analysis]

In test 4, the strength of the edges of the cockpit (cell) is analysed. Two washers, 50 mm in diameter, are located on both sides of the cockpit at the same height as the top of the cockpit, 250 mm in front of the

C-C plane. The defined load of 50 kN at an angle of 90° to the center of the car plane – Pic. 5. The cell is fixed with the floor and the rear part of the cockpit.
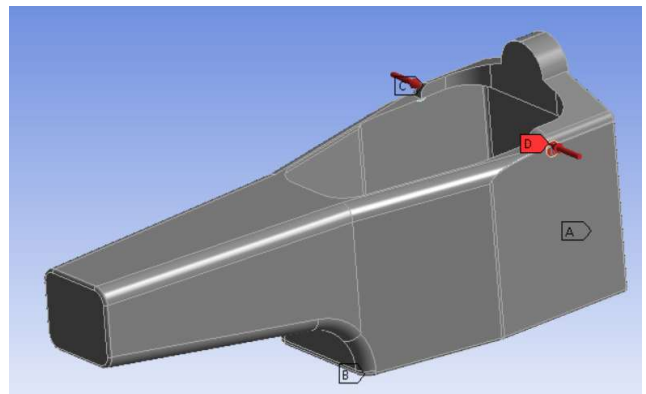
Pic. 5. View of the survival cell with test load conditions no. 4 [own analysis]

The last test no 5 also includes checking the cockpit floor and is carried out the same way as in the test no. 3, with the difference that load value is changed up to 15 kN and the place where the structure is loaded – Pic. 6. The center of the load bearing washer is halfway across the cell and 600 mm in front of the C-C plane (see Pic. 1). The cell is fixed in the same way as during test no. 3.
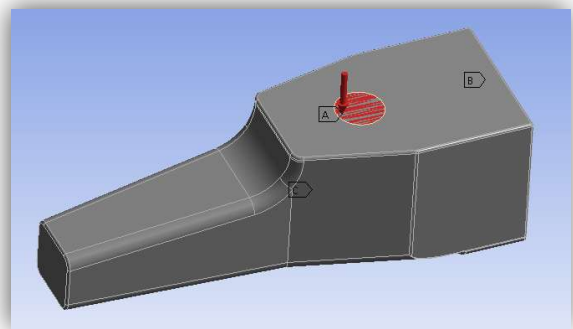
Pic. 6. View of the survival cell with test load conditions no. 5 [own analysis]

Defining the materials of the sandwich structure

The survival cell is used in conditions of high static and dynamic loads. Since the cell should be designed as a monocoque structure, resistant to deformation and at the same time it should have a high potential in terms of impact energy absorption, it was proposed to adopt a solution in the form of sandwich structure. Such a structure consist of facing adhesively bonded to the core. Polymer composites made of laminates based on epoxy resin reinforced with carbon fibers have been proposed as the cladding material. On the

other hand, the honeycomb solution was adopted as the core of the sandwich structure – Pic. 7, while it was assumed that the core cells would be made of an aluminum or titanium alloy [3]. The honeycomb core, in addition to high compressive strength, is characterized by favorable energy-consuming properties, which depend, among others, on the geometric dimensions of cells [5]. In the proposed solution, it was assumed that the core would be made of cells with geometric dimensions in the range of 3¸4 mm. The selection of materials for individual elements of the sandwich structure was also guided by the recommendations related to the most favorable weight of the final product. Hence, aluminum alloys and titanium alloys were proposed for the core material, and carbon composite for the facings.

Pic. 7. Honeycomb core view [5]

Aluminum and titanium alloys are characterized by favorable relative parameters, i.e. strength parameters related to the material density. The performance properties of selected materials, including their fire resistance, are also important. For futher considerations, an aluminum panel with a honeycomb structure called AHC-032-Q-10 of the manufacturer Easy Composites with a cell size of 3.2 mm was adopted. The parameters of the basic material from which the core is made are presented in Table 1. The honeycomb panel made of series 5 titanium alloys, which is also used in aviation structures, has better strength properties. For the purposes of the work, the American Elements honeycomb panel made of titanium with a mesh size of 3 mm called TI-M-02-HYCB was selected. The parameters of the titanium alloy as the base material for the production of the core are also presented in Table 1.

A polymer composite material based on epoxy resin reinforced with carbon fibers was proposed for the cladding. Two types of material were selected, from Toray. M60J fibers are high-modulus carbon fibers that are dedicated to car construction, and the other T800H are intermediate-module fibers. The parameters of composite materials for claddings are also presented in Table 1.

Table 1. Mechanical properties of the materials used [11, 12, 13]

Material name	Young's modulus [GPa]	Poisson number
Aluminum honeycomb AHC-032-Q-10 (aluminum alloy)	70	0.4
Titanium honeycomb TI-M-02-HYCB (titanium alloy)	116	0.4
Toray M60J	54.9	0.3
Toray T800H	39.2	0.3

Young's modulus of cell fillers adopted for calculations are the percentages of materials in individual layers. The honeycomb panel has a 4% share material (the surface of the walls has such a share in the entire surface of the material). On the other hand, the Young's modulus of claddings takes into account the quasi-isotropic structure of cladding and the supersaturation of the material with epoxy resin.

With the above-mentioned materials, three models of different sandwich panels were prepared, the characteristics of which are presented in Table 2. For the calculations, the quasi-isotropic orientation of the layers of the cladding composite material was assumed [0°/45°/-45°/90°/-45°/45°/0°]. This kind of ply orientation has little effect on the stiffness of the cover material as compared to the unidirectional orientation of the fibers in the ply, which was verified numerically. By the way, the quasi-isotropic facings of the sandwich structure facings are a more advantageous solution as the mechanical characteristics of the facings are independent of the load direction.

The analyzed panels of sandwich structures have an unchanged structure, their claddings are made of the same numbers of layers (seven) of the same thickness. They differ, however, in the types of carbon fibers used in the cladding layers as well as the thickness and type of core material of the sandwich structure. This difference affects the overall thickness of the panel as well as the total weight of the overall survival chamber structure.

Table 2. Characteristics of sandwich panels [own analysis]

Panel name	Carbon fiber material	Honeycomb plate material	The thickness of one layer of carbon fiber [mm]	The thickness of the honeycomb layer [mm]	Number of layers	Total thickness spacer panel [mm]	Total mass [kg]
Sandwich panel 1	TORAY M60J	Titanium	0.12	1.82	7+1+7	3.5	10
Sandwich panel 2	TORAY M60J	Aluminum	0.12	2.5	7+1+7	4.18	10.2
Sandwich panel 3	TORAY T800H	Aluminum	0.12	4	7+1+7	5.68	10.45

CAD Model

In order to be able to perform calculations and visually present static tests, a CAD model was designed in the SolidWorks program (an environment for the preparation of a geometric model). The survival cell model was prepared on the basis of the Formula 1 Technical Regulations of 2020. The minimum allowable dimensions defined in Pic. 1 have been adopted. The model was made using the thin-walled plate method. The view of the model adopted for the calculations is presented in Pic. 8.
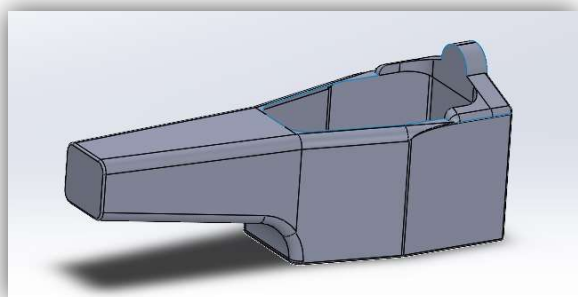
Pic. 8. Survival cell model [own analysis]

The calculations by the finite element method of the survival cell, in accordance with the guidelines for static tests, were performed in the Ansys Workbench program. The materials for the model were defined in accordance with the above-mentioned guidelines. After converting the model from the graphical environment to the calculation environment, the orientation of the model in the coordinate system was defined and a computational grid with an element size of 27 mm was generated – Pic. 9. The number of elements was 28955 and the number of nodes was 28971.
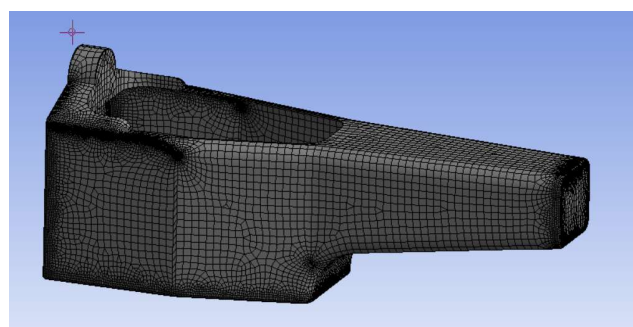
Pic. 9. Model in the Ansys Workbench software [own analysis]

The elements of the sandwich panel, for the purposes of calculations, are connected with each other with contact elements of the Bonded type.

Analysis of the results of the survival cell calculations

For each type of test, calculations were made for the panel, taking into account three different material solutions. The obtained results are presented in turn for individual tests

a) Test no. 1

The calculation results for this test are presented in Table 3. Pictures 10, 11, 12, 13, 14 and 15 show the displacements in the direction of the load (X axis) and the map of reduced stresses, respectively.

Table 3. Test results no. 1 for different sandwich panels [own analysis]

Sandwich panel no.	Displacement of X [mm]	Displacement of Y [mm]	Displacement of Z [mm]	Stress (max value) [MPa]	Deformation
1	7.72	0.87	0.18	715.12	0.005
2	6.79	0.83	0.18	511.07	0.005
3	11.13	1.4	0.31	381.22	0.011
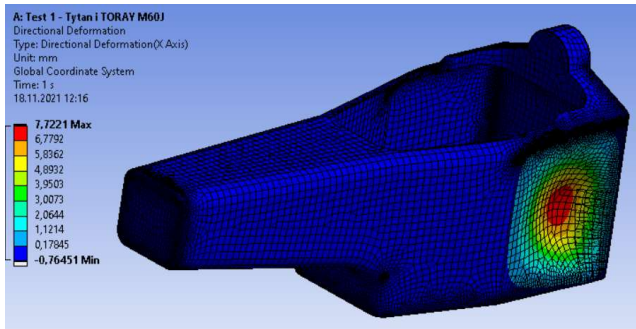
Pic. 10. Survival cell view with a map of displacements in the direction of the X axis of panel no. 1 [own analysis]
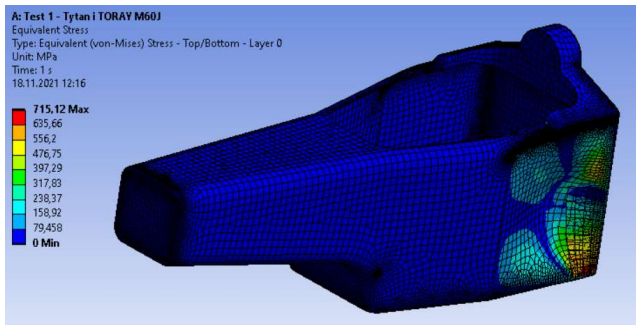
Pic. 11. View of the survival cell with a map of reduced stresses (von Mises) of panel no. 1 [own analysis]

Pic. 12. Survival cell view with a map of displacements in the direction of the X axis of panel no. 2

Pic. 13. View of the survival cell with a map of reduced stresses (von Mises) of panel no. 2

Pic. 14. Survival cell view with a map of displacements in the direction of the X axis of panel no. 3 [own analysis]

Pic. 15. View of the survival cell with a map of reduced stresses (von Mises) of panel no. 3 [own analysis]

The smallest displacements in the X direction were obtained for panel no. 2, and the lowest values of reduced stress for panel no. 3.

b) Test no. 2

The calculation results for this test are presented in Table 4. Pic. 16, 17, 18, 19, 20 and 21 show the displacements in the direction of the load (X axis).

Table 4. Test results no. 2 for different sandwich panels [own analysis]

Sandwich panel no.	Displacement of X [mm]	Displacement of Y [mm]	Displacement of Z [mm]	Stress (max value) [MPa]	Deformation
1	6.45	2.18	0.57	628.77	0.004
2	6.02	1.96	0.55	600.61	0.004
3	18.24	6.22	1.74	548.97	0.008

Pic. 16. Survival cell view with a map of displacements in the direction of the X axis of panel no. 1 [own analysis]
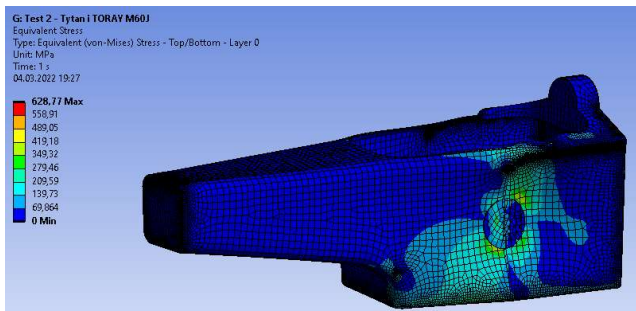
Pic. 17. View of the survival cell with a map of reduced stresses (von Mises) of panel no. 1 [own analysis]
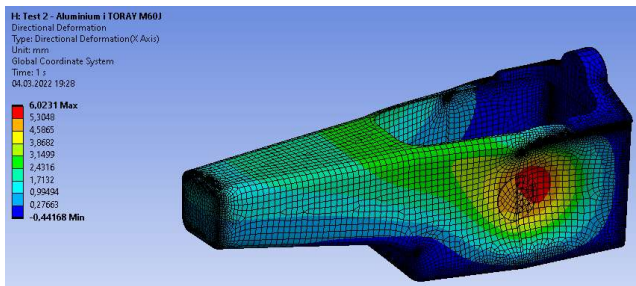
Pic. 18. Survival cell view with a map of displacements in the direction of the X axis of panel no. 2 [own analysis]

Pic. 19. View of the survival cell with a map of reduced stresses (von Mises) of panel no. 2 [own analysis]

Pic. 20. Survival cell view with a map of displacements in the direction of the X axis of panel no. 3 [own analysis]

Pic. 21. View of the survival cell with a map of reduced stresses (von Mises) of panel no. 3 [own analysis]

The smallest displacement was obtained by sandwich panel no. 2, while the lowest stress was achieved by panel no. 3 and it underwent the greatest displacement in the X direction.

c) Test no. 3

The calculation results for this test are presented in Table 5. Pic. 22, 23, 24, 25, 26 and 27 show the displacements in the direction of the load (Y axis).

Table 5. Test results no. 3 for different sandwich panels [own analysis]

Sandwich panel no.	Displacement of X [mm]	Displacement of Y [mm]	Displacement of Z [mm]	Stress (max value) [MPa]	Deformation
1	6.52	46.44	0.07	1317.3	0.007
2	4.22	29.15	0.047	1173.3	0.005
3	6.52	50.35	0.13	451.55	0.011
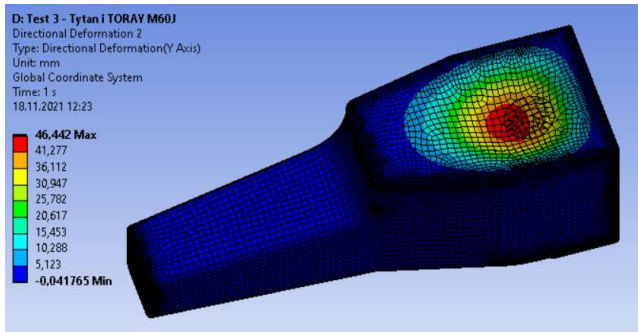
Pic. 22. Survival cell view with a map of displacements in the
direction of the Y axis of panel no. 1 [own analysis]
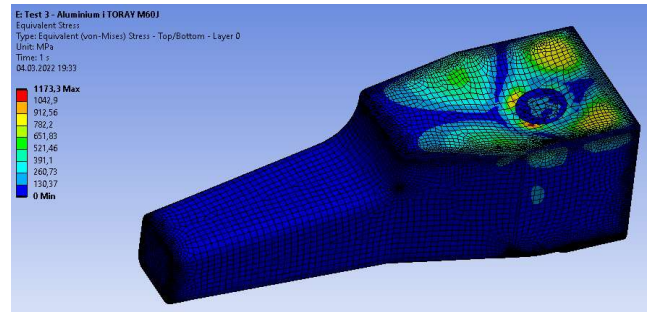
Pic. 25. View of the survival cell with a map of reduced stresses
(von Mises) of panel no. 2 [own analysis]
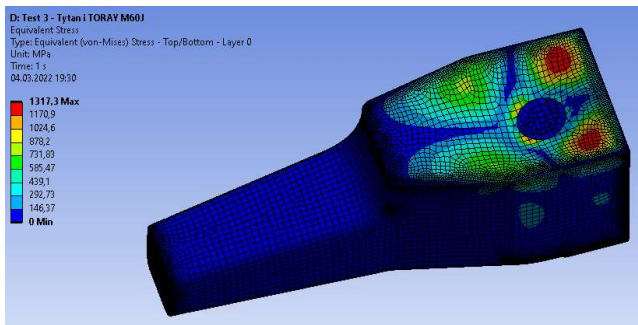
Pic. 23. View of the survival cell with a map of reduced stresses
(von Mises) of panel no. 1 [own analysis]
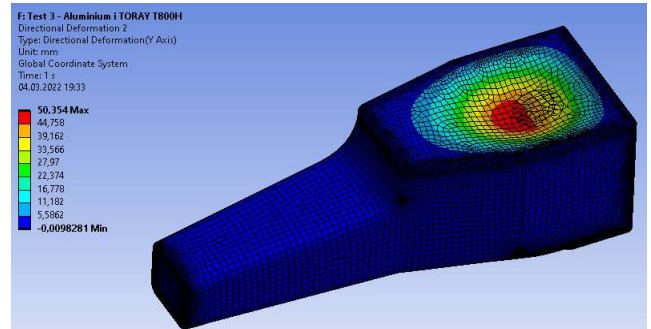
Pic. 26. Survival cell view with a map of displacements in the
direction of the Y axis of panel no. 3 [own analysis]
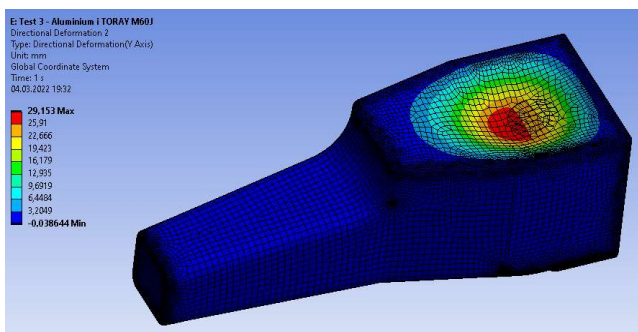
Pic. 24. Survival cell view with a map of displacements in the
direction of the Y axis of panel no. 2 [own analysis]
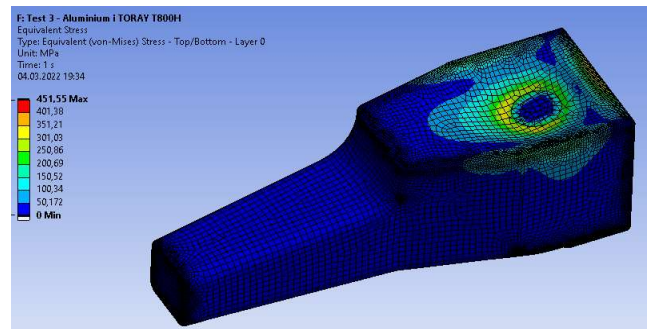
Pic. 27. View of the survival cell with a map of reduced stresses
(von Mises) of panel no. 3 [own analysis]

Again, the lowest values of displacements and stresses were obtained for sandwich panel no. 2, while the largest values for sandwich panel no. 3.
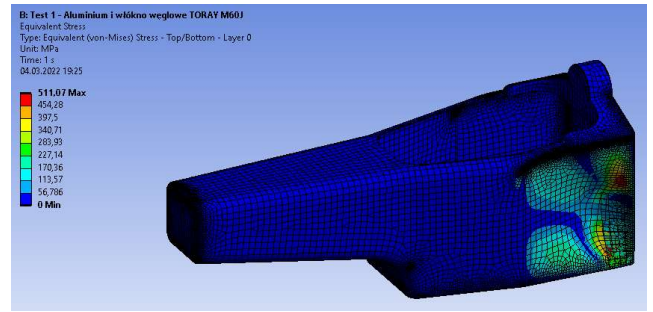
d) Test no. 4

The calculation results for this test are presented in Table 6. Pic. 28, 29, 30, 31, 32 and 33 show the displacements in the direction of the load (X axis).

Table 6. Test results no. 4 for different sandwich panels [own analysis]

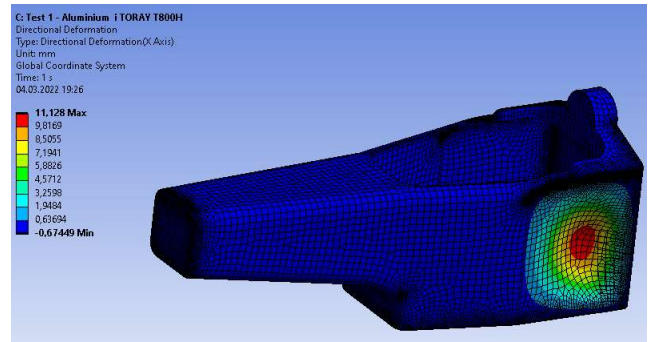| Sandwich panel no.	Displacement of X [mm]	Displacement of Y [mm]	Displacement of Z [mm]	Stress (max value) [MPa]	Deformation
1	10.66	6.64	3.79	3309.8	0.014
2	5.02	2.849	2.29	1797.8	0.009
3	14.16	8.88	6.53	723.7	0.026
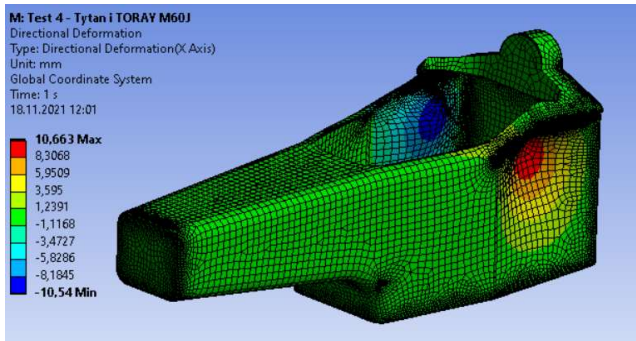
Pic. 28. Survival cell view with a map of displacements in the direction of the X axis of panel no. 1 [own analysis]
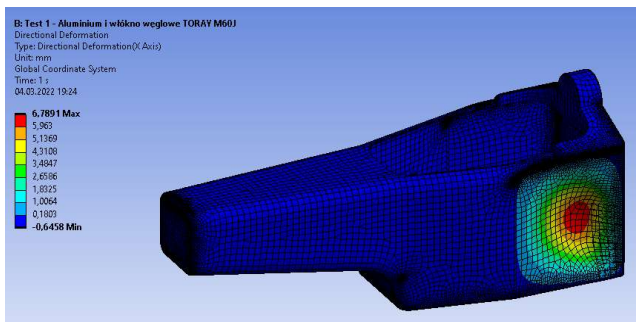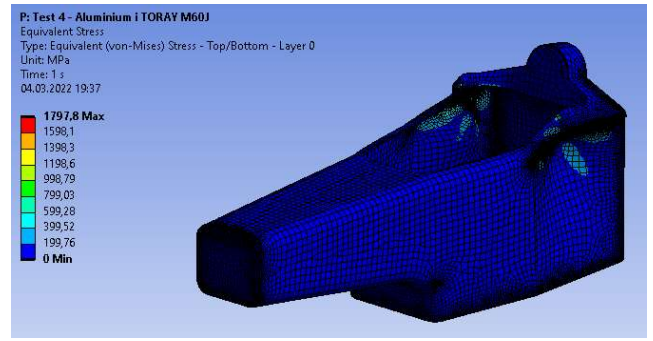

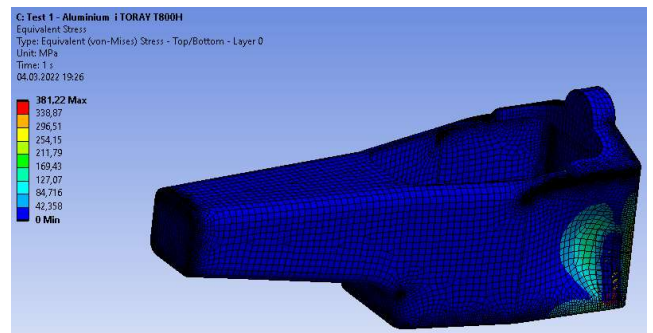Pic. 31. View of the survival cell with a map of reduced stresses (von Mises) of panel no. 2 [own analysis]
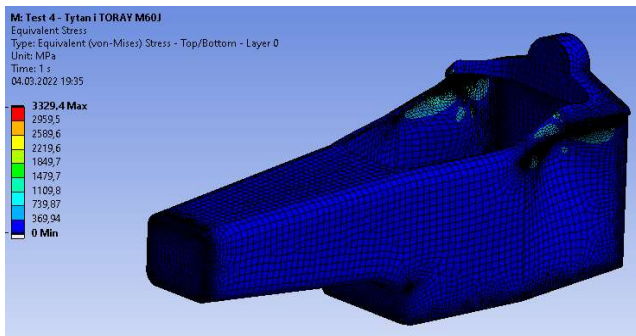
Pic. 29. View of the survival cell with a map of reduced stresses (von Mises) of panel no. 1 [own analysis]
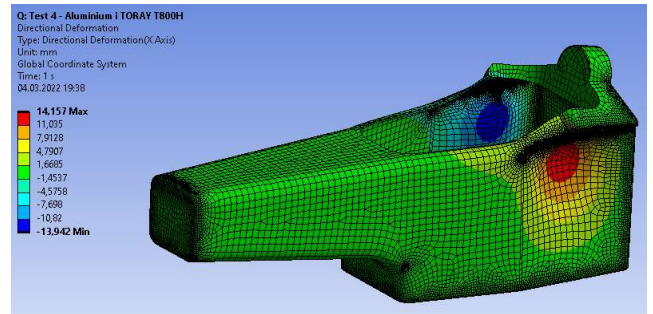
Pic. 32. Survival cell view with a map of displacements in the direction of the X axis of panel no. 3 [own analysis]
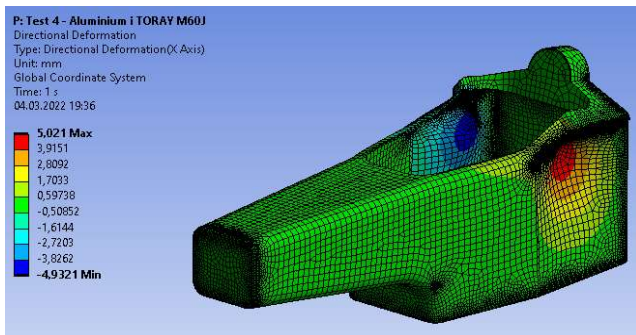
Pic. 30. Survival cell view with a map of displacements in the direction of the X axis of panel no. 2 [own analysis]
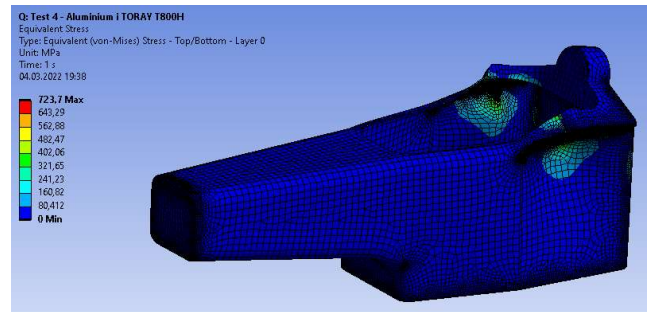
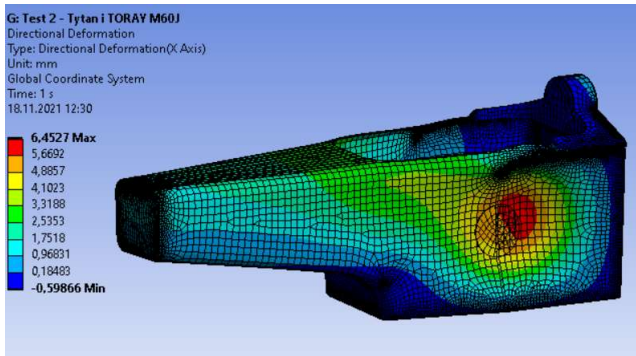Pic. 33. View of the survival cell with a map of reduced stresses (von Mises) of panel no. 3 [own analysis]

Analysing the obtained results, in the case of the first two panels, the stresses exceeded the allowable stresses.

e) Test no. 5

The calculation results for this test are presented in Table 7, while Pic. 34, 35, 36, 37, 38 and 39 show the displacements in the direction of the load (Y axis).

Table 7. Test results no. 5 for different sandwich panels [own analysis]

Sandwich panel no.	Displacement of X [mm]	Displacement of Y [mm]	Displacement of Z [mm]	Stress (max value) [MPa]	Deformation
1	9.01	48.03	0.25	1607.4	0.008
2	6.33	33.54	0.19	1130.8	0.006
3	9.84	57.22	0.36	653.27	0.014
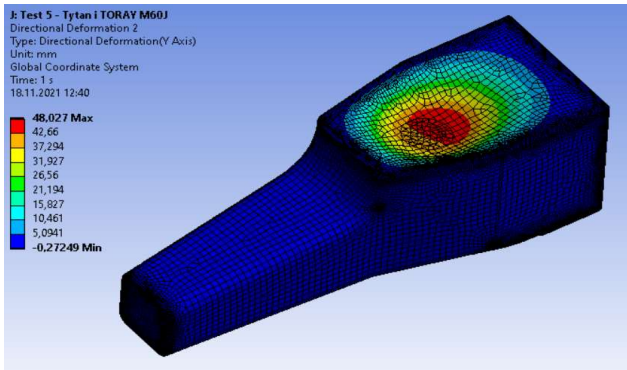
Pic. 34. Survival cell view with a map of displacements in the direction of the Y axis of panel no. 1 [own analysis]
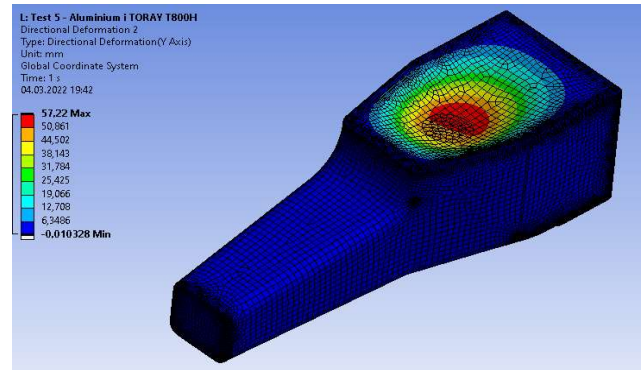
Pic. 35. View of the survival cell with a map of reduced stresses (von Mises) of panel no. 1 [own analysis]
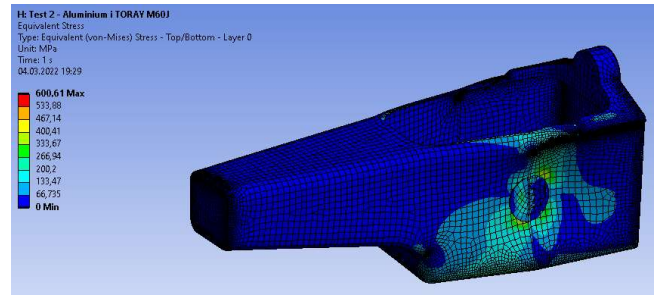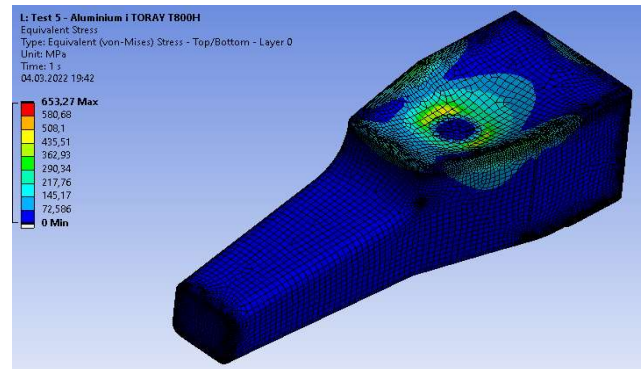

Pic. 36. Survival cell view with a map of displacements in the direction of the Y axis of panel no. 2 [own analysis]
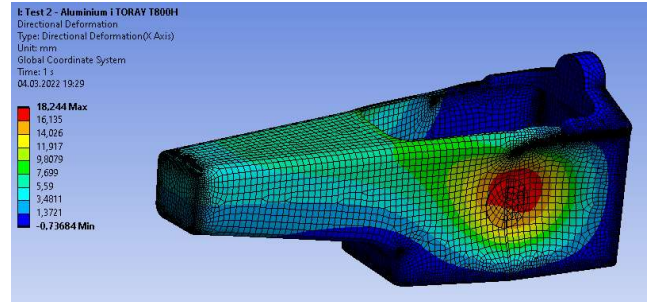

Pic. 37. View of the survival cell with a map of reduced stresses (von Mises) of panel no. 2 [own analysis]
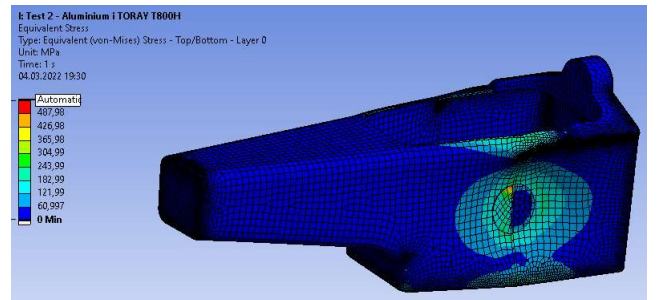

Pic. 38. Survival cell view with a map of displacements in the direction of the Y axis of panel no. 3 [own analysis]
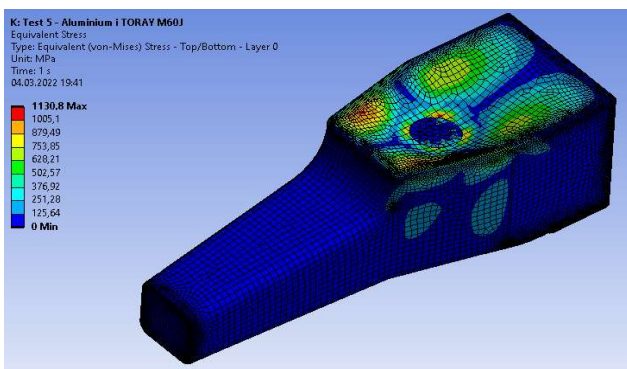
Pic. 39. View of the survival cell with a map of reduced stresses (von Mises) of panel no. 3 [own analysis]

By analyzing the obtained results, the smallest displacements and stresses were obtained for sandwich panel no. 2.

Conclusions

Based on the analyses, it can be concluded that:

- the thickness of the panel has a greater impact on the stiffness of the panel (susceptibility to deformation) and its strength properties than the type of material it is made of. For example, in panel no. 1, made of titanium cellular filler and facings based on high-modulus carbon fiber M60J, higher values of displacement were observed than in a panel made of cellular filler prepared on the basis of aluminum alloy and the same facings. Despite the use of a titanium alloy sandwich structure for the production of the core, i.e. a material with more favorable strength properties than aluminum alloy, panel no. 1 as a material for the construction of the cell turned out to be a worse solution.
- there was a difference in stress when simulating the same static load test across the individual sandwich panels. This is due to the different stiffness of individual panels, which depends on the value of the material parameters of the materials used.

- in further analyses concerning this project, local structural reinforcements with additional layers of carbon fiber can be used, the shape and dimensions of the survival cell can be changed, and other materials for the construction of sandwich panels can be used, e.g. Toray TC346 [7], which is a new material specially developed for Formula 1 racing cars.

Bibliography

[1] Rendall I. 1991. "The power and the glory (a century of motor racing)". *BBC Books.*

[2] Savage G. 2009. "Development of penetration resistance in the survival cell of a Formula 1 racing car". *Elsevier*

[3] Savage G. 2001, "Anales De Mecanica de la Fractura, vol. 18". Baiona: 274.

[4] Thompson R. W., Matthews F.L., O'Rourke B.P. 1995. "Load attachment for honeycomb panels in racing cars". *Elsevier.*

[5] Baumgart C., Halle T., Weigelt C., Krüger L., Aneziris C.G. 2013. "Effect of honeycomb cell geometry on compressive properties: Finite element analysis and experimental verification". *Science and Technology of Materials.*

[6] Savage G. 2001. "Proc. materials science, its nucleation and growth". *Imperial College London.*

[7] Wright P. 1999. "RaceCar Engineering" 9(9):13.

[8] FIA. 19.06.2020. *"2020 Formula One Technical Regulations".* Issue 3.

[9] Hayesa Alethea, Wang Aijun, Dempsey Benjamin, McDowell David. 2004. "Mechanics of linear cellular alloys" *Elsevier.*

[10] Savage G. 2009. "Formula 1 Composites Engineering". *Elsevier.*

[11] Quinn J.A. 2002. "Composites – Design Manual. Issue 3". *James Quinn Associates Ltd.*

[12] https://www.easycomposites.co.uk

[13] https://www.americanelements.com/titanium-honeycomb-7440-32-6

Eduardo Valente[1], Camelia Avram[2], Adina Astilean[3], José Machado[4]

A SYSTEMATIC APPROACH FOR MICROSCOPIC MODELS BASED ON CELLULAR AUTOMATA FOR ROAD TRAFFIC

SYSTEMATYCZNE PODEJŚCIE DO MODELI MIKROSKOPOWYCH OPARTYCH NA AUTOMATACH KOMÓRKOWYCH DLA RUCHU DROGOWEGO

Abstract

The transportation infrastructure is one of the most important resources for a country's economic and social well-being. The effectiveness of a country's street network will decide whether it develops further or stagnates. With the increasing number of vehicles on the road and the effects of urbanization, traffic roads are being subjected to a variety of requests and uses for which they were not designed, sized, or predicted. Because of the critical relevance of traffic roads, research must begin to lessen the effects of traffic jams in the streets, determine the appropriate number of traffic lanes, and integrate real-time traffic information into GPS systems. The goal of modeling a traffic-road system is to either build new traffic systems or gain a better knowledge of existing traffic systems so that they can be optimized. The accuracy, performance, stochastic and dynamic behavior of the model produced will be evaluated using a simulation of a genuine traffic system. This paper provides microscopic models based on cellular automation to replicate the behavior of various automobiles on a set of urban streets in Cluj Napoca city downtown. This model includes streets with multiple traffic lanes, various types of vehicles such as automobiles, buses, and trams, intersections with multiple possible upcoming streets controlled by traffic lights, bus stops inside and outside the traffic lane, tram stops inside the traffic lane, pedestrian crosswalks, and parking areas alongside and transversely with the right traffic lane of a street. TCA (Traffic Cellular Automata) is a proposed model that produces adequate findings in urban traffic theory. The results were obtained in both free-flow and traffic-jam conditions.

Keywords: Urban-traffic theory, cellular automaton, simulation, modeling, traffic-elements

Streszczenie

Infrastruktura transportowa jest jednym z najważniejszych zasobów zapewniających dobrobyt gospodarczy i społeczny kraju. Skuteczność sieci ulic danego kraju zadecyduje o dalszym rozwoju lub stagnacji. Wraz z rosnącą liczbą pojazdów na drogach i skutkami urbanizacji, drogi drogowe są przedmiotem różnych wymagań i zastosowań, do których nie zostały zaprojektowane, zwymiarowane ani przewidziane. Ze względu na krytyczne znaczenie dróg, badania muszą zacząć łagodzić skutki korków na ulicach, określić odpowiednią liczbę pasów ruchu i zintegrować informacje o ruchu drogowym w czasie rzeczywistym z systemami GPS. Celem modelowania układu ruch-droga jest albo zbudowanie nowych układów ruchu, albo uzyskanie lepszej wiedzy o istniejących układach ruchu, aby można je było zoptymalizować. Dokładność, wydajność, zachowanie stochastyczne i dynamiczne wytworzonego modelu zostaną ocenione za pomocą symulacji rzeczywistego systemu ruchu. W tym artykule przedstawiono mikroskopowe modele oparte na automatyzacji komórkowej w celu odtworzenia zachowania różnych samochodów na zbiorze miejskich ulic w centrum miasta Cluj Napoca. Model ten obejmuje ulice z wieloma pasami ruchu, różnego rodzaju pojazdy, takie jak samochody, autobusy i tramwaje, skrzyżowania z wieloma możliwymi zbliżającymi się ulicami sterowanymi przez sygnalizację świetlną, przystanki autobusowe wewnątrz i poza pasem ruchu, tramwaje przystanki wewnątrz pasa ruchu, pieszy przejścia dla pieszych oraz parkingi wzdłuż i w poprzek z prawym pasem ruchu ulicy. TCA (Traffic Cellular Automata) to proponowany model, który daje odpowiednie wyniki w teorii ruchu miejskiego. Wyniki uzyskano zarówno w warunkach swobodnego przepływu, jak i w korku.

Słowa kluczowe: teoria ruchu miejskiego, automat komórkowy, symulacja, modelowanie, elementy ruchu

[1] Eduardo Valente MSc, University of Minho; MEtRICs Research Center; Campus of Azurém; 4800-058 Guimarães; Portugal, e-mail: E_Valeeeente@live.com.pt

[2] Camelia Avram PhD, Technical University of Cluj Napoca, Cluj Napoca, Romania, e-mail: camelia.avram@aut.utcluj.ro, ORCID: 0000-0002-7394-5051.

[3] Adina Astilean PhD, Technical University of Cluj Napoca, Cluj Napoca, Romania, e-mail: adina.astilean@aut.utcluj.ro

[4] José Machado Dr. habil, PhD (corresponding author), University of Minho, MEtRICs Research Center; Campus of Azurém; 4800-058 Guimarães; Portugal, e-mail: jmachado@dem.uminho.pt, ORCID: 0000-0002-4917-2474.

1. Introduction

The continuous increase of the global number of vehicles circulating in the constant number of urban traffic roads has become one of the main problems for modern society. The impact generated by the saturation and consequent congestion of the traffic networks reflects directly and reduces the life quality for the citizens. The major disadvantages for the citizens of these blocks are waiting too much time, physical resources spent in excess, and the possible apparition of stressful situations. In this context computing simulations can have an important role, allowing different ways to control and manage urban traffic [7].

The most innovative solutions called ITS (Intelligent Transport Systems) employ the latest technological products and have a high market price. Its main goal is to collect information related to vehicular traffic roads in urban and suburban areas and their subsequent use to optimize and correct traffic circulation. The characte-ristics of this type of technology make it particularly suitable for the use of mathematical models and computer simulations with high computing capacity [4].

In fact, vehicular traffic is a complex system with features to the model. Indeed, it was one of the first simulated systems by the ancestors of digital computers in the middle of the twentieth century [8]. In general, a traffic model represents the behavior of a group of vehicles traveling on a road or a circuit. There are different modeling strategies according to the level of resolution required for the subsequent simulation; macroscopic, mesoscopic, and microscopic models [18]. In those simulations, the microscopic models based on cellular automata have been highlighted from the other principal computational models for vehicular traffic simulation, due to their capacity to represent the main traffic features using simple rules. In Germany, for example, an approach based on cellular automata is used to predict the traffic situation for the next hour, from the data obtained by sensors scattered around the road's country network [18].

Due to the extreme importance of the traffic-roads, research must be initialized to reduce the effects of traffic jams in the streets, sizing the optimal number of traffic lanes, and to implement in Global Position Systems information about the traffic conditions (the possibility of traffic congestions in each path, the existence or not of car-crushes, or works in the street) in real-time. Modeling a traffic-road system intends to design new traffic systems, or a better understanding of the existing traffic systems to optimize them. The simulation of a real traffic system will evaluate the accuracy, the performance, the stochastic and dynamic behavior of the model created.

The main target of this work is the creation of an urban traffic model using the cellular automaton approach. This model contains the main traffic elements present in urban traffic as streets with multiple traffic lanes, different types of vehicles as automobiles, buses, and trams, intersections with multiple possible upcoming streets controlled by traffic lights, bus stops inside and outside of the traffic lane, tram stops inside of the traffic-lane, crosswalks for pedestrians, parking areas alongside and transversely with the right traffic lane of a street.

Creating a systematic and easily changeable imple-mentation for different urban traffic scenarios is the biggest advance that the author intends to reach.

The concrete aims highlighted in this work are:
- Characterization of the urban traffic, explaining its main variables and relations among them.
- Overall framework of the cellular automata theory converging for TCA (Traffic Cellular Automata) theory and its implementation in the software UPPAAL [2, 16, 17].
- Detailing the construction process until the final model and its characteristics are considered.
- Definition of the entire group of Cluj-Napoca's streets implemented in the simulation.
- Simulation and validation of the results obtained by the model suggested.

2. Urban traffic theory

Historically, traffic congestion was thought to be a challenge that only existed in major cities. The traffic difficulties that plagued densely populated metropolitan areas began to spread to the suburbs over time. Advances in transportation technology have made it possible for more people to drive, as well as the busy modern lifestyle has resulted in traffic congestion issues even in tiny communities. With this chaotic environment in place, the need for solutions to improve road traffic circulation has arisen, and road traffic simulators play an important role [4].

A thorough understanding of road traffic dynamics is required to aid in the selection of the most efficient and appropriate strategies. Simulations that mimic the final effect of traffic change parameters may be particularly useful in improving road traffic circulation in this scenario [7].

Road traffic, in general, contributes to climate change and environmental degradation. Innovation in sustainable mobility will help to reduce environmental pollution [11].

Road traffic models and in particular the microscopic ones represent a fundamental resource in the

management of road networks. Real progress in the study of traffic has been obtained with the introduction of the models based on cellular automata (CA) [1, 5, 6, 12, 15].

Because of their simplicity in simulating unrealistic vehicle behavior and the versatility of cellular automata to be implemented on a variety of platforms, traffic models based on cellular automata have a high computing efficiency. Parallel processing is a term that refers to the process of the other tiny traffic, on the other hand, car-following models, for example, are more computationally intensive, but they include more realistic driver behaviors and detailed vehicle characteristics [10, 11, 13, 19].

In this section, the fundamental concepts of the urban traffic theory will be presented. Firstly, the main physical variables involved in the traffic road problems (flow, average speed, and density) are shown, as well as different approaches to express those variables. Afterward, relational diagrams between these variables are depicted and their theoretical behaviors are exposed. A presentation of some microscopic models for traffic road simulation will close this chapter [7].

2.1. Fundamental concepts of the urban traffic flow (traffic parameters)

The traffic behavior can be evaluated by the following variables: flow (J), average speed ($\bar{v}$), and density (ρ). These parameters are called traffic parameters, i.e., those variables that help to determine the road condition at a particular time. Traffic flow is defined as the vehicles quantities which pass through a road section in each period and its unities are vehicles per time unit. The average speed is given by space units traveled by those vehicles per time unit. The density is determined by the number of vehicles per space unit [9, 18].

In this section different methods to calculate the urban traffic parameters are presented. The different expressions provide the necessary background for the utilization of urban traffic parameters in the course of this work [5, 7, 9, 13].

The traffic characteristics are ranging in time and space. To simplify these variations, commonly medial values for the traffic parameters are adopted. These medial values may be temporal or spatial values. Thus, there are different expressions for the traffic variables, when one traffic road is considered, in a one-time interval, is called temporal average, or a lane stretch in a time instant, is called a spatial average [5, 7, 9, 13].

2.2. Relational diagrams

Several empirical studies have been conducted to understand the behavior of vehicles on roads, i.e., the way that the variables presented in the previous section interact and how they are related. In this section, the principal diagrams that describe the relational behavior of the real traffic parameters are presented, such as the relation between the flow with the density, the flow with the speed, and density with the speed [5, 7, 9, 13].

Fundamental traffic diagram (Traffic flow & density)

The diagram that relates the traffic flow with the density is the principal diagram wildly used, due to its strong connection with the saturation level of the traffic lane. The diagram is called a fundamental diagram, has three different phases [3], and is displayed in Figure 1.
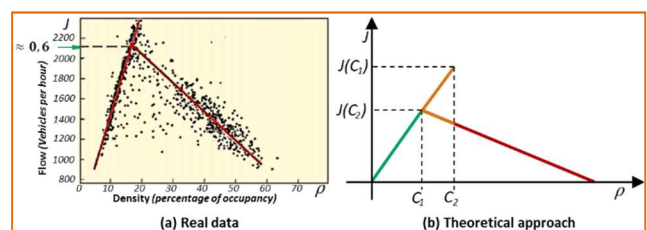
Fig. 1. Fundamental traffic diagram[1]

(i) Low-density region, called free traffic flow. This phase generically, allows the drivers to have the desired speed, approaching the maximum permitted speed. The diagram in this region has a linear growth with a density ranging from $0 < \rho < c_1$, presented in Figure 1(b). It can be also observed in Figure 1(a), the maximum flow in this region occurs approximately 2100 vehicles per hour or 0.6 vehicles per second.

(ii) Median density region, $c_1 < \rho < c_2$ Figure 1(b), where the traffic flow is not exclusively defined by density. The traffic configuration directly influences its flow and may cause a free or congested flow. In this region, the middle density is denominated meta-stable region.

(iii) High-density region, $\rho > c_2$, Figure 1(b), where the traffic flow drops as the density increases. The large concentration of vehicles causes them to cluster in traffic jams and a vehicle that leaves a place from the traffic jam will find congestion just ahead. This type of traffic is characterized by the behavior start and stop.

The meta-stable region of median density is characterized by the hysteresis effect. In the first phase, the drivers can maintain their speeds with $\rho > c_1$ (the direction a, Figure 2). This behavior continues until the density $\rho \leq c_2$ when the distance between vehicles is no longer enough to allow movement. From this moment, when the driver decelerates, also causes a deceleration in the following vehicles, creating

a traffic jam (direction b, Figure 2). On the other hand, (direction c, Figure 2) if the flow goes from congested to free; the density decreases, the traffic flow will increase linearly until it becomes a free flow (point d in Figure 2) [7].

Relation Flow & Speed

Another important relationship is the flow with the speed, shown in Figure 3, where V_f is the final average speed, it has a value slightly below the maximum traffic lanes speed since in a free flow, not all vehicles are permanently at maximum speed. The speed that provides a maximum traffic flow J_{max} is called optimal speed V_0 [7].

Also, can be observed in Figure 3, when the vehicles are circulating at maximum or minimum speed the traffic flow has the minimum value. This occurs, when the vehicles circulate at low speed, and traffic jams are created which, despite the high density, generate a low vehicles flow. When the vehicles are at high-speed little interactions occur between them, and consequently, the density is lower, generating a low vehicle flow. For this reason, the maximum traffic flow (J_{max}) occurs with a speed below the maximum value, at a point where the density of vehicles is bigger before the traffic jams start [7, 14].
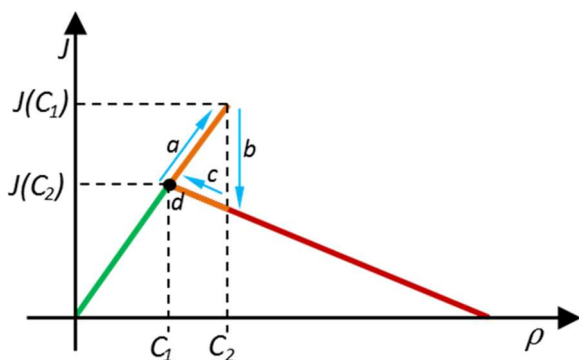
Fig. 2. Hysteresis effect[1]
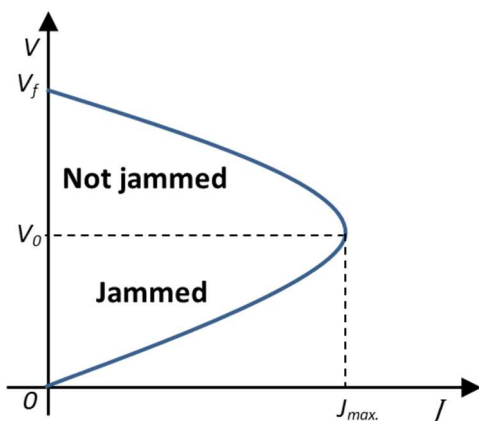
Fig. 3. Theoretical scheme of the speed-flow relation[1]

___
[1] Image adapted from [7].

Relation Density & Speed

The diagram presented in Figure 4, shows how the speed decreases with the traffic-lane saturation. Due to its monotonically decreasing behavior, some mathematical models represent this diagram only as a linear function.
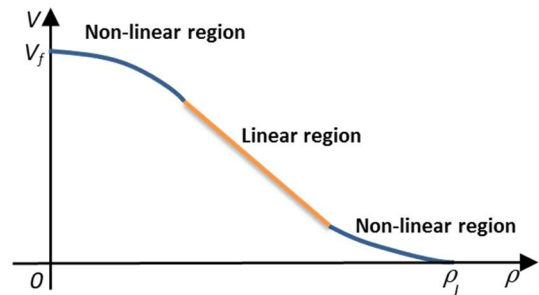
Fig. 4. Theoretical scheme of the density-velocity relation

2.3. Some models for simulation of vehicular traffic

Mathematical models for traffic simulation can be divided into three different approaches: Macroscopic, Mesoscopic, and microscopic models.

The macroscopic analyses describe the global behavior of traffic streams. Therefore, they relate the density, flow, and average speed parameters of the vehicles [18].

The mesoscopic models represent the behavior of a group of vehicles, i.e., bases its traffic analyses in a group of vehicles that behaves according to some logical grouping criteria: an expedition, congestion behavior, etc. [18].

Microscopic models are the ones that focus on the individual behavior of each vehicle to obtain the global behavior of a traffic road. They consider the interrelated parameters which determine the vehicle's dynamics. For example, knowing the acceleration of each vehicle at each time instant its position and speed can be known, after a time interval [18].

In the next section, a brief description of microscopic models is presented.

2.4. Microscopic Models

A type of microscopic modeling that has been largely used in traffic simulation is based on cellular automata, due to its versatility and simplicity. The first probabilistic model that reproduced the basic traffic conditions with the use of simple transition rules was proposed in [10].

One of the most studied models in traffic road simulation is the microscopic model, using the persecution model (car-following) which was developed at the end of the 1950s. This model has as a first

objective the translation of speed variation of the tracker vehicle. The speed variation is a response function of the speed stimulus between a vehicle and the vehicle in its front, called leader vehicle. A schematic representation of a car-flowing model is presented in Figure 5 [7].
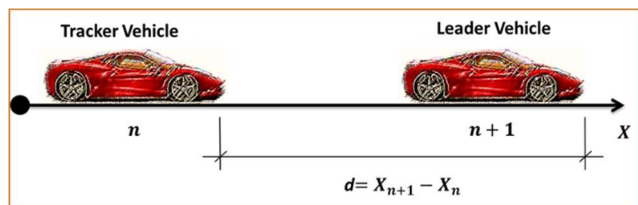
Fig. 5. Scheme of the car-following model

In general, the car-following modes are centered on the following relation:

[Response]n ∞ [Stimulus]n+1

The vehicle n = 1, 2, … can only accelerate or decelerate as a response to different flow conditions. The equation (1) represents the car-flowing model's vehicle's analyzed speed (v_n), the speed difference between it and the leader vehicle (Δv_n), and the distance between these vehicles (d_n) among others [14].

$$\ddot{x}_n(t) = f(v_n(t), d_n(t), \Delta v_n(t)) \qquad (1)$$

Road layout and the physical environment

When cellular automaton analogy is applied to vehicular road traffic flows, the physical environment of the system represents the road the vehicles are driving on. In a classic single-lane setup for traffic cellular automata, the layout consists of a one-dimensional grid. Each cell can either be empty or occupied by exactly one vehicle (single-cell models). Another possibility is to allow a vehicle to occupy several consecutive cells (multi-cell models) (Nagel, 1996).

An example of the time-space dynamics of TCA is represented in Figure 6, where two consecutive vehicles i and j are driving on a 1D grid. A typical discretization scheme assumes $\Delta T = 1$ s and $\Delta X = 7.5$ m corresponding to speed increments of $\Delta V = \Delta X / \Delta T = 27$ km/h. The spatial discretization corresponds to the average length that a vehicle occupies in a traffic jam. (In this context, its width is not considered). The temporal discretization is based on a typical driver's reaction time [10].

In Figure 6, the time axis is oriented downwards, the space axis extends to the right. The TCA's configuration is shown for two consecutive time steps t and t + 1, during which two vehicles i and j propagate through the grid.
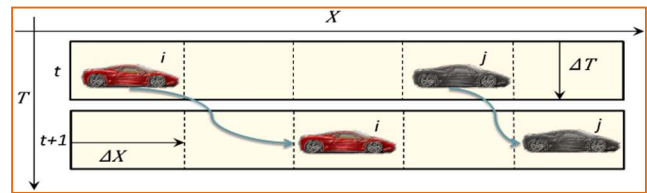
Fig. 6. Schematic diagram of a single-lane traffic cellular automaton (TCA)

With respect to the layout of the system, two main cases can be distinguished: closed and open systems. They correspond to periodic (or cyclic) versus open boundary conditions respectively. A closed system is usually implemented as a closed ring of cells and the number of vehicles is always conserved. An open system considers an open road.

Vehicle movements and the set of rules

The circulation of the individual vehicles in a traffic flow is described by a set of rules that reflects the car-following and lane-changing behavior, evolving in time and space. This set of rules included in TCA is consecutively applied to all vehicles in parallel. The system's state is changed through synchronous position updates of all the vehicles: for each vehicle, the new speed is calculated, after its position is updated according to its new speed and finally a possible lane-change maneuver is considered. It is furthermore assumed that a driver does not react to events between consecutive time iterations.

For single traffic-lane models, it is assumed that vehicles act as anisotropic particles, i.e., they only respond to frontal stimuli. The car-following stimuli are the states of the direct frontal neighborhood of each vehicle. The radius of this neighborhood should be large enough so that vehicles are able to move without collisions. Typically, this radius is equal to the maximum speed that a vehicle can achieve, expressed in cells per time step.

From a microscopic point of view, the process of a vehicle following its predecessor is expressed using the relation stimulus-response. Typically, this response is the speed or the acceleration of a vehicle. In TCA models, a vehicle's stimulus is mainly composed of its speed and the distance to its leader. As a direct response, the vehicle's new speed is adjusted. In a strict sense, this approach only leads to the avoidance of accidents. Some models incorporate anticipation stimuli. These forms of "anticipation" only consider leaders' reactions. When these effects are considered, the traffic flow is more stable and laminar avoiding abrupt braking and strong accelerations.

3. Uppaal modelling and simulation

This section is described the modeling process until the final UPPAAL model that covers and represents the study case.

Firstly, when the author faced the problem, simplistic models were created and as far as the project was developed the models became more complex. Some features such as places, transitions, functions, and channels from the simple models were changed or erased. Thus, each example present in this chapter defines a concrete problem and the models' evolution until the creation of the final model that contains all the features needed to implement in the study case.

The first subsection presents a model with one traffic lane and one automobile. In the second subsection, the complexity increases, and two models are presented to describe a traffic lane with several automobiles traveling. The third subsection is described the model which contains four traffic lanes connected by an intersection and the automobiles will choose the next street to continue their journey. A fourth model is a group of four traffic lanes connected in an intersection and are allowed to travel three different vehicles: automobiles, buses, and trams in free flow. The fifth subsection presents a model with traffic lanes where the three previous vehicles can circulate and be added to other traffic elements (bus and tram stops inside and outside of the traffic lane, crosswalks for pedestrians, parking areas, and traffic lights).

The author was always concerned with the creation of general models that can be easily extended or implement new situations and features. For this reason, the previous definition of the street cell using the function list was erased and in this new model, in similarity with the automobiles' definition was used the function typedef to create the streets in the global declarations.

3.1. Model with one traffic lane and one automobile

To implement this scenario in UPPAAL was necessary to develop two automata: the automaton street and the automaton automobile. An automobile only has two possible states: STOPPED or MOVING. The movement of the automobile is coordinated by the sensors at the beginning and at the end of the street which will define if the automobile is in or out of the traffic lane considered.

3.2. Model with one traffic lane and several automobiles

The model presented previously is extended with several features like changing traffic lanes, speed monitoring, acceleration/deceleration, and creating and managing queues.

The intersections are modeled as sections with multiple exits. For simulation purposes, vehicles will have two types of trajectories: random movement on the simulated map (at the end of each section with multiple exits – intersection – the next segment is randomly selected) and predefined path (at the beginning of the simulation for this type of automobiles the list with streets to follow is predefined)

This model has potentialities to be extended to new traffic scenarios and to be implemented in other types of vehicles and traffic elements.

Based on real-life road traffic measurements the average flow on the cells of analyzed streets is calculated and is used as weights in the UPPAAL model. The random choice of the next segment is weighted based on real-time road traffic measurements.

3.3. Street with multiple possible choices as an upcoming street with automobiles, buses, and trams moving in a free flow

Once the behavior of a traffic lane with several automobiles traveling with three possible next streets was already modeled, the next level of complexity is to create different types of vehicles. Two new classes of vehicles were defined: buses and trams. The difference between an automobile and a bus is its length. The bus is longer than an automobile and has a defined route to move by the pre-established bus stops. The tram is also bigger than an automobile and in similarity with a bus has a defined route to move by the tram stops.

In this model, we consider free-flow traffic (the bus or tram travel without stops) and traffic with predefined stops (on specific traffic lane cells with bus or tram stations).

The principal new feature considered in this model is that a bus will occupy two street cells and a tram will occupy three street cells. When a bus or a tram reaches an intersection with multiple next streets, they will always choose the same street to move in its predefined route. Therefore, to have multiple routes of trams or buses can be created different types of buses or trams in the simulation. Consequently, the simulation will have groups of buses or trams covering different areas of the city.

In this model and in all the subsequent models the automobiles will continue to have homogeneous distributions by the next possible traffic lanes: 50% in the case of two next possible streets and 33% when the intersection has three next possible streets.

Figure 7 is schematically represented the model with several automobiles, buses, and trams moving in a street, and at the end of the street is chosen another

street. The distribution of the traffic flow with the rules admitted for buses, trams, and automobiles was explained, and they are depicted in this scheme. The first automobile (black) which arrives at the intersection (blue rectangle) will continue to travel in the street ID 1, the second automobile to reach the intersection (green) will choose the street ID 2, the third automobile (blue) will choose the street ID 3, and this cycle of choice will continue for the subsequent automobiles. In the case of the buses which arrive at the intersection, they will always continue to move in the street ID 2. The trams which arrive at the intersection will have similar behavior to the buses but instead of choosing the street ID 2, they will always choose the street ID 3.
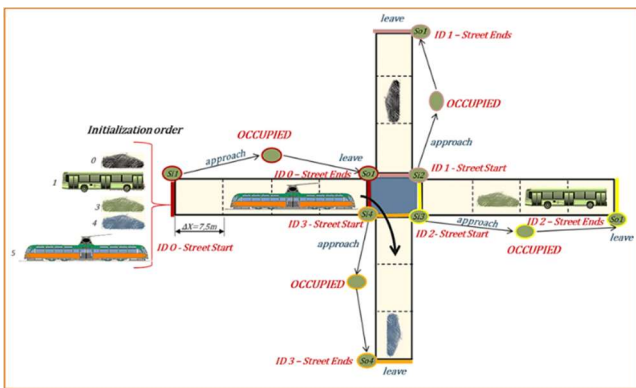
Fig. 7. Schematic representation of the model traffic lane with several automobiles, buses, and trams traveling with three possible next streets

Also, should be considered the buses that are not in service or buses that are traveling on long-distance trips and assume trucks equal in size to the buses. For this reason, in the subsequent models, buses with random destinations as automobiles will be considered. This percent of traffic elements is small, but to be as accurate as possible buses that are not included in the bus stop and have no predefined route will be considered, including long-distance buses and trucks.

This new model, contrarily to the previous model, is constituted by four templates: street, automobile, bus, and tram because it considers three different types of vehicles.

In the global declarations firstly is declared the number of automobiles, buses, trams, and streets, using the function typedef. In this model, it will be present three automobiles, one bus, one tram, and four streets.

The automaton street will be the "brain" of the simulation has all the information regarding the traffic conditions, set of rules and consequent transition rules, and possible interactions between the different vehicles.

Figure 9 shows the configuration of the street automaton for the model one traffic lane and different vehicles traveling with three possible next streets.

Figure 10 and Figure 11 present the bus and tram automaton respectively. In the red oval are highlighted the differences between them and the automobile automaton.
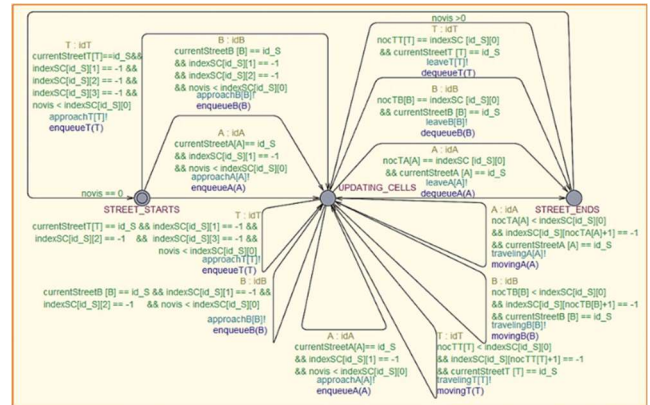
Fig. 9. Street automaton for the model traffic-lane with automobiles, buses, and trams
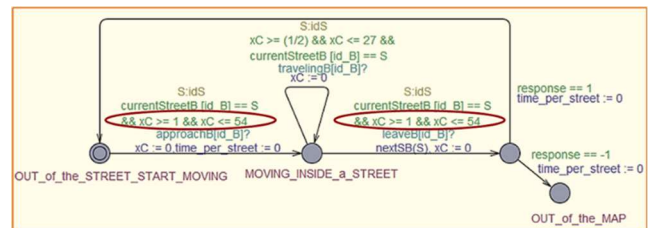
Fig. 10. Bus automaton for the model traffic-lane with different vehicles traveling with three possible next streets
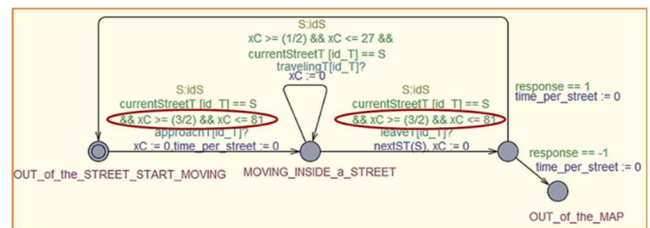
Fig. 11. Tram automaton for the model traffic-lane with different vehicles traveling with three possible next streets

For the streets considered in the case study, the traffic behavior is not exclusively influenced by the state of the street cells, as considered in the previous model. The vehicles interact with others traffic elements present in the street as crosswalks, bus stations, and tram stations. In this new model are added this interaction between vehicles and the traffic elements contained in the group of the streets of this case study.

The automobiles can interact with the following traffic elements implemented:
- Crosswalks for pedestrians.
- Parking placed transversely on the right side of the traffic lane.

- Parking placed alongside on the right side of the traffic lane.

The buses can interact with the following traffic elements implemented:
- Crosswalks for pedestrians.
- Bus stops inside of the traffic lane.
- Bus stops outside of the traffic lane, on the right side of the traffic lane.

The trams can interact with the following traffic elements implemented:
- Crosswalks for pedestrians.
- Tram-stops inside of the traffic lane.

3.4. Global declaration of the model containing different traffic-elements

To implement these traffic elements were needed to instantiate in the matrix indexSC, new negative numbers which will have a different meaning than an empty cell, affecting the behavior in the vehicles. The elements present inside of the street (crosswalks, bus stops inside of the street, and tram stops inside of the street) were coded in the respective street ID, with a negative number.

However, to create the traffic elements outside of the street were necessary to define adjacent streets to implement the exit movement that a vehicle will execute for the adjacent street where is located the traffic-element. The implementation rule is the following: if a traffic lane has in its right side an exterior traffic element (parking places transversely, parking places alongside and bus-stops outside of the street) the street ID-1 will have the respective negative digit of the traffic element and in the street, ID-2 will be necessary to create the border of the street that will give information that the vehicle cannot move to another street ID on the right.

Summarily, the different negative digits that a matrix indexSC can have will give the instructions for an interaction between a vehicle and a traffic element. The meaning (the traffic-element) of the negative digits is the following: (description of the matrix number of cells per different street with different traffic elements)

-1 - Empty cell,

-2 - Bus station inside of the traffic lane,

-3 - Tram station inside of the traffic lane,

-4 - Crosswalks for pedestrians,

-5 - Possible Park place alongside for automobiles in the right side of the street,

-55 - Border of a parking place alongside for automobiles with the right side of the street,

-6 - Possible Park places for automobiles in transversal with the right side of the street (the right place),

-66 - Border of a park places for automobiles in transversal with the right side of the street (the right place),

-7 - Possible Park places for automobiles in transversal with the right side of the street (left place),

-77 - Border of a park places for automobiles in transversal with the right side of the street (left place),

-22 – Bus station outside of the right side of the street,

-222 - Border of a bus station outside of the right side of the street,

-8 - Street's end and cells without meaning for the simulation.

The succeeding Figures will be explained how to encode the different configurations of the traffic lanes containing different traffic elements in the matrix indexSC.

3.5. Implementation of traffic elements inside of the traffic lane

This simulation contains traffic elements inside of a street that will affect the traffic circulation for the respective vehicle. The traffic elements inside of the street considered are bus stops, tram stops, and crosswalks for pedestrians.

In Figure 12 the generic configuration of a bus stop inside of a street is presented. In this example, the street is constituted with four cells (the first element of the matrix) and the street cell which contains the bus stop is encoded with the digit -2. All the other cells are encoded with -1, (empty cells) and the last element of the matrix (-8) means that is the end of the street.
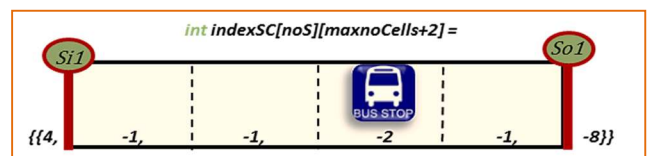
Fig. 12. Bus stop inside of the traffic lane implemented in the matrix indexSC

In Figure 13 the generic configuration of a tram stop inside of a street is presented. In this example, the street is constituted with four cells (the first element of the matrix) and the cell with a tram stop is encoded with the number -3. All the other cells are encoded with -1 and the last element of the matrix (-8) means that is the end of the street.
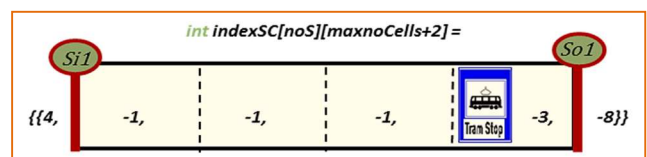
Fig. 13. Tram stop inside of the traffic lane implemented in the matrix indexSC

In Figure 14, a traffic lane with a crosswalk for pedestrians is presented. In this example, the street is constituted with four cells (the first element of the matrix) and the cell with a crosswalk is encoded with the number -3. All the other cells are encoded with -1 and the last element of the matrix (-8) means that is the end of the street.
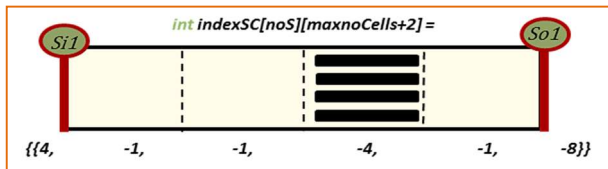
Fig. 14. Crosswalk encoded in the matrix indexSC

These three previous traffic elements inside of the traffic-lane (crosswalks, bus, and tram stop inside of a street) when the vehicles are moving, created the necessity of control variables, to restore the traffic element inside of the street's cell (inside of the matrix indexSC) in the same position. In Figure 14, the eighteen control variables generated in the global declaration are presented. At the beginning of the simulation, all the variables are set with the value 0 and now that interacts with the respective traffic element, its value will change for 1.

In Figure 15 the generic configuration of a parking area transversely with the right side of a street is presented. In this example, the street is constituted with four street cells (first element of the street ID 2) and all the other street cells are encoded with -1, (empty cells) and the last element of the street ID 2 (-8) means that is the end of the street. Once in this microscopic model, the width of the street and the vehicles are not considered, two adjacent traffic lanes for implementation of the parking area were created.
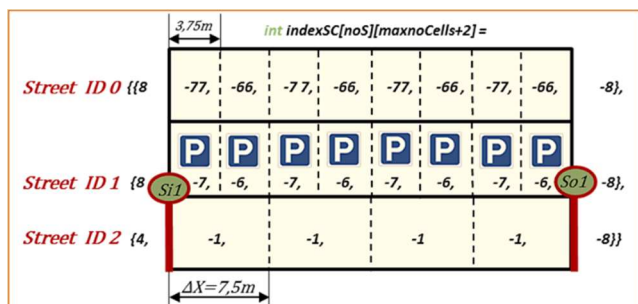
Fig. 15. Parking area for automobiles in transversal with the right side of a traffic lane

In Figure 16 the generic configuration of a parking area in parallel with the right side of a street is depicted. In this example, the street is constituted with four street cells (first element of the street ID 2) and all the other street cells are encoded with -1, (empty cells)

and the last element of the street ID 2 (-8) means that is the end of the street. Once in this microscopic model, the width of the street and the vehicles are not considered, two adjacent traffic lanes for implementation of the parking area were created.
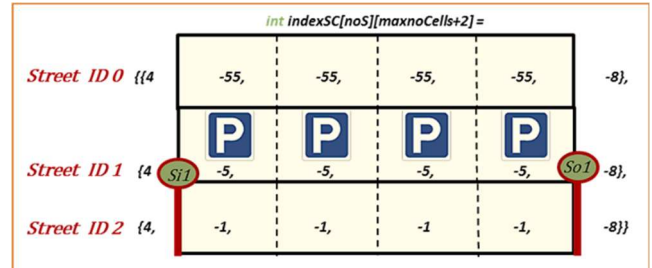
Fig. 16. Parking area for automobiles alongside the right side of a traffic lane

In Figure 17 the generic configuration of a bus stop outside of the traffic lane on the right side of a street is depicted. In this example, the street is constituted with four street cells (first element of the street ID 2) and all the other street cells are encoded with -1, (empty cells), and the last element of the street ID 2 (-8) means that is the end of the street. Once in this microscopic model, the width of the street and the vehicles are not considered were created two adjacent traffic lanes to implement the boarding area and unloading area.
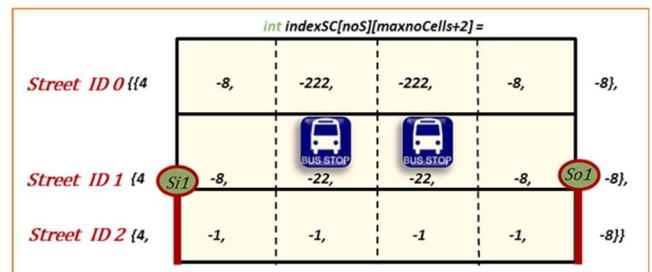
Fig. 17. Bus stop outside of the right side of a traffic lane

3.6. Automaton Automobile

The automaton automobile only evolves from the initial location if it was detected an automobile by the sensor Si1 present at the beginning of a street. The channel approachA will be activated and the clock time_cellA[id_A] will have a value between 0.5 times unites and 27-time units which is the time necessary to cross one street's cell with 7.5 meters with a range of velocity between 1 and 50 km/h.

After entering a street, the automobile will receive the channel travelingA from the street automaton always that the street's cell in its front is free and will update its position inside of the street. And if the cell in its front is a crosswalk the channel stopped_in_NCCWA is activated. In a crosswalk was

admitted that the clock time_cellA[id_A] will have a value between 0.5 times unites and 50-time units because the automobile can be forced to stop if pedestrians were crossing the traffic lane. In the place INTERACTING_INSIDE_a_STREETbefore PARKING two situations can occur: If there are no parking places on the right side of the street the automobile reaches the end of the street, or if exist possible parking places in its right and if the driver desires to park the vehicle will be parked during a period. When an automobile reaches the last street's cell, the channel leaveA will be activated and the function nextCA will be updated. This function has the algorithm of choice between the possible next streets. If the value of the auxiliary variable response is 1 the value of the currenStreetA will be updated and the automobile continues to move inside of the considered map but in another street ID. If the value of response is equal to -1 means that there are no possible next streets, and the automobile will be out of the map remaining blocked in the place OUT_of_the_MAP. In the second case when an automobile evolves for one of these places: parked PARKED_ALONGSIDE or PARKED TRANSVERSELY RIGHT or PARKED_ TRANSVERSELY_LEFT the automobile will stop during a period. If the automobile is parked alongside a parking place the time consider for the clock time_cellA[id_A] is between 7200 and 10800-time units, which correspond to a parking time between 2 or 3 hours. If the automobile is parked in a transversal parking place the time consider for the clock time_cellA[id_A] is between 21600 and 28800-time units, which correspond to a parking time between 6 or 8 hours. This last interval of parking time can be considered for the people that are going to work during a normal workday. After having been parked the automaton evolves to the place INTERACTING_INSIDE_a_STREET_after_PAR-KING and in this place the automobile can interact with other vehicles and traffic- elements but if in the same street that it was parked exist free parking places, the automobile cannot park again. This behavior is like the real driver's behavior because after being parked for a period the driver normally wants to continue his trip and not park again a few meters further in the same street. Thus, after leaving the street where the automobile was parked and if the automobile is traveling in another street with free parking places it can park again.

Figure 18 shows the configuration of the automaton automobile for the model of several vehicles' interaction with different traffic elements.

Fig. 18. Automaton automobile for the model several vehicles interaction with different traffic-elements

3.7. Automaton Bus

The automaton bus was reconfigured and has five places:

- OUT_of_the_STREET_START_MOVING: when a bus is moving in a direction to the beginning of the street.
- MOVING_INSIDE_a_STREET: when a bus was detected by the sensor Si1 and since there is inside of the street traveling interacting with other vehicles and traffic-elements.
- STOPPED_in_BUS_STATION_OUTSIDE_of_the_STREET: when a bus is stopped outside of the street to board and unload passengers.
- OUT_of_the_STREET_END_MOVING: when a bus was detected by the sensor SO1.
- OUT_of_the_MAP: when a bus was detected by the sensor SO1 and there are no possible next streets and is out of the considered map.

The automaton bus-only evolves from the initial location if it was detected a bus by the sensor Si1 present at the beginning of a street. The channel approachB will be activated and the clock time_cellB[id_B] will have a value between 1-time unit and 54-time units which is the time necessary to across two street's cells with 7.5 meters with a range of velocity between 1 and 50 km/h.

After entering in a street, the bus will receive the channel travelingB from the street automaton always that the street's cell in its front is free and will update its position inside of the street. If the cell in its front is a crosswalk the channel stopped_in_NCCWB is activated. In a crosswalk was admitted that the clock time_cellB[id_B] will have a value between 0.5 times unites and 50-time units because the bus can be forced to stop if pedestrians were crossing the traffic lane. If the cell in its front is a bus stop inside of a street the channel stopped_in_bus_Station_inside_Street[id_B] is activated. In a bus stop inside of the street and in accord with the book "Transit Capacity and Quality Service Manual" the following values for the busiest bus stops may be adopted, considering their location: 60s downtown, 30s peripheral zone very busy and 15s typical peripheral zone. In all the bus stops was

admitted that the clock time_cellB[id_B] will have a value between 60 times unites and 30-time units which corresponds a bus stops located downtown and in peripheral zones of the city in similarity with the study case. In the place MOVING_INSIDE_a_STREET two situations can occur: if there is no bus stops on the right side of the street the bus reaches the end of the street, or if exist a bus stop outside of the street the bus is forced to go out of the traffic lane and the automaton evolves to the place STOPPED_in_BUS_STATION_OUTSIDE_of_the_STREET.

When a bus reaches the last street's cell, the channel leaveB will be activated and the function nextCB will be updated. This function has the algorithm of choice between the possible next streets. If the value of the auxiliary variable response is 1 the value of the currenStreetB will be updated and the bus continues to move inside of the considered map but in another street ID. If the value of response is equal to -1 means that there are no possible next streets, and the bus will be out of the map remaining blocked in the place OUT_of_the_MAP. In the second case when a bus evolves for the place STOPPED_in_BUS_STATION_OUTSIDE_of_the_STREET the bus will stop during the period previously explained. After having been stopped the bus evolves to the place MOVING_INSIDE_a_STREET and in this place the bus can interact with other vehicles and all the traffic-elements even if in the same street that it was stopped outside of the street in a bus stop exist another bus stop outside of the street.

Figure 19 shows the configuration of the automaton bus for the model of several vehicles interacting with different traffic elements.

Fig. 19. Automaton bus for the model several vehicles interaction with different traffic elements

3.8. Automaton Tram

The automaton tram has four places:
- OUT_of_the_STREET_START_MOVING: when a tram is moving in direction to the beginning of the street.

- MOVING_INSIDE_a_STREET: when a tram was detected by the sensor Si1 and since there is inside of the street traveling interacting with other vehicles and traffic-elements.
- OUT_of_the_STREET_END_MOVING: when a tram was detected by the sensor SO1.
- OUT_of_the_MAP: when a tram was detected by the sensor SO1 and there are no possible next streets and is out of the considered map.

The automaton tram only evolves from the initial location if it was detected a tram by the sensor Si1 present at the beginning of a street. The channel approachT will be activated and the clock time_cellT[id_T] will have a value between 1.5 times unites and 81-time units which is the time necessary to across three street cells with 7.5 meters with a range of velocity between 1 and 50 km/h.

After entering a street, the tram will receive the channel travelingT from the street automaton always that the street's cell in its front is free and will update its position inside of the street. If the cell in its front is a crosswalk the channel stopped_in_NCCWT is activated. In a crosswalk was admitted that the clock time_cellT[id_T] will have a value between 0.5 times unites and 50-time units because the tram can be forced to stop if pedestrians were crossing the traffic lane. If the cell in its front is a tram stop inside of a street the channel stopped_in_tram_Station_inside_Street[id_T] is activated. In all the tram stops was admitted that the clock time_cellT[id_T] will have a value between 30 times units and 60 based on the same values for the buses. In the place MOVING_INSIDE_a_STREET when a tram reaches the last street's cell, the channel leaveT will be activated and the function nextCT will be updated. This function has the algorithm of choice between the possible next streets. If the value of the auxiliary variable response is 1 the value of the currenStreetT will be updated and the tram continues to move inside of the considered map but in another street ID. If the value of response is equal to -1 means that there are no possible next streets, and the tram will be out of the map remaining blocked in the place OUT_of_the_MAP.

Figure 20 shows the configuration of the automaton bus for the model of several vehicles interacting with different traffic elements.

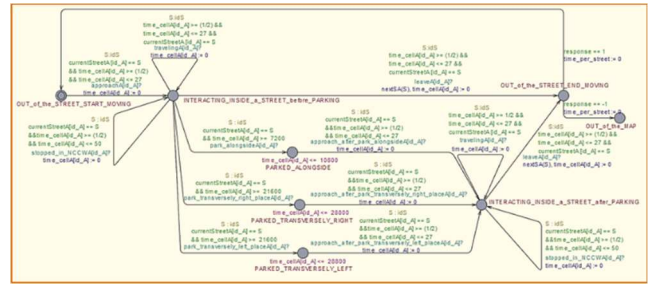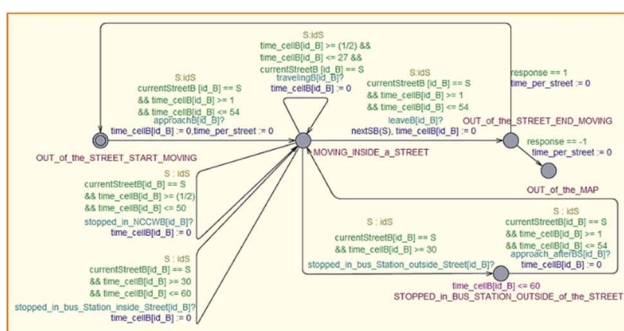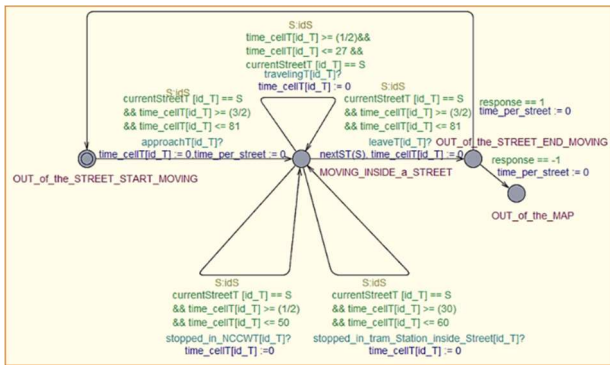Fig. 20. Automaton tram for the model several vehicles interaction with different traffic elements

Some relevant features of this model:

- The physical environment is a two-dimensional grid of rectangular cells. The street cells, the crosswalk cells, the bus stop cells, the tram stop cells, the alongside parking cells are equal in size (7.5 meters in length). The transversal parking cells have a different size (3,75 meters in length) and for this reason, this model has a non-homogeneous grid of cells.
- It is a multiple cells model because an automobile occupies one street cell, a bus occupies two street cells, and a tram occupies three street cells in each time iteration.
- The possible states of the cell are thirteen: be occupied by an automobile, a bus, or a tram, be empty, to contain a crosswalk, to contain a bus stop inside of the street, to contain a tram stop inside of the street, to contain a parking place alongside with right side of the street, to contain a left parking place transversely with the right side of the street, to contain a right parking place transversely with the right side of the street and to contain a bus stop outside of the right side of the street.
- variables and the matrix idexSC to extend the size of the neighborhood is different for each cell and this model is not anymore anisotropic because the automobiles and buses also receive stimulus from the right side.
- This model is a dynamic system with a closed number of automobiles buses, trams, and streets, being the evolution in space and time depending on different rules to satisfy the real traffic rules.
- The time is a stochastic feature, and its choice is completely nondeterministic. In an instant t, a vehicle can circulate in a cell at the velocity of 50 km /h and in the instant t+1 it can move at 2 km/h. This model has presented heavy breaks and accelerations even if the street is completely free.

- It is a realistic model, once considering different types of vehicles (automobiles, buses, and trams).
- This model can be easily extended. The number of streets and vehicles can be easily changed, is only necessary to define in global declaration those the map, define the inputs of the traffic flow in the simulation (vectors currentStreetA, currentStreetB and currentStreetT), define the next upcoming streets for the different vehicles (matrices indexMap AUTOMOBLIE, indexMapBUS, and indexMapTRAM), set up the variables responsible to count the number of cells traveled (nocTA, nocTBF, nocTBB, nocTTF, nocTTM, and nocTTB) for each vehicle, and define the matrix indexTL.

In fact, this model has the potentialities to simulate different traffic scenarios. It can be largely improved but due to the time restriction for this project the author defined a list of possible next improvements in this model.

4. Simulations

Figure 21 presents the map chosen for simulation to validate all the complex presented features. The map is inspired by Cluj Napoca downtown. Some of the designed features previously presented are artificially added to the city model for tests and validation purposes.

To implement the considered scenario 90 automobiles, 10 buses, and 9 traffic lanes were declared. Intersection A is completely considered, and a part of intersection B is also included.

An extensive list of interrogations that can be used in this type of simulation was previously presented in [17]. Based on the interrogations in UPPAAL we can establish the variation of the number of automobiles inside of the traffic lanes.

The left traffic lane before intersection A, of the street Piața Mihai Viteazu (direction street George Barițiu) is constituted by 8 street cells which is also the maximum number of vehicles allowed to travel. This street has an input of traffic flow of 30 automobiles and 5 buses. At the end of this street, all the buses mandatorily will continue their trip in the right traffic lane of the street Piața Mihai Viteazu (direction Street Dávid Ferenc). The automobiles will be equally distributed by the left and right traffic lane of the street Piața Mihai Viteazu (direction Street Dávid Ferenc) and in the Street Piața Mihai Viteazu (direction street George Barițiu) left traffic-lane after the intersection A.
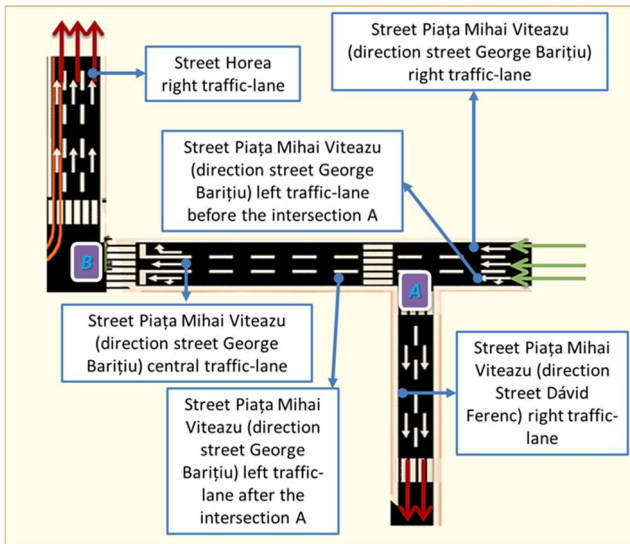
Fig. 21. Representation of the considered map in the simulation in UPPAAL

Figure 22 presents the variation of the number of automobiles inside of this traffic lane. Can be observed that the number of vehicles inside of this traffic lane never exceeds 10 vehicles. During the time considered the number of vehicles is not floatable, continuing the entire simulation in a traffic fluid regime.
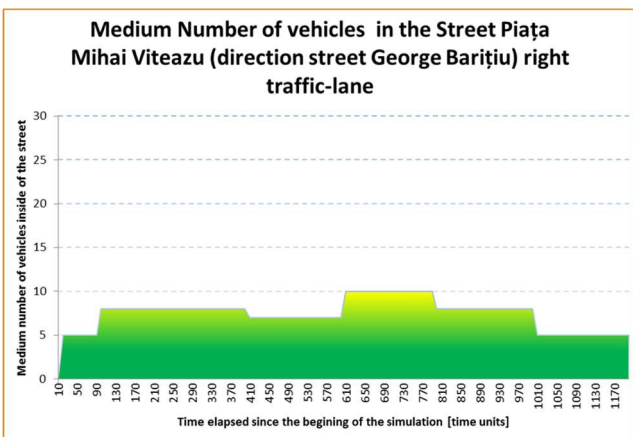
Fig. 22. Evolution of the medium number of vehicles in the street Piața Mihai Viteazu (direction street George Barițiu) right traffic-lane

Figure 23 presents the variation of the number of automobiles inside of this traffic lane is presented. Can be observed that the number of vehicles inside of this central traffic lane of the street Piața Mihai Viteazu never exceeds 15 vehicles. During the time considered the traffic behaves in a fluid regime.

In Figure 24 the variation of the number of automobiles inside of this traffic lane is presented. Can be observed that the number of vehicles inside of this traffic lane of the street Piața Mihai Viteazu never exceeds 6 vehicles. During the time considered the traffic behaves in fluid regime until 370 time units elapsed and after the traffic started to get congested until 800 time units. Due to the small length of this street, it will have a moment of peak traffic corresponding to the maximum number of vehicles inside traveling. When a big group of vehicles left the street and is propagating to the others traffic lanes the number of vehicles inside starts to be smaller and interacting again in a fluid regime.
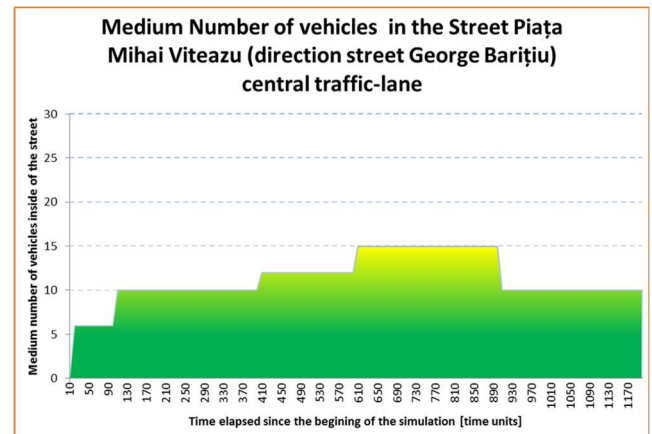
Fig. 23. Evolution of the medium number of vehicles in the street Piața Mihai Viteazu (direction street George Barițiu) central traffic-lane
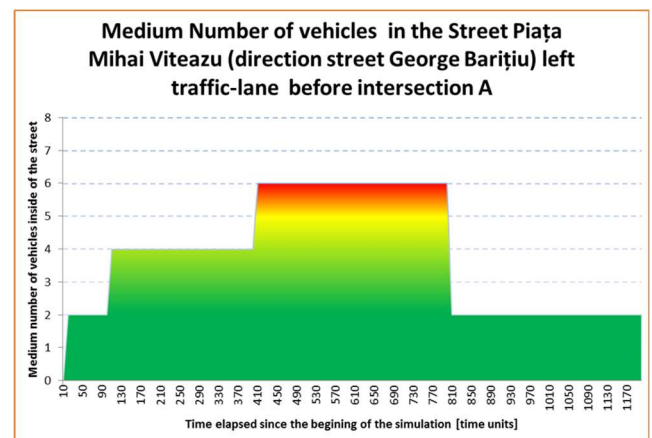
Fig. 24. Evolution of the medium number of vehicles in the street Piața Mihai Viteazu (direction street George Barițiu) left traffic-lane before the intersection A

The right traffic-lane, of the street Horea, is constituted by 14 street cells which is also the maximum number of vehicles allowed to travel. This traffic lane will receive 33% of the number of automobiles (10 automobiles) and 5 buses which started the trip in the Street Piața Mihai Viteazu (direction street George Barițiu) right traffic-lane before the intersection B. At the end of this street, all the automobiles are considered outside of the map.

In Figure 25 the variation of the number of automobiles inside of this traffic lane is presented. Can

be observed that the number of vehicles inside of this traffic lane never exceeds 10 vehicles. During the time considered the traffic behaves in the fluid regime and pre-congested regime.
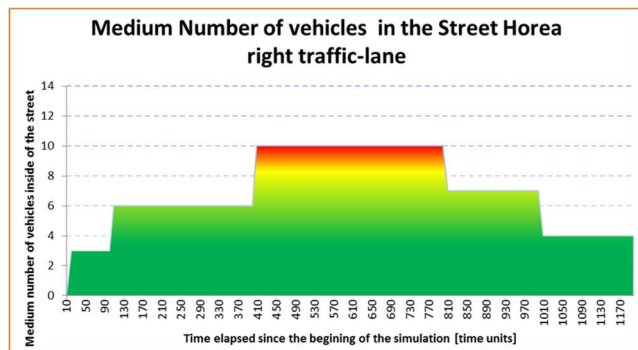
Fig. 25. Evolution of the medium number of vehicles in the Street Horea right traffic-lane

These results were obtained by queries implemented in UPPAAL graphical interface Verifier. The results obtained with the model proposed are appropriate in the context of the urban traffic theory.

5. Conclusions

The cellular automata allow the observation of different phenomena, managing to dissect its components in individual variables, and can understand how local changes affect the whole grid of cells.

Using microscopic models brings a large amount of data to analyze. In an urban area, where are several elements involved in road traffic, is compulsory to analyze the interactions between them to reduce traffic jams, fuel costs and to improve the quality of life.

It would be interesting to implement different kinds of vehicles like ambulances, fire trucks, and police automobiles with high priority than the others, works in the street, bus and tram schedules, and crosswalks controlled with traffic lights.

Implementing the adaptive safety distance for a vehicle depending on the chosen value of velocity, and the distance that splits it from the vehicle in front (number of free cells in its front) based on the functions presented previously would be also an interesting topic to analyze. With this implementation will be created smooth transitions of the values of velocity between two consecutive street cells.

References

[1] Alur, R., Dill, D.L., "A Theory of Timed Automata," In Theoretical Computer Science, vol. 126, 183-235, 1994.

[2] Behrmann, G., David, A., Larsen, K.G. "A tutorial on UPPAAL". In Proceedings of the 4th international school on formal methods for the design of computer, commu- nication, and software systems (SFM-RT'04). LNCS 3185, 2004.

[3] Chowdhury, D., Santen, L.; Schadschneider, A., "Statistical physics of vehicular traffic and some related systems," Physics Reports, v. 329, pp. 199-329, 2000.

[4] Clark, J., Daigle, G., "The importance of simulation techniques in its research and analysis", Proceedings of the 1997 Winter Simulation Conference, USA, 1997.

[5] Daigle, G., Clark, J., "The Importance of Simulation Techniques In Its Research And Analysis," in Winter Simulation Conference, pp. 1236-1243, 1997.

[6] Hanumappa, D., Ramachandran, P., "Cellular Automata Model for Mixed Traffic Flow with Lane Changing Behavior", Modelling and Simulation in Engineering, vol. 2021, 2021.

[7] Lima, E.B., "Modelos microscópicos para simulação do tráfego baseados em autômatos celulares.", Dissertação de Mestrado em Computação, Universidade Federal Fluminense, Niterói, Brazil, 2007.

[8] Lindberg, T., Peterson, A., Tapani, A., "A simulation model of local public transport access at a railway station", RaillLille 2017, International Conference on Railway operations modeling and analysis, pp. 922-944, 2017.

[9] May A.D., "Traffic Flow Fundamentals", Prentice Hall, 1997.

[10] Nagel, K., Schreckenberg, M., "A cellular automaton model for freeway traffic", Journal de Physique I, France, pp. 2221-2229, 1992.

[11] Nguyen, J., Powers, S.T., Urquhart, N., Farrenkopf, T., Guckert, M., "An overview of agent-based traffic simulators", Transportation Research Interdisciplinary Perspectives, Volume 12, 2021.

[12] Regragui, Y., Moussa. N., "A Cellular Automata Model for Urban Traffic with Multiple Roundabouts", Chinese Journal of Physics, Physical Society of the Republic of China, 2018.

[13] Rodaro, E., Yeldan, O., "A multi-lane traffic simulation model via continuous cellular automata", 2018.

[14] Rothery, R., et all "Traffic flow theory. Transportation Research Board (TRB)", Special Report, pp. 165, 1998.

[15] Tian, J., Zhu, C., Jiang, R., "Cellular automata approach to synchronized traffic flow Modelling", 2018.

[16] Vaandrager, F., "A First Introduction to Uppaal", Institute for Computing and Information Sciences, Radboud University Nijmegen, Netherlands.

[17] Valente, E., Avram, C., Machado, J., Aștilean, A., "An Innovative Approach for Modelling Urban Road Traffic Using Timed Automata and Formal Methods", Jour. of Advanced Transportation, vol. 2018, Article ID 6269526, 15 pages, 2018.

[18] Vico, F.J., Basagoiti, F.J., García-Platas, R., Lobo, D., "Modelado y simulación del tráfico en vías urbanas y periurbanas en base a la estimación de tiempos de recorrido", ETSI Informática, Universidad de Málaga and Tecnologías Viales Aplicadas, TEVA, SL, Malaga, 2005.

[19] Zhao, H.T., Zhao, X., Jian-Cheng, L., Xin, L.Y., "Cellular automata model for Urban Road traffic flow Considering Internet of Vehicles and emergency vehicles", Journal of Computational Science, Volume 47, 2020.

Andrzej Loska[1], Dorota Palka[2], Alicja Bień[3], Katarzyna Substelny[4]

A WAY OF SUPPORTING THE SERVICING OF PRODUCTION MACHINES USING REVERSE ENGINEERING AND 3D PRINTING TECHNIQUES

SPOSÓB WSPOMAGANIA SERWISOWANIA MASZYN Z WYKORZYSTANIEM INŻYNIERII ODWROTNEJ I TECHNIKI DRUKU 3D

Abstract

The use of machines and devices causes their components to wear out, which leads to damage. The easiest and fastest method of repair is to replace this element with a new one. The problem arises when the desired element is not available on the market, technical documentation is unavailable or the costs of acquiring a new element are too high. In such a situation, engineering reconstruction, also known as reverse engineering, is used, which allows for the reconstruction of technical documentation and the production of a new product thanks to additive technology. The article presents the process of reverse engineering and the types of additive manufacturing technology. The aim of the article is to present the possibilities of using the reverse engineering method and 3D printing in the reconstruction of sample machine parts. The work uses the FDM (Fused Deposition Modeling) spatial production technology. The relevance of the article is confirmed by the possibility of its practical use in the field of machine servicing support.

Keywords: reverse engineering, 3D printing, CAM computer support, machine servicing, machine operation

Streszczenie

Eksploatacja maszyn i urządzeń powoduje, że ich podzespoły zużywają się, a to prowadzi do uszkodzeń. Najprostszą i najszybszą metodą naprawy jest wymiana tego elementu na nowy. Problem pojawia się, gdy pożądany element nie jest dostępny na rynku, niedostępna jest dokumentacja techniczna lub koszty pozyskania nowego elementu są zbyt wysokie. W takiej sytuacji zastosowanie znajduje rekonstrukcja inżynierska nazywana również inżynierią odwrotną, która pozwala na odtworzenie dokumentacji technicznej oraz wykonanie nowego produktu dzięki technologii addytywnej. W artykule przedstawiono proces przebiegu inżynierii odwrotnej oraz rodzaje technologii wytwarzania przyrostowego. Celem artykułu jest przedstawianie możliwości zastosowania metody inżynierii odwrotnej oraz druku przestrzennego w rekonstrukcji przykładowych części maszyn. W pracy wykorzystano technologię wytwarzania przestrzennego FDM (Fused Deposition Modeling). Zasadność artykułu potwierdza możliwość jego praktycznego wykorzystania w zakresie wspomagania serwisowania maszyn.

Słowa kluczowe: inżynieria odwrotna, druk 3D, wspomaganie komputerowe CAM, serwisowanie maszyn, eksploatacja maszyn

1. Introduction

One of the key problems affecting the effectiveness of production or service processes is the exploitation potential of the technical means involved in them. This results in the need for constant analysis of wear of machine and device elements, as well as to plan and optimize the operating processes carried out in parallel. This is reflected in the adopted exploitation policy, the guidelines of which relate to current activities, but the effects are significant in the long term [9]. The key aspect of the operational policy is the approach to the method and scope of servicing machines in a technically and economically effective manner. High maintenance costs as well as the difficult economic situation force entrepreneurs to intensively search for opportunities to reduce these costs [3, 7, 12, 19].

---

[1] PhD Eng. Andrzej Loska Assoc. Prof. (corresponding author), Silesian University of Technology, Faculty of Organisation and Management. Department of Production Engineering, ul. Roosevelta 26-28, 41-800 Zabrze, Poland, email: andrzej.loska@polsl.pl, ORCID: 0000-0003-0041-795X.

[2] MSc. Eng. Dorota Palka, Silesian University of Technology, Faculty of Organisation and Management. Department of Production Engineering, ul. Roosevelta 26-28, 41-800 Zabrze, Poland, e-mail: dorota.palka@polsl.pl ORCID: 0000-0002-1441-4197.

[3] MSc. Eng. Alicja Bień, e-mail: ala.bien@interia.pl

[4] MSc. Eng. Katarzyna Substelny, e-mail: katarzyna.substelny@gmail.com

In operational practice, the greatest care is usually attached to machines and devices heavily loaded, requiring constant and frequent diagnostic and maintenance supervision throughout their life cycle. Technical facilities with high reliability and high durability are deliberately omitted in these activities, as they do not cause current problems in the production processes carried out [6, 8]. The result of high reliability and durability of some elements of machines and devices is:

- long trouble-free operation time,
- limitation or loss of their technical and organizational serviceability after a long trouble-free period of use.

Undoubtedly, the first aspect is unquestionably positive. But in this article the authors have focused on the second aspect, which, paradoxically, is a consequence of the positive dimension of the first aspect. As a result of technically and organisationally justified lack of service interest in highly durable and reliable elements of machines and devices, the necessity and the possibility of restoring their operational potential in the event of their natural wear disappears with time [1]. In practice, after a long, usually many years, period of use and the implementation of many production cycles, a situation that makes further operation impossible appears quite suddenly. A long period that goes beyond the typical period of life over time results in the abandonment of service care, and thus difficulties in accessing replacement parts, and even the lack of documentation allowing for their reproduction.

As a solution to such a problem, the authors propose the use of reverse engineering methods, including the methods of rapid prototyping and 3D printing technology. This allows for the introduction of changes to the manufactured machine elements, their complete modification and the production of unique tools, not produced in series, but necessary to carry out an unforeseen repair [4, 19]. Therefore, in the further part of the article, the authors demonstrated the method of servicing selected machines, taking into account the reverse engineering method, the method of rapid prototyping and 3D printing of used elements.

The aim of the article is to present the possibilities of using the reverse engineering method and 3D printing in the reconstruction of sample machine parts. The relevance of the article is confirmed by the possibility of its practical use in the field of machine servicing support. Each chapter of the article supports the achievement of this goal.

2. Reverse engineering in exploitation processes

The method of reverse engineering or engineering reconstruction consists in transforming a real, existing object into its digital representation. The relationship between the described processes is shown in Fig. 1.
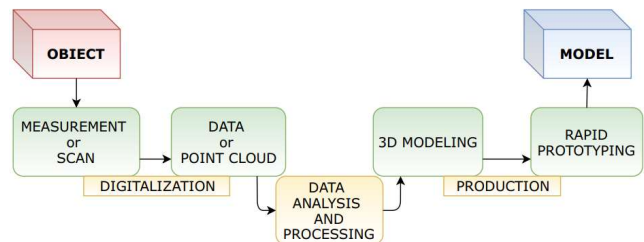
Fig. 1. Scheme of procedures in engineering reconstruction

The form of a 3D model is most often created through the scanning process, and this process is called digitization. In the era of existing technical solutions, manual measurements more and more often seem insufficient, although they are still used in practice. On the basis of the reconstructed object, it is possible to prepare technical documentation. In traditional CAD methods, the development of a 3D model consists in providing dimensions from the existing technical documentation or creating technical documentation along with the resulting model of the object. The next step is to transform the virtual model into a real object.

The key stage of engineering reconstruction is rapid prototyping technology. It is used primarily for precise and repeatable production of elements using additive manufacturing. The high accuracy of mapping the geometric features of the models enables their use for structural, assembly and functional analyzes. Rapid prototyping technology is based on the creation of three-dimensional physical objects, layer by layer, from computer models. This process is also known as additive manufacturing [12, 19].

3. Production methods incremental - review of techniques and tools

The first additive technique was developed by Chuck Hull in 1984. He defined and patented stereolithography as the successive formation of a spatial object thanks to thin layers of hardened ultraviolet material. Two years later, he founded the company 3D Systems, which was involved in the production and sale of 3D printers. As part of the company's activity, the STL (stereolithography) file format [18], which is indispensable nowadays, has been developed (Alternative extensions of the STL abbreviation were created secondary: Standard Tessellation Language and Standard Triangulation Language). Stereolithography

is an additive manufacturing process that belongs to the family of photopolymerization. Currently, the Chuck Hull method is known as SLA (from the name stereolithography), printing from a light-cured resin, hardened with a laser beam. The workbench is immersed in a container with resin, and then the laser beam defines the shape of the object in the XY plane, hardening the resin. After the process is finished, the table is raised to the height of the next layer and the process is repeated [12, 13, 14]. The DLP (Digital Light Processing) method is characterized by a similar production process. The difference is in the way the layer is cured, namely the light emitted by the projector mounted under the resin container. In this way, the entire layer is hardened simultaneously [10, 17]. Another incremental technique, Fused Deposition Modeling, was developed in 1988 by Scott Crump. FDM means positioning or deposition of a fused material. Currently, it is one of the most popular methods due to the availability of amateur printers using thermoplastics. The printing process consists of heating the plastic material supplied to the printer head in the form of a line and bringing it to a semi-liquid state. The layers are applied in the XY plane, then the table is lowered down or the head is raised up to the height of the next layer. The process is repeated layer by layer, and the semi-liquid plastic sticks together under the influence of high temperature and solidifies to form a uniform structure [13, 16]. 3D printing techniques from powdered plastics are also known. The Selective Laser Sintering (SLS) method uses polyamides that are selectively sintered by a laser beam. After the end of the process, the object comes out of the lump of unbaked powder. A similar process is characterized by the EBM method, the basic material of which is powdered metals and an electron beam is used to bind the molten metal [10, 18]. The CJP method, whose name comes from the English words Color Jet Printing, is similar to the principle of operation of the above techniques. It allows you to obtain a multi-color printout similar to standard CMYK printers. The sintered metals are hardened by the point application of a binder, which allows the powder to stick together at the point of application. The printing head is responsible for the application, its structure is similar to that of a traditional inkjet head. This solution allows the use of the binder together with colored pigments. The semi-fluid, deliquescent consistency of the material makes it possible to blur the boundaries between successive layers, which significantly affects the quality of the object [2]. Printing systems made of powdered plastics or metals are used only in the industrial sector and their cost can even reach several million zlotys. There are also other specialized methods of additive manufacturing [5, 7, 11, 18]:

1. LMD (Laser Metal Deposition) – laser metal deposition. The technology allows for the simultaneous creation of new layers of the object and their hardening, which increases the resistance of models to loads.
2. LENS (Laser Engineered Net Shaping) – laser execution of the final shape and dimensions. The method is one of the innovative incremental techniques that can be used to apply protective layers.
3. NPJ (Nanoparticle Jetting) – jet spraying of nanoparticles. A method that uses a mixture of various metal nanoparticles as a working material.
4. EBAM (Electron Beam Additive Manufacturing) like EBM, this method uses an electron beam to melt the material and requires the creation of vacuum conditions.

The choice of the best 3D printing technology depends primarily on the needs of the contractor. Each of the technologies is characterized by individual features, such as: time, cost and accuracy of the printout. In addition, the most important issue determining the choice of technology is the material used to manufacture the object. The appropriate mechanical properties of the material are crucial for their application.

4. Reconstructive servicing of a selected duplicating machine – a case study

The described problem of servicing machines with the use of engineering reconstruction methods of its elements was based on a practical case. In this case, the reconstruction of selected elements of the Nashuatec 4525 duplicating machine (copiers) was carried out. The high reliability of this machine and the rapid development of printing technology meant that the described Nashuatec 4525 copier was withdrawn from production. Thus, it fulfilled the previously formulated operational problem criteria for objects with high reliability, the lifetime of which significantly exceeds the average operation time. Currently, there are no new devices or spare parts available on the market, only accessories such as toners, sheets and paper are available. There is no possibility to purchase spare parts, and thus the lack of serviceability of the machine resulted in the need to develop technical documentation and reconstruct the damaged elements.

The elements that had worn out and needed to be reconstructed were:

a) knob, cooperating with the fusing heating unit,
b) a gear wheel located on the rear wall of the copier, mating with the gear wheel on the developer.

The location of the damaged elements is shown in Fig. 2.

Fig. 2. Nashuatec 4525 duplicating machine with used parts location

The knob cooperating with the fusing heating unit is a part of the unit which consists of, among others, two rollers. One of these shafts is held in place by a play knob. This mechanism is designed to prevent paper jams. A damaged knob and mating element are shown in Fig. 3.

As a result of wear and tear caused by long-term operation, the knob was permanently damaged. Its upper part has been significantly damaged. Due to the location of the damage, this loss completely prevents further use of the knob.

The process of reconstruction of the used element consists of the following stages:

a) development of a 3D model,
b) development of construction documentation,
c) development of the executive program code,
d) print of a new element
e) performance operational tests.

Fig. 3. Knob that mates with the fusing heating unit: a) knob defective, b) mating element

The first stage of the reconstruction of the damaged element was its measurement and the development of a 3D model. For this purpose, traditional measurement methods (calliper) and the Fusion 360 software were used. The next steps of modeling and the final modeling effect are shown in Fig. 4.

a)   b)   c)
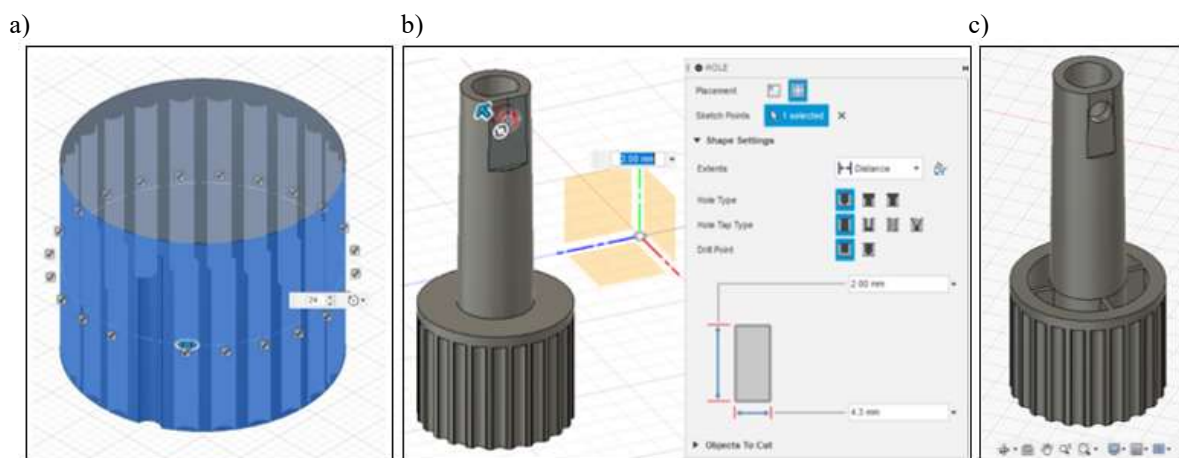
Fig. 4. Stages of modeling the reconstructed element: a) creating the knob grooves,
b) creating a bolt hole in the element's shaft, c) the final modeling effect

Based on the prepared 3D model of the reconstructed element, the necessary drawings of the construction documentation were developed, selected components of which are shown in Fig. 5. The construction documentation contains information necessary for the subsequent stages of manufacturing the reconstructed element.
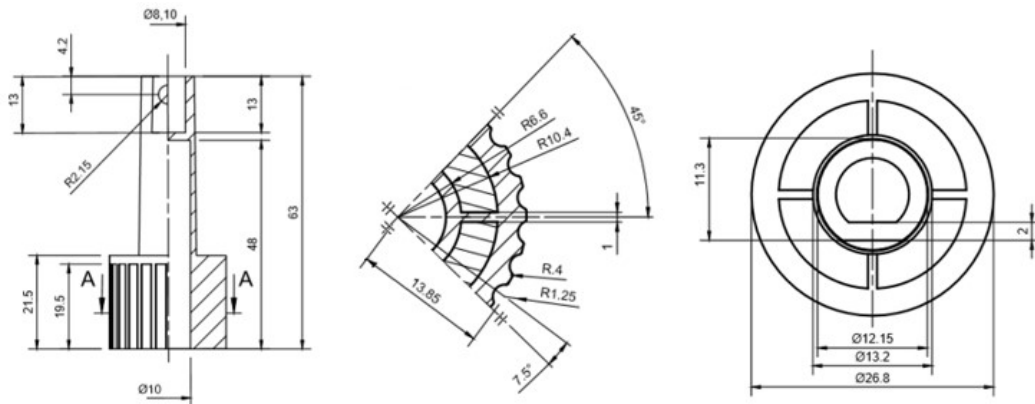
Fig. 5. Prepared technical documentation of the reconstructed element

Based on the developed 3D model of the reconstructed element, as well as construction documenttation, a program was developed that allows for printing a new element. For this purpose, the design of the 3D model was exported to the STL format. STL files are a conventional form of commands to be performed by a 3D printer, at the same time it is a file format compatible with the CAD environment and dedicated software for the printer. The Z-SUITE software dedicated to the Zortrax M 200 plus printer was used here. This software made it possible to assign detailed printing parameters, in particular:

1. Parameters related to the type and characteristics of the material from which the product will be made. In this case, it is the Z-ULTRAT filament. This material is based on plastic and ensures high quality and durability of the models, thanks to which it can be used for a variety of functional prototypes, spare parts for machines or sample consumer products. In addition, this material is easily subject to chemical and mechanical treatment, it allows you to print models with physical properties similar to products manufactured with the use of injection molds [20].

2. Object filling parameters: structure and material density given as a percentage and precision given in tenths of a millimeter, decisive for the strength and quality of the manufactured element (Fig. 6).

3. Parameters determining the method of production. In order to ensure the smoothness of the surface of the object, it is most often produced on a thin platform, moreover, in the production of geometrically complex objects, it is worth using supports supporting the model during its production. An important element for the strength of the element is the dispersion of the seam. The seam is the point where the application of a new layer of material begins and ends, at the same time this area is most likely to break (Fig. 6).
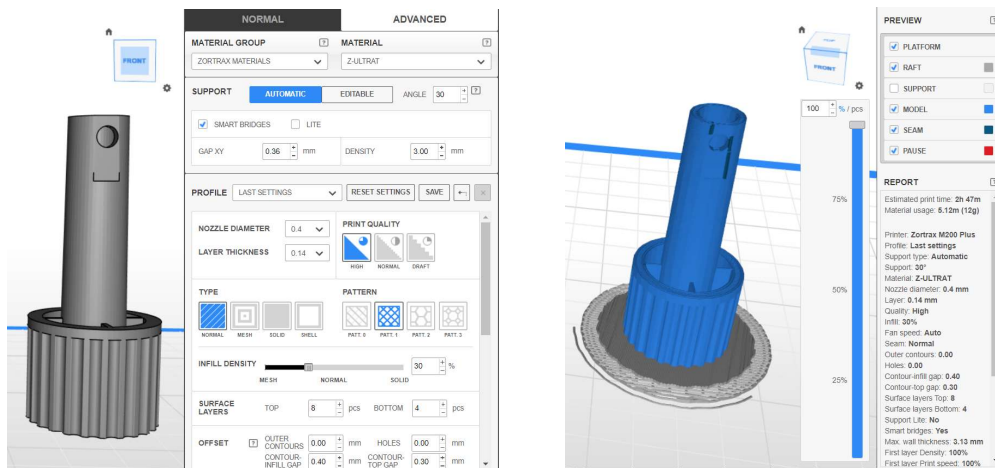
Fig. 6. Parameters of 3D printing and the manufacturing process of the reconstructed knob

The next stage resulting directly from the previous stages and their consequences is the execution (printing) of a new element. A Zortrax M200 PLUS 3D printer was used for printing, using the technology of layered application of melted filament. The printing process was estimated at 2 hours 47 minutes, and the material consumption at 12g. The printing process is shown in Fig. 7.
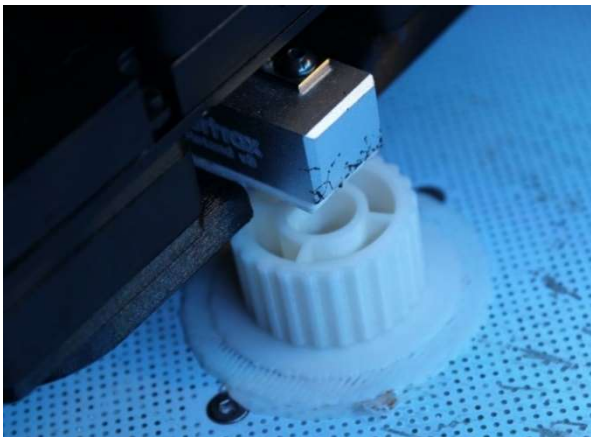
Fig. 7. The printing process

A comparison of the original damaged and new reconstructed element is shown in Fig. 8.

Fig. 8. Comparison of damaged and reconstructed knob

The comparison process was carried out in geometric and operational aspects. It was confirmed that the geometrical features (form, dimensions) of the printed element correspond to the values included in the previously prepared construction documentation. In addition, it has been observed that the resulting element overlaps the shaft, and the flattening of the figure itself at this stage significantly inhibits the movement of the knob in relation to the shaft. In addition, the hole at the root is large enough not to block the screw, and small enough so that the screw head does not pass through it. The grooves increase the

grip of the knob. The element placed on the shaft is shown in Fig. 9.

Fig. 9. Visualization of operational verification of the reconstructed element

The second reconstructed element of the above-mentioned copying machine was a gear wheel. This element is located on the rear wall of the copier and cooperates with the gear wheel on the developer. The damaged gear wheel and counter wheel is shown in Fig. 10.

Fig. 10. Visualization of the reconstructed gear wheel with the mating gear wheel

Similarly to the presented reconstruction process of the knob, the reconstruction of the gear wheel was started with its measurements with traditional tools.

This enabled him to make a geometric model using the Inventor software. The next steps of the object modeling process and its final effect are shown in Fig. 11.

The developed 3D model allowed for the preparation of construction documentation (Fig. 12).
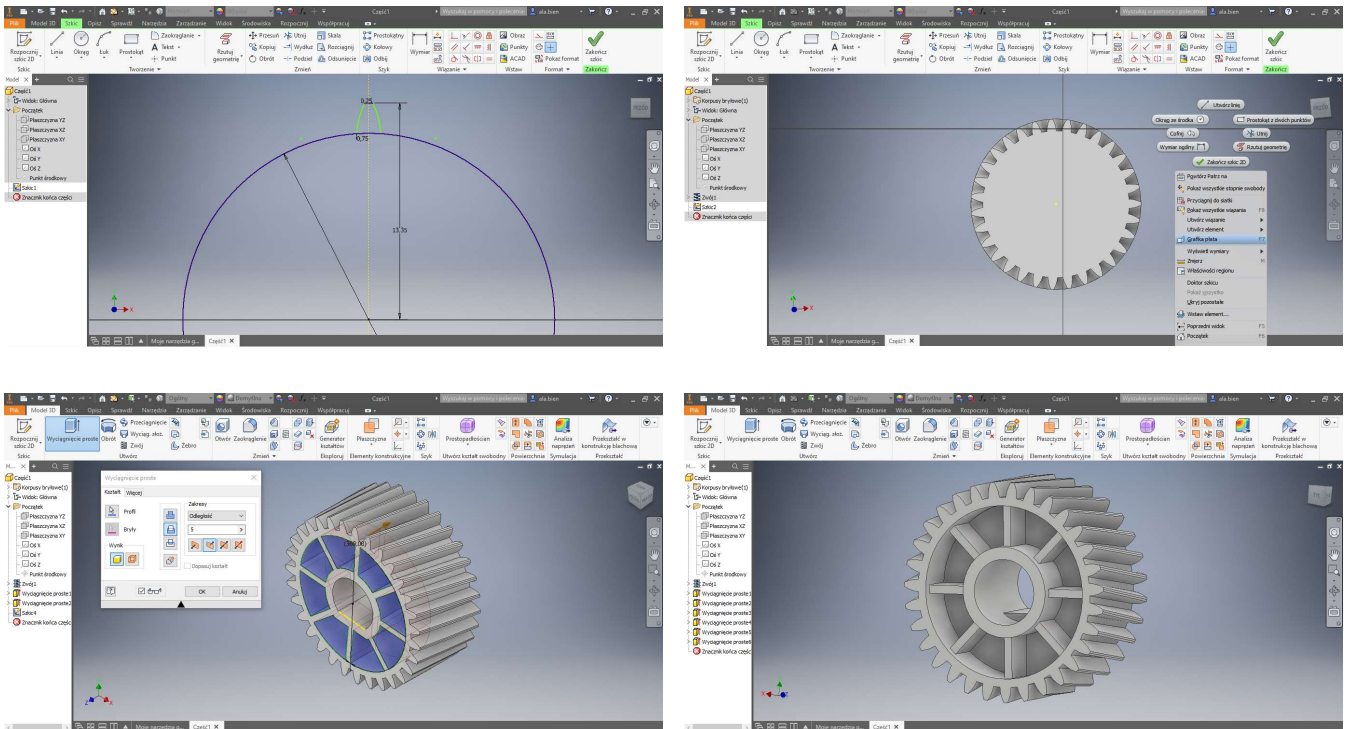
Fig. 11. Modeling steps in the engineering reconstruction of a gear wheel
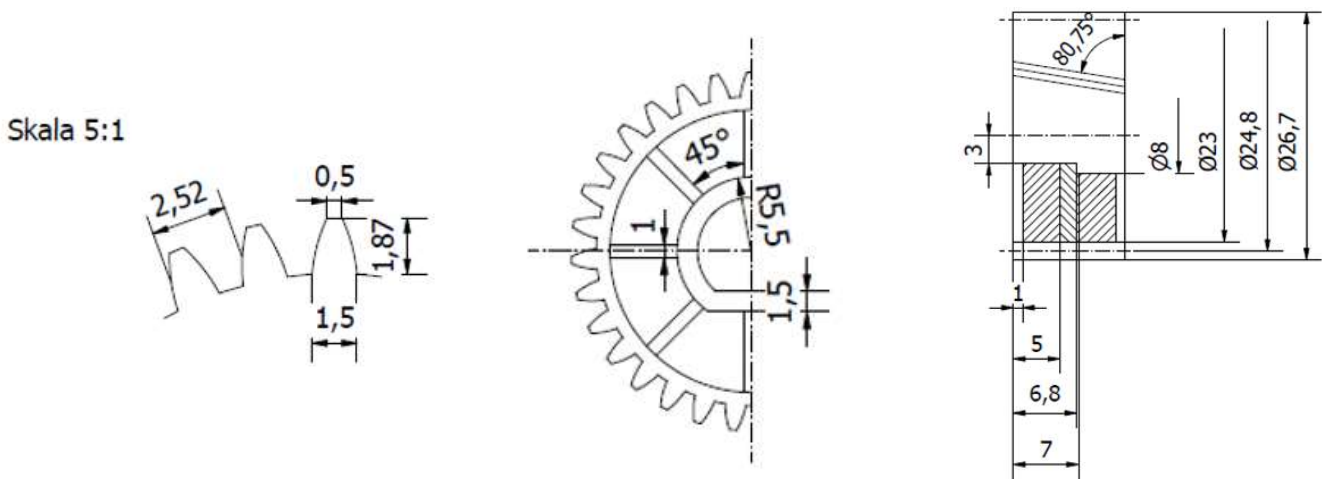
Fig. 12. Technical documentation of the reconstructed gear wheel

Based on the construction documentation, the code in the STL format was prepared, which was the basis at the prining. Printing time was estimated at 56 minutes and material consumption at 6g.

The selected options and parameters are shown in Fig. 13.

The next steps for printing a gear wheel are shown in Fig. 14.
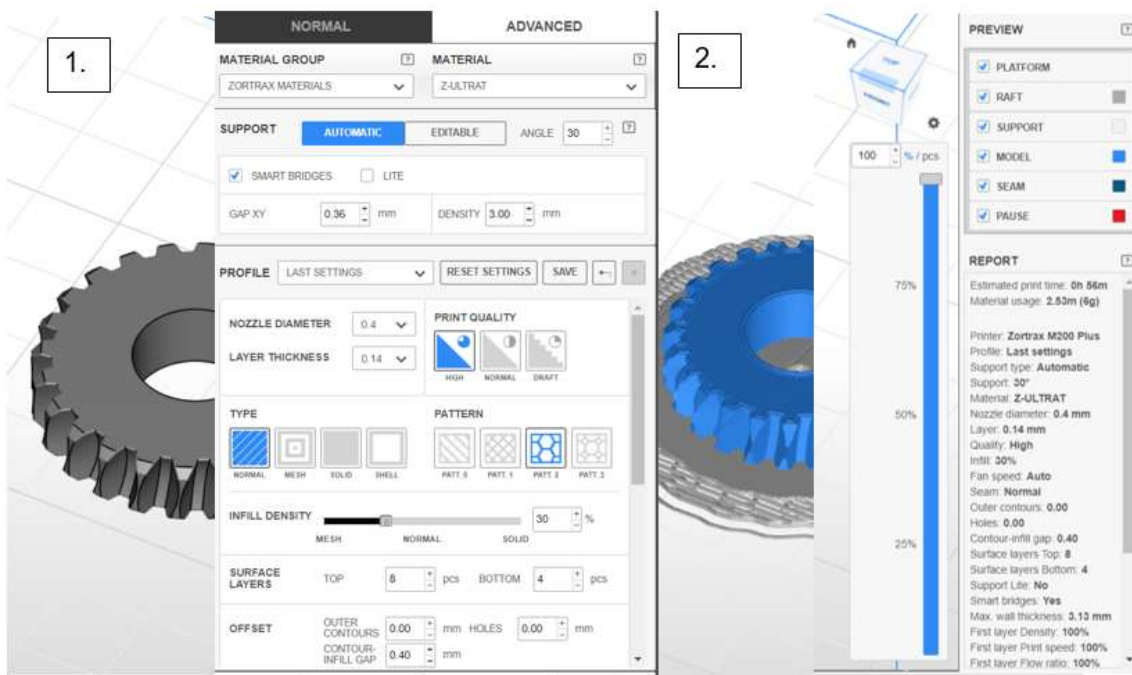
Fig. 13. Parameters of 3D printing and the manufacturing process of the reconstructed gear wheel
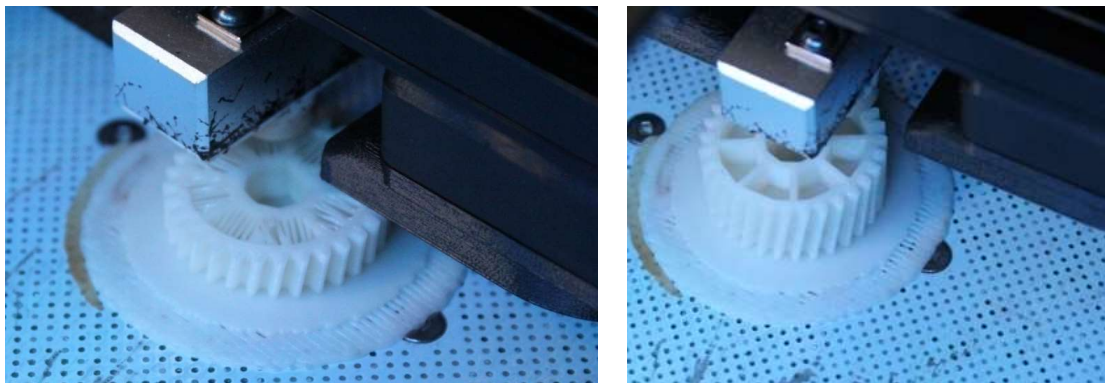
Fig. 14. Visualization of the manufacturing process of a reconstructed gear wheel

The structural and functional verification carried out showed that all geometric features of the gear wheel were reproduced in accordance with the requirements (tooth pitch, tooth shape, wheel diameter, and wheel bore). It was observed that the new gear wheel meshes properly with the wheel on the developer, as shown in Fig. 15.
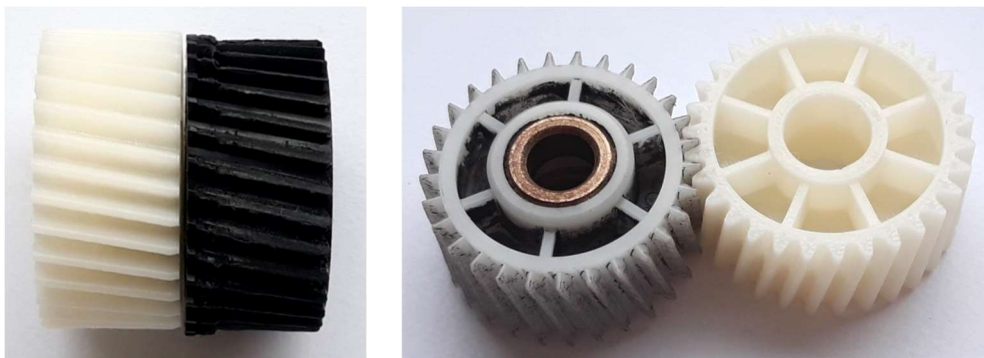
Fig. 15. Comparison of the damaged and reconstructed gear wheel

5. Conclusions

In the current difficult market situation, the approach to the issue of maintenance is essential for the future of enterprises. The slightest failure generates downtime and this usually causes costs and losses. These costs can be much higher when the failure is related to a spare part that is not available on the market. The inability to repair a damaged machine causes a need, which is answered by the method of reverse engineering.

There are many different ways to make reconstructive engineering activities effective, and there are also many IT tools for modeling or developing technical documentation. The quality of the final element is related to the methods, programs and equipment used. Their significant diversity allows for the appropriate selection of solutions for the selected element, taking into account many factors – the level of geometric complexity, the essence of aesthetic values, the function of fulfilling the element, etc.

3D printing turns out to be particularly useful when you need to create a single object. This technique eliminates the need to run the entire production line. It significantly reduces costs, time and workload that must be put into the production process. Additionally, the precision or quality of the manufactured objects does not differ from traditional methods.

The use of modeling and 3D printing, characterized by high accuracy of mapping with reality, can also be used to verify the features of the object, e.g. strength tests. Having a digital version of a real element also allows you to make improvements to it without generating additional costs. These improvements may be related to changes in the geometry of the object or the selection of an alternative, better material.

Bibliography

[1] Antosz K., Chandima R.R.M. 2019. „Spare parts' criticality assessment and prioritization for enhancing manufacturing systems' availability and reliability". Journal of Manufacturing Systems 50: 212-225.

[2] Caban J., Szala M., Kęsik J., Czuba Ł. 2017. „Wykorzystanie druku 3D w zastosowaniach automotive". Autobusy: technika, eksploatacja, systemy transportowe 18(6): 573-579.

[3] Fidali, M. 2018. „Szybki dostęp do części zamiennych, czyli technologie przyrostowe w służbie utrzymania ruchu". Utrzymanie Ruchu 4: 64-68.

[4] Gebler M., A.J.M. Schoot Uiterkamp, C. Visser. 2014. „A global sustainability perspective on 3D printing technologies". Energy Policy 74: 158-167.

[5] Gościański M., Dudziak B. 2015. „Próby technologiczne napawania elementów technicznych metodą Laser Metal Deposition (LMD)". Technika Rolnicza Ogrodnicza Leśna, 4: 24-28.

[6] Knofius N., van der Heijden M.C., Zijm W.H.M. 2019. „Moving to additive manufacturing for spare parts supply". Computers in Industry 113: 103-134.

[7] Li, Feng, et al. "Increasing the functionalities of 3D printed microchemical devices by single material, multimaterial, and print-pause-print 3D printing." Lab on a Chip 19.1 (2019): 35-49.

[8] Lolli F., Coruzzolo A.M. Peron M., Sgarbossa F. 2022. „Age-based preventive maintenance with multiple printing options". International Journal of Production Economics 243: 108-339.

[9] Loska A. 2020. „The way of exploitation assessment in the conditions of object-oriented servicing of selected production machines and equipment". Technologia i Automatyzacja Montażu, 1: 4-9.

[10] Maines, E. M., Porwal, M. K., Ellison, C. J., & Reineke, T. M. (2021). Sustainable advances in SLA/DLP 3D printing materials and processes. Green Chemistry.

[11] Napadłek W., Chrzanowski W., Woźniak A. 2017. „Przyrostowe technologie 3D w odbudowie kształtu zużytych eksploatacyjnie łopat turbin parowych". Autobusy: technika, eksploatacja, systemy transportowe 18: 1147--1151.

[12] Palka, Dorota. "Use of reverse engineering and additive printing in the reconstruction of gears." Multidisciplinary Aspects of Production Engineering 3.1 (2020): 274-284.

[13] Peltola, Sanna M., et al. "A review of rapid prototyping techniques for tissue engineering purposes." Annals of medicine 40.4 (2008): 268-280.

[14] Rutkowski K., Ocicka B. 2020. „Rozwój druku 3D i jego wpływ na zarządzanie łańcuchem dostaw". Przegląd Mechaniczny 4: 30-37.

[15] Siemiński P., Budzik G. 2015. „Techniki przyrostowe. Druk 3D. Drukarki 3D". Oficyna Wydawnicza Politechniki Warszawskiej.

[16] Szmidt A., Rębosz-Kurdek A. 2017. „Sposoby doskonalenia druku 3D w technologii FDM/FFF". Mechanik 90: 258-261.

[17] Ślusarczyk P. 2018. „Nowe technologie druku 3D z metali. STAL Metale & Nowe Technologie. 9-10.

[18] Tatarczak J., Krzysiak Z., Samociuk W., Kaliniewicz Z., Krzywonos L. 2017. „Przegląd nowoczesnych technologii druku 3D obiektów metalowych". Mechanik 90: 612-614.

[19] Wyleżoł M. 2019. "Inżynieria odwrotna i technologie rapid prototyping w utrzymaniu ruchu". Utrzymanie Ruchu 1: 66-70.

[20] Zortrax, Strona internetowa, (dostęp online 5.12.2021) www.zortrax.com

Tomasz Trzepieciński[1], Ľuboš Kaščák[2]

ASSESSMENT OF FRICTIONAL PERFORMANCE OF DEEP DRAWING QUALITY STEEL SHEETS USED IN AUTOMOTIVE INDUSTRY

OCENA WŁAŚCIWOŚCI TARCIOWYCH BLACH STALOWYCH GŁĘBOKOTŁOCZNYCH STOSOWANYCH W PRZEMYŚLE MOTORYZACYJNYM

Abstract

This article presents the results of tribological tests of three grades of deep-drawing quality steel sheets used in the automotive industry. The frictional properties of the sheets were anaysed using a strip drawing test. Friction tests were performed under dry friction and lubrication conditions using machine oil L-AN 46. Additionally, friction tests of pre-strained sheets were also carried out. Cylindrical countersamples with different surface roughness were used. Relationship between the surface roughness, pressure force, lubrication conditions and the value of the friction coefficient were evaluated. It was found that increasing the roughness of the countersamples increased the value of the friction coefficient in both friction conditions analysed. The greater the pressure force, the lower efficiency of lubrication. The effectiveness of reducing the value of the friction coefficient ranged from 20-30% and depended on the pressure force, roughness of the countersamples and the degree of specimen pre-straining.

Keywords: coefficient of friction, friction, sheet metal forming, steel sheet

Streszczenie

W artykule przedstawiono wyniki badań tribologicznych trzech gatunków blach stalowych głębokotłocznych stosowanych w przemyśle motoryzacyjnym. Do oceny właściwości tarciowych blach wykorzystano test przeciągania pasa blachy. Testy tarcia przeprowadzono w warunkach tarcia suchego i smarowania olejem maszynowym L-AN 46. Dodatkowo przeprowadzono badania tarcia blach poddanych odkształceniu wstępnemu. Zastosowano przeciwpróbki walcowe o różnej chropowatości powierzchni. Pozwoliło to na określenie relacji pomiędzy chropowatością powierzchni, wartością nacisku, warunkami smarowania oraz wartością współczynnika tarcia. Stwierdzono, że zwiększenie chropowatości przeciwpróbek powodowało zwiększenie wartości współczynnika tarcia w obydwu zastosowanych warunkach tarcia. Im większa siła docisku tym efektywność smarowania olejem maszynowym zmniejszała się. Efektywność zmniejszania wartości współczynnika tarcia wahała się w zakresie 20-30% i zależała od siły nacisku, chropowatości przeciwpróbek oraz stopnia wstępnego odkształcenia próbek.

Słowa kluczowe: współczynnik tarcia, tarcie, kształtowanie blach, blacha stalowa

1. Introduction

One of the key phenomena in sheet metal forming (SMF) is the friction between the surfaces of the tool and the workpiece material [2]. The initial topography of the sheet surface under the influence of large deformations constantly evolving during the forming process [1]. The wear resulting from the mechanical interaction of materials in contact is a phenomenon that makes it difficult to obtain products with the suitable surface quality [21]. The technologist has

many means and methods of selecting optimal lubrication conditions in order to increase the lubrication efficiency and reliability of the forming process [19, 20].

Friction and wear is an indispensable physical phenomenon accompanying the contact of two bodies [12]. It is assumed that approx. 23% of world energy consumption comes from tribological contacts [9]. 20% of this energy is used to overcome friction, and 3% is the cost of regenerating worn parts due to failure or wear. The phenomenon of friction occurring in the

---

[1] DSc, PhD, Eng. Tomasz Trzepieciński, Assoc. Prof. (corresponding author), Rzeszow University of Technology, Faculty of Mechanical Engineering and Aeronautics, Department of Manufacturing Processes and Production Engineering, al. Powstańców Warszawy 8, 35-959 Rzeszów, Poland, e-mail: tomtrz@prz.edu.pl, ORCID: 0000-0002-4366-0135.

[2] Ľuboš Kaščák, doc. Ing., PhD, Institute of Technology and Material Engineering, Faculty of Mechanical Engineering, Technical University of Košice, Košice, Slovakia, ORCID: 0000-0001-5642-9998.

SMF processes differs significantly from the phenomena occurring at low loads and in the kinematic pairs due to the high influence of plastic deformation that can intensify many phenomena in the contact zone [14]. The value of friction coefficient strongly depends on the roughness of the contacting surfaces and the value of normal pressures. Friction is a phenomenon that has a key impact on the plastic flow of the material, the quality of the surface of the finished product, and also directly affects the wear of tools [8, 25].

Friction during sheet forming is a complex function of the physical and mechanical properties of the tool and workpiece, forming parameters, sheet and tool topography and lubrication conditions [18]. SMF is one of the most important forming technology, especially in the engineering, automotive and aviation industries. During SMF, the relative movement of the tool and the workpiece makes the properties of the deformed material (e.g. hardness, topography and surface roughness) and preparation of the tool surface (e.g. texture, protective coating, thermomechanical properties) of great importance [27]. In order to optimally design the forming process, improve SMF conditions and finally control tribological phenomena, it is necessary to understand the interactions between tribological and surface engineering aspects [6].

The strip drawing test is the basic tribological test used to model the friction conditions in the flange of the drawpiece. In this method, the countersample surfaces represented tool surfaces are pressed against the sheet metal strip, which is simultaneously drawn [24]. The sheet metal strip is pulled between non-rotating countersamples with flat [15] or cylindrical shape [5, 24]. The change of friction conditions is realized by changing the sliding speed, radius of the countersamples, surface roughness of countersamples and lubrication conditions [19, 22]. Many authors have used the strip drawing test to determine the value of the coefficient of friction over a wide range of process parameters. The frictional behavior of sheets made of aluminum alloys 5754, 6111 and 6451 was the subject of research carried out by Masters et al. [15]. It was found that the coefficient of friction increases with the degree of sheet deformation, but the use of waxy solid lubricants helps to minimize this effect, keeping the friction coefficient constant with sample deformation up to 10%. The problem of the influence of the drawing speed and directional surface topography on the value of the friction coefficient and the change of the surface topography under mixed lubrication conditions in the strip drawing test was presented by Roizard and von Stebut [17]. Coello et al. [3] tested the electron beam textured galvanized steel sheet TRIP700 in a strip drawing test with flat dies. It was found that the microhydrodynamic conditions of boundary lubrication arise due to the plastic deformation of surface asperities, which creates high pressure in the volume of the lubricant filling the valleys surface topography.

In this paper, the results of tribological tests of three grades of deep-drawing steel sheets used in the automotive industry are presented. To assess the frictional performance of sheet metals the strip drawing test was used. Friction tests were performed under dry friction and lubricated conditions. Additionally, friction tests of pre-strained sheets were carried out. Cylindrical countersamples with different surface roughness were used.

2. Experimental investigations

2.1. Test material

In the friction tests the steel sheets of different deep drawing quality i.e., SB, BSB and Z II T were used. The basic mechanical parameters of the sheets (Table 1) were determined using an uniaxial tensile testing machine. Specimens for tensile test were cut along the sheet rolling direction (0°) and transversely (90°) in relation to the sheet rolling direction. Based on the measurement data, the work hardening characteristics of the examined sheets were determined. True stress-true strain relations were approximated by the Hollomon equation $\sigma = K \cdot \varepsilon^n$, where σ = true stress, ε – true strain, K – strength coefficient, n – strain hardening exponent.

Table 1. Selected mechanical parameters of sheets tested

Material	Specimen orientation	Yield stress $R_{p0,2}$, MPa	Ultimate tensile stress R_m, MPa	Strength coefficient K, MPa	Strain hardening exponent n
SB	0°	162	310	554	0.21
	90°	163	312	530	0.21
BSB/SSB	0°	151	282	494	0.221
	90°	153	281	475	0.21
Z II T	0°	166	313	543	0.22
	90°	171	321	551	0.241

2.2. Friction test

Assessment of friction performance of steel sheets has been carried out using strip drawing test simulator (Fig. 1). The test consists in pulling a sheet metal strip between two stationary countersamples with a cylindrical surface. Friction test considered is easy to carry out. Strip drawing test is characterized by possibility of uncomplicated measurement of the forces necessary to determine the value of the friction coefficient.
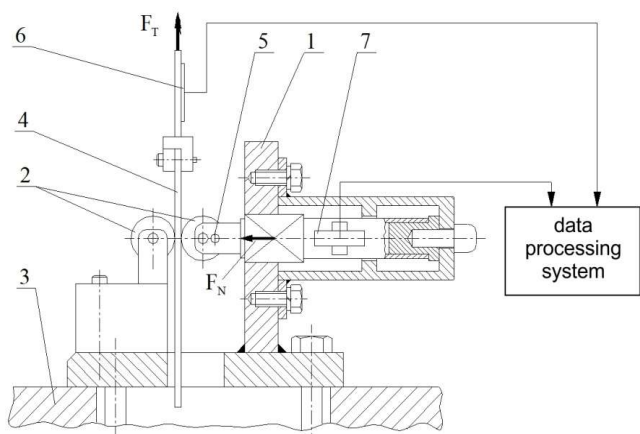
Fig. 1. Schematic view of strip drawing test: 1 – frame, 2 – countersamples, 3 – base, 4 – specimen, 5 – fixing pin, 6,7 – load cell

Friction test specimens approximately 200 mm long and 20 mm wide were cut along the sheet rolling direction. Countersamples in the form of rolls with a diameter of 20 mm were made of cold work tool steel. Three sets of countersamples with the following roughness parameters Ra = 0.32 μm, Ra = 0.63 μm and Ra = 1.25 μm, were used in the tests. The tests were carried out in dry friction and lubricated (L-AN 46 machine oil) conditions. In order to eliminate the influence of external factors, the surfaces of the samples and rolls were degreased with acetone. On the basis of the prepared data set, the value of the friction coefficient μ was determined according to the relationship:

$$\mu = \frac{F_T}{2F_N} \qquad (1)$$

where: F_T – friction force, F_N – pressure force.

The value of the pressure force was considered in the range between 0.4 kN and 2 kN.

3. Results and discussion

The general relationship that can be noticed was the reduction of the value of coefficient of friction with the increase of the clamping force at both lubricated and dry friction conditions (Fig. 2). This may be due to the fact that after a certain load value is exceeded, the relationship between the friction force and the clamping force is nonlinear, and the friction coefficient (as defined by Amontons' law) does not have a constant value and changes with increasing pressure. This effect is especially visible during friction with cylindrical countersamples for which the contact surface changes nonlinearly with pressure force. This relation has been also observed by Kirkhorn et al. [11], Trzepieciński et al. [23] and Trzepieciński and Fejkiel [24].

The friction occurring at high pressures may significantly differ from the phenomena occurring at low loads and in the kinematic pairs due to the high influence of plastic deformation that can intensify many phenomena in the contact zone [29]. In comparison with conventional kinematic pairs, in SMF processes, the material strength of one element of the friction pair (tool) is assumed to be much greater than the strength of the workpiece material, which undergoes intentional plastic deformation [4]. In such conditions, the share of the adhesion mechanism and the mechanical interaction of the surface asperities is dominant. The reduction of the value of friction coefficient by the use of lubricant depends on the roughness of the countersamples and the value of the contact force FN. The greater the contact pressure, the lubrication efficiency tends to reduce.

In general, increasing the surface roughness of the countersamples increases the value of the coefficient of friction of Z II T sheets in both applied friction conditions (Fig. 3). However, the increase in the value of the friction coefficient does not exceed the value of 0.06 when the roughness of countersamples changes from 0.32 μm to 1.25 μm. Such a nature of changes in the friction coefficient in the lubricated conditions proves the high contribution of the mechanism of mechanical interaction of the surface asperities in the conditions of cooperation of rollers with high surface roughness and the workpiece surface. In spite of the increase in the volume of lubricant pockets that can hold the oil, the value of the coefficient of friction increases. In the range of low contact forces, the lubricant to a greater extent reduced the coefficient of friction. Similar conclusions can be drawn for SB and BSB sheets
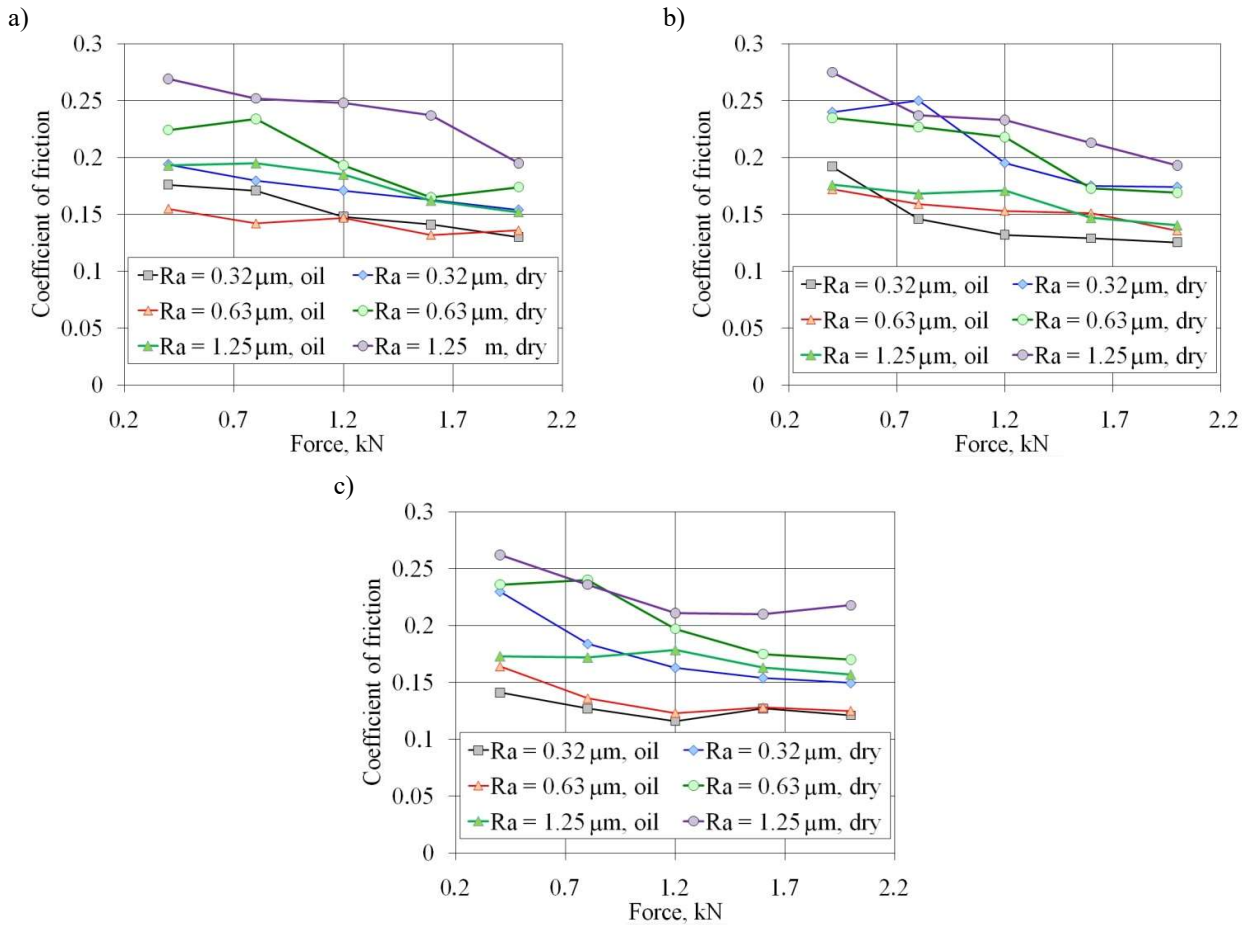
Fig. 2. Effect of pressure force F_N on the value of coefficient of friction for the following grades of steel: a) SB, b) BSB and c) Z II T
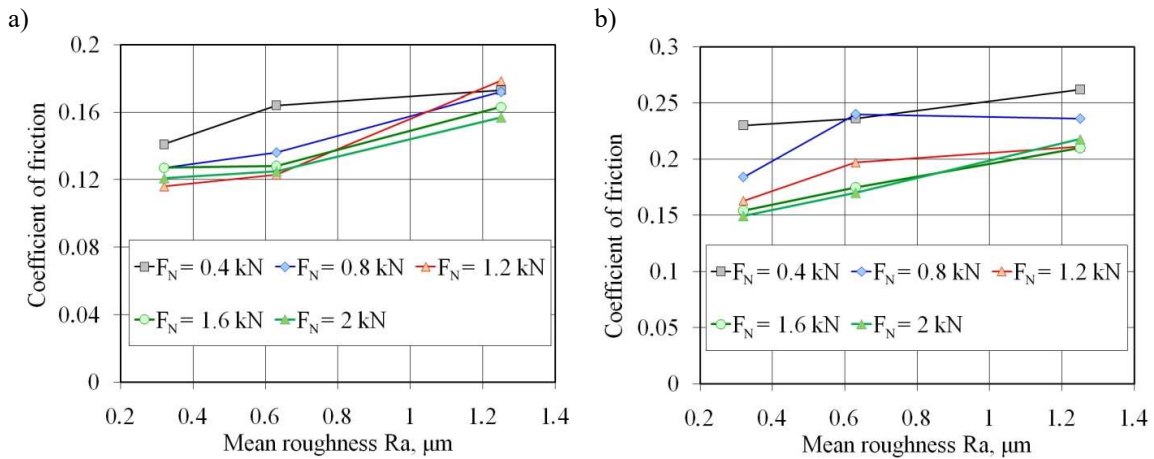
Fig. 3. Effect of average roughness of countersamples on the value of coefficient of friction for Z II T tested at a) lubricated conditions and b) dry friction

The highest average lubrication efficiency of BSB and Z II T sheets was recorded for the pressure force FN = 0.8 kN. For this pressure force, the lubrication resulted in a reduction of the value of friction coefficient by about 20-30%. Increasing the pressure force above value of 0.8 kN increases the value of the friction coefficient. The contact force under lubrication conditions determines the pressure of the lubricant in the closed lubricant pockets. And when the surface roughness of countersamples is high, then the friction force determines the intensification of the phenomenon of ploughing of the sheet surface by the hard asperities of the tool surface.

Changes in the properties of the surface layer of the samples are related to the change of friction conditions. The most frequently used 3D parameters

were used to describe changes in surface roughness during sheet metal forming. The measurements of the surface roughness of the sheet metal after the friction tests (Table 2) did not give an unambiguous answer to the question about the influence of friction conditions on the change of surface roughness of workpiece. Sheet strips after friction tests carried out with the use of countersamples with a roughness of Ra = 0.63 µm and at an initial pressure force 1.2 kN were selected for the analysis of surface roughness change. The friction process of steel sheets was accompanied by a decrease in the Sa (Fig. 4) and Sq (Table 2) parameters. No clear relationship was observed between the coefficient of friction and mean roughness Ra of sheets. Meanwhile, the lubrication of the sheet surface significantly reduced the number of summits per surface area of specimens compared to the dry friction conditions (Table 2).

Table 2. Selected spatial parameters of the sheet metal surface roughness before and after the SDT (Sa – the mean roughness, Sds – the summit density, Sdq – root mean square gradient)

Material	Friction conditions	Sq, µm	Sds, n_p/mm^2*	Sdq, µm/µm
SB	original surface	1.89	272	0.103
	dry friction	1.46	319	0.0902
	lubrication	1.64	290	0.0995
BSB	original surface	2.21	320	0.133
	dry friction	1.56	343	0.0849
	lubrication	1.4	303	0.0874
Z II T	original surface	2.08	312	0.131
	dry friction	1.58	311	0.109
	lubrication	1.48	283	0.0926

* n_p – number of summits
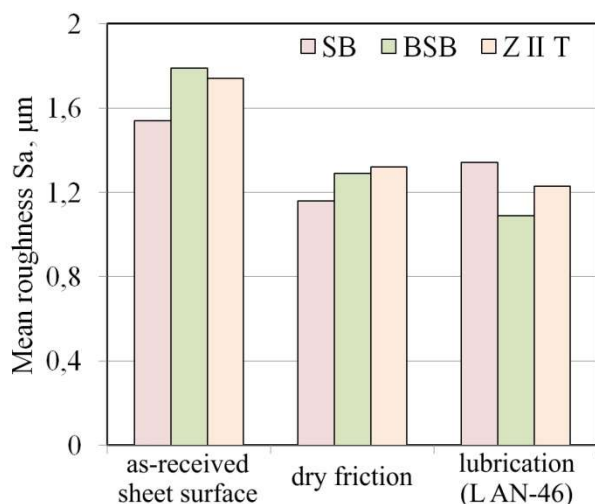
Fig. 4. Effect of test conditions on the mean roughness Sa

In the next part of the investigations, the pre-stretched samples were tested. For this purpose, the samples were stretched on the uniaxial tensile testing machine in order to obtain true strains ε equal to 0.095,

0.14 and 0.182. The most important parameters of surface roughness of the pre-strained samples were measured with the use of a Taylor Hobson Subtronic 3+ measuring system. On the basis of the results (Table 3), it was found that the values of the parameter Ra measured along (0°) rolling direction and transversely (90°) to this direction were proportional (Fig. 5). It should be emphasized that the values of Ra and Rz parameters increase with the increase of the true strain of the sheet strips. Moreover, in the whole range of true strains of the specimens, the value of the roughness parameter Ra increases almost linearly (Fig. 5). The change in roughness parameters measured in two perpendicular directions (0° and 90°) shows a different character. Mean spacing of profile irregularities increases in the direction of sheet strip stretching and decreases in the lateral direction.

Table 3. The influence of sample pre-strain on the change in the value of 2D roughness parameters of SB sheet surface (Ry – the maximum height, Rz – the maximum height of the assessed profile, Sm – mean spacing of profile irregularities)

Orientation	True strain φ	Surface roughness parameters		
		Ry, µm	Rz, µm	Sm, µm
0°	0	10.2	8.8	149
	0,095	11.1	9.6	167
	0,14	14	12	196
	0,182	14.2	12.4	177
90°	0	12.4	9.4	160
	0,095	18	11.2	146
	0,14	22.2	13.8	145
	0,182	18.5	14.3	152
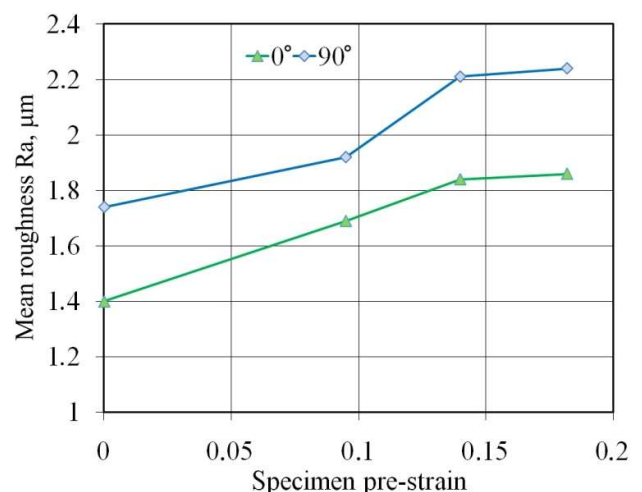
Fig. 5. Effect of specimen pre-strain on the value of mean roughness measured at rolling direction (0°) and transverse to the rolling direction (90°)

The value of the friction coefficient decreases with increasing contact force and true strain of pre-strained samples. Pre-straining process caused both a change in

the surface topography and mechanical properties of the sheet material as a result of work hardening phenomenon. The lowest values of the coefficient of friction were recorded during friction with the participation of a countersample with surface roughness Ra = 0.63 µm, tested in both analysed friction conditions (Fig. 6). The pre-strained samples tested with the countersample with roughness Ra = 1.25 µm were characterized by the lowest lubrication effi-

ciency. Due to the high surface roughness of the countersample in the form of open lubricant pockets and high hardness caused by the severe work hardening, the lubricant was not able to effectively reduce the frictional resistance. During friction with the countersample with mean roughness Ra = 0.63 µm, after exceeding the pressure force FN of about 1 kN, the stabilization of the value of friction coefficient with increasing load is visible.

a)

b)

c)
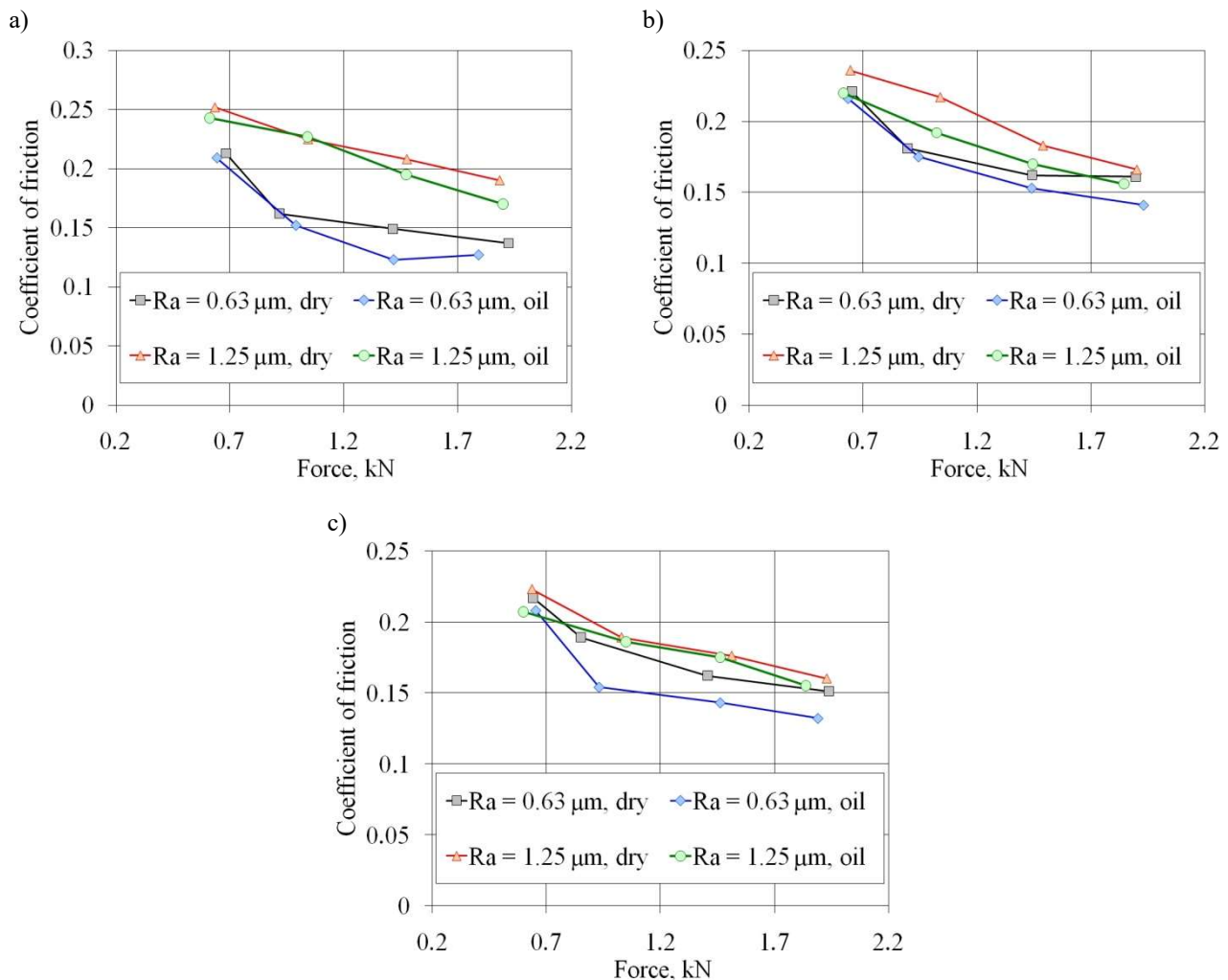
Fig. 6. Effect of force F_N on the value of coefficient of friction for pre-strained sheets a) φ = 0.095, b) φ = 0.139 and c) φ = 0.182

During the plastic working of metals there is initially a small effective contact area. The surfaces stick to each other only by the peaks of the asperities, which then, under the influence of the pressure forces, are plastically deformed until the contact surface created in this way is sufficient to transfer the load [10, 28]. The asperities of the surface are sheared and elastically deformed, which increases the real contact area. For small values of the surface roughness parameters, adhesion is the dominant tribological pheno-

menon occurring during metallic contact. As the surface roughness increases, the influence of adhesion decreases, while the share of the mechanical ploughing of the asperities during the contact of two metallic bodies increases [2].

In the conditions of dry friction, the coefficient of friction is the main factor limiting the movement of the workpiece material on the surface of the tools [16]. Under loading, the asperities deform elastically and plastically, changing the topography of the surface and

lubricant flow between asperities [13]. In the case of elastic-plastic metals, the increase in pressure during sliding movement causes an increase in the real contact surface, which may lead to a reduction in the volume of the lubricant pockets [7]. Closed lubricant pockets are separated from the outer edges of the material and hold the lubricant in the closed volume of the valleys. Under load, the pressure of the lubricant in pockets increases, forming a kind of hydrostatic cushion [7]. Open lubricant pockets located on the edges of the surface are not able to hold the lubricant during the friction process. According to the theory of lubricating pockets presented in [26], an increase in the friction coefficient is observed in the conditions of open lubricant pockets and its reduction in the presence of closed lubricant pockets.

4. Conclusions

In sheet metal forming processes the friction is the result of two main mechanisms: adhesion in the areas of real contact and resistance resulting from the mechanical interaction of the peaks of surface asperities as a result of flattening and ploughing of the workpiece surface by asperities of the hard surface of tool. The results of SDT presented in this article allow the following conclusions to be drawn:

- in the friction conditions with cylindrical countersamples, the increase in pressure force is accompanied by a decrease in the value of the friction coefficient,
- the greater the contact pressure, the lubrication efficiency tends to reduce,
- increasing the roughness of the countersamples increases the value of the friction coefficient in both analysed friction conditions,
- in the range of low contact pressure forces, the lubricant to a greater extent reduced the coefficient of friction,
- the lubricant reduced the value of the friction coefficient by about 20-30% depending on the roughness of the countersamples and the pressure force,
- the lubrication of the sheet surface significantly reduced the number of summits per surface area of specimen compared to the dry friction conditions,
- pre-straining of the specimens increased the maximum height of the assessed profile.

References

[1] Azushima Akira, Junji Miyamoto, Hideaki Kudo. 1998. „Effect of Surface Topography of Workpiece on Pressure Dependence of Coefficient of Friction in Sheet Metal Forming". CIRP Annals 47 (1): 479, 482.

[2] Chodoła Łukasz, Daniel Ficek, Ireneusz Szczęsny, Tomasz Trzepieciński, Łukasz Wałek. 2021. "Modelling of the draw bead coefficient of friction in sheet metal forming". Technologia i Automatyzacja Montażu 3: 3-9.

[3] Coello Juana, Valentin Miguel, Alberto Martínez, F. J. Avellaneda, A. Calatayud A. 2013. „Friction behaviour evaluation of an EBT zinc-coated trip 700 steel sheet through flat friction tests". Wear 305: 129-139.

[4] Dharavath Baloji, Dinesh Varma, Swadesh K. Singh, M.T. Naik. 2021. Understanding frictional behaviour of ASS316L in sheet metal forming. Materialtoday: Proceedings 44: 2855-2858.

[5] Evin Emil, Miroslav Tomáš, Marek Výrostek. 2016. „Verification the numerical simulation of the strip drawing test by its physical model". Acta Mechanica Slovaca 20 (1): 14-21.

[6] Figueiredo Luiz, Amilcar Ramalho, Marta C. Oliveira, Luís F. Menezes. 2011. „Experimental study of friction in sheet metal forming". Wear 271 (9-10): 1651-1657.

[7] Gåård Anders. 2018. „Wear in Sheet Metal Forming". Licentiate Thesis. Karlstad: Kalstad University Studies.

[8] Han S.S. 1997. „The influence of tool geometry on friction behavior in sheet metal forming". Journal of Materials Processing Technology 63 (1-3): 129-133.

[9] Holmberg Kenneth, Ali Erdemir 2017. „Influence of tribology on global energy consumption, costs and emissions". Friction 5: 263-284.

[10] Jurkovic Martin, Zoran Jurkovic, Stipo Buljan. 2006. „The tribological state test in metal forming processes using experiment and modelling". Journal of Achievements in Materials and Manufacturing Engineering 18 (1-2): 383-386.

[11] Kirkhorn Lanny, Kenneth Frogner, Mats Andersson, Jan-Eric Ståhl. 2012. „Improved tribotesting for sheet metal forming". Procedia CIRP 3: 507-512.

[12] Kirkhorn Lanny, Volodymyr Bushlya, Mats Andersson, Ståhl. 2013. "The influence of tool steel microstructure on friction in sheet metal forming". Wear 302 (1-2): 1268-1278.

[13] Kmiotek Małgorzata, Tomasz Iwan. 2021. „Numerical simulation of flow through microchannels of technical equipment with triangular and rectangular elements of roughness". Technologia i Automatyzacja Montażu 4: 16-23.

[14] Makhkamov Anvar, Dipak Wagre, António M. Baptista, Abel D. Santos, Luís Malheiro. 2017. „Tribology testing to friction determination in sheet metal forming processes". Ciência & Tecnologia dos Materiais 29 (1): e249-e253.

[15] Masters Lain G., David K. Williams, Rajat Roy. 2013. „Friction behaviour in strip draw test of pre-stretched high strength automotive aluminium alloys". International Journal of Machine Tools Manufacture 73: 17-24.

[16] Menezes Pradeep L., Kishan Kumar, Kishore, Satish V. Kailas S.V. 2009. „Influence of friction during forming processes–a study using a numerical simulation technique". International Journal of Advanced Manufacturing Technology 40: 1067-1076.

[17] Roizard Xavier, Jürgen von Stebut. 1995. „Surface asperity flattening in sheet metal forming – a 3D relo-

cation stylus profilometric study". International Journal of Machine Tools Manufacture 35: 169-175.

[18] Shisode Meghshyam, Javad Hazrati, Tanmaya Mishra, Matthijn de Rooij, Carel ten Horn, Jeroen van Beeck, Ton van den Boogaard. 2021. "Modeling boundary friction of coated sheets in sheet metal forming". Tribology International 153: 106554.

[19] Shisode Meghshyam P., Javad Hazrati, Tanmaya Mishra, Matthijn de Rooij, Ton van den Boogaard. 2020, „Modeling Mixed Lubrication Friction for Sheet Metal Forming Applications". Procedia Manufacturing 47: 586--590.

[20] Shisode Meghshyam, Javad Hazrati, Tanmaya Mishra, Matthijn de Rooij, Ton van den Boogaard. 2021. Journal of Materials Processing Technology 291: 117035.

[21] Szyszka Grzegorz, Daniel Kwiatanowski, Jarosław Sęp, Katarzyna Antosz. 2021. „Automatic compensation of errors of multi-task machines in the production of aero engine cases". Technologia i Automatyzacja Montażu 1: 29-39.

[22] Trzepieciński Tomasz. 2019. „A study of the coefficient of friction in steel sheets forming". Metals 9(9): 988.

[23] Trzepieciński Tomasz, Anna Bazan, Hirpa G. Lemu. 2015. "Frictional characteristics of steel sheets used in automotive industry". International Journal of Automotive Technology 16 (5): 849-863.

[24] Trzepieciński Tomasz, Romuald Fejkiel. 2017. "On the influence of deformation of deep drawing quality steel sheet on surface topography and friction". Tribology International 115: 78-88.

[25] Vierzigmann Ulrich H., Marion Merklein, Ulf Engel. 2011. „Friction conditions on sheet-bulk metal forming". Procedia Engineering 19: 377-382.

[26] 1050 Vollertsen Frank. 2011. „Size effects in micro forming". Key Engineering Materials 473: 3-12.

[27] Wang Chunge, Rui Ma, Juan Zhao, Jun Zhao. 2017. „Calculation method and experimental study of coulomb friction coefficient in sheet metal forming". Journal of Manufacturing Processes 27: 126-137.

[28] Wang Dan, Yang He, Li Heng. 2014. „Advance and trend of friction study in plastic forming". Transactions of Nonferrous Metals Society of China 24: 1263-1272.

[29] Zabala Alaitz, Eneko Sáenz de Argandoña, Daniel Cañizares, Iñigo Llavori, Nagore Otegi, Joseba Mendiguren. 2022. „Numerical study of advanced friction modelling for sheet metal forming: Influence of the die local roughness". Tribology International 165: 107259.

Lidia Gałda[1], Dariusz Pająk[2]

ANALYSIS OF THE APPLICATION OF SIC CERAMICS AS A TOOL MATERIAL IN THE SLIDE BURNISHING PROCESS

ANALIZA ZASTOSOWANIA CERAMIKI SIC JAKO MATERIAŁU NARZĘDZIOWEGO W PROCESIE NAGNIATANIA ŚLIZGOWEGO

Abstract

The paper presents results obtained by SiC ceramic implementation for slide burnishing. Analyzes of the effect of the burnishing force and feed on selected surface texture parameters were conducted. The influence of technological parameters was assessed according to the analysis of variance. The burnishing force and feed affected most of the examined surface texture parameters in the analyzed ranges. Optimal values were found for the technological parameters. In most cases, the minimum of height parameters were achieved for 80 N of burnishing force and 0,063 mm/rev of feed. Limitations in the increase in the burnishing force were also found.

Keywords: slide burnishing, surface texture, SiC ceramic

Streszczenie

W artykule przedstawiono wyniki uzyskane w badaniach nagniatania ślizgowego z zastosowaniem ceramiki SiC. Przeprowadzono analizy wpływu siły nagniatania i posuwu na wybrane parametry struktury geometrycznej powierzchni. Wpływ parametrów technologicznych oceniono na podstawie analizy wariancji. Siła nagniatania i posuw wpłynęły na większość badanych parametrów struktury geometrycznej powierzchni. Wyznaczono optymalne wartości parametrów technologicznych. W większości przypadków minimalne wartości parametrów wysokościowych osiągano dla siły nagniatania równej 80 N i przy posuwie równym 0,063 mm/obr. Zidentyfikowano również ograniczenia dotyczące maksymalnej siły nagniatania.

Słowa kluczowe: nagniatanie ślizgowe, struktura geometryczna powierzchni, ceramika SiC

1. Introduction

Reliability of the automated assembly systems is extremely important. Mounting systems are composed of many elements that work under specific load conditions. One of the factors increasing the durability and reliability of machines and the entire systems is the reliability and durability of their components. The durability of machine elements, depending on the loads, is often significantly influenced by the quality of the surface. Various techniques, e.g. burnishing treatment, can be used to improve the surface quality. Burnishing is used as a final machining of the technological process of parts of machines. The goals of burnishing applications are the increase in fatigue strength, wear resistance, corrosion resistance, dimensional accuracy, kinematic pairs, and others such

as reflection ability. Przybylski [14] defined the burnishing process as the finishing method of the surface when the plastic deformation of the surface layer takes place as a result of interaction between the hard and smooth tool and the processing surface. According to the implementation purpose, the special kind of burnishing, type of tool, and technological parameters range are considered. Slide burnishing is usually applied to smooth the surface by reducing the surface irregularities remained after the prior process. In some cases, changes in the surface layer such as hardening and compressive stress generation caused an increase in fatigue strength, wear, and corrosion resistance. Although the burnishing has many advantages such as machining without chips, high effectiveness of surface smoothing, high safety of

---

[1] DSc, PhD, Eng. Lidia Gałda, Assoc. Prof. (corresponding author), Rzeszow University of Technology, Faculty of Mechanical Engineering and Aeronautics, 12 Powstańców Warszawy, 35-959 Rzeszów, Poland, Tel. +48 17 8651904, e-mail: lgktmiop@prz.edu.pl, ORCID: 0000-0001-8603-9907.

[2] MSc. Eng. Dariusz Pająk, Rzeszow University of Technology, Faculty of Mechanical Engineering and Aeronautics, 12 Powstańców Warszawy, 35-959 Rzeszów, Poland, Tel. +48 177432456, e-mail: pajak@prz.edu.pl

operating, non-complicated construction of burnishing tools, and others, there are still some disadvantages. Taking into account the plastic deformation effect (in cold conditions) during burnishing, there are several limits in industrial applications. The material of the workpiece should be processable at the surrounding temperature. Another limitation is the stiffness of the system: machine, fixture, workpiece, and tool. Slide burnishing is typically applied to process hard machine parts after the thermal process or with diffusive or galvanic coatings. But it could be used for machine parts of medium or small hardness, especially when the value of burnishing force should be low, such as in processing thin-wall workpieces or objects of small dimensions. In such cases, slide burnishing is an option to finish the surface.

Today, a wide range of hard materials for burnishing tools is emerging starting from different kinds of steel and synthetic diamond ending in special composites. Jaworska et al. [7] worked out the method of direct synthesis of carbon, silicon, and titanium under self-propagating high-temperature synthesis conditions. The diamond composite with Ti_3SiC_2 was used to make cylinder-shaped burnishing tools. Korzyński et al. [12] applied a cylinder-shaped tool of diamond composite tool with a ceramic Ti_3SiC_2 binding phase for slide burnishing. The authors achieved beneficial effects on the fatigue strength of burnished steel elements compared to that of ground workpieces. The increase in fatigue strength was about 18%. Great results in the reduction of the height of the surface texture were presented by Świrad [17]. Due to the application of Ti_3SiC_2 ceramic as a burnishing tool the values of the decrease in the amplitude parameters of surface texture such as Sa, St, and Sz were more than ten times lower than after grinding (without burnishing). Konefał et al. [9] examined the corrosion resistance of stainless steel X6CrNiMoTi17-12-2 and compared the results obtained after different finishing methods. They found that slide burnishing with a spherical diamond tool could improve corrosion resistance, provided that the machined surface has the appropriate texture. Korzyński [10] analyzed a theoretical model of smoothing by the slide burnishing with a tool with a rounding radius of 4 mm and compared it with experimental results. The investigation result made with the application of the low-hardness steel showed good agreement with the results of the model analyses. The author concluded that the post-burnishing surface roughness first of all depended on the pressure force. The optimum burnishing force due to the model was in the range of 25-170 N depending on the hardness, initial surface roughness, and material of the workpiece. The burnishing force obtained experimentally varied from 20 to 150 N depending on other parameters applied. Radziejewska et al. [15] applied a new hybrid method that combined the laser alloying process and slide burnishing. The authors found that the slide burnishing (with sintered carbides) applied to the alloyed material led to a reduction in surface roughness and the generation of compressive stresses in the surface layer. El-Tayeb et al. [3] carried out ball burnishing on aluminum 6061 with different technological parameters. The authors found values of burnishing force of 160 N and speed of 330 rpm that determine the optimum of surface qualities and tribological properties.

Recently, SiC ceramics were of interest in research in the field of fabrication and special applications of ceramic products. D. Jianxin et al. [8] studied hot pressing of SiC/(W,Ti)C laminated ceramic nozzles. There was the problem of high erosion wear at the nozzle entry area during the sand blasting process. They found that the laminated ceramic nozzles have higher erosion wear resistance than homologous stress-free ceramic nozzles. Researchers have put a lot of effort into improving the properties of porous SiC ceramics. Liu et al. [13] developed the fabrication of cordierite-bonded porous SiC ceramics from α-SiC, α- Al_2O_3 and MgO using graphite powder as the pore-forming agent. The flexural strength of 26 MPa was achieved at the open porosity of 44,51%. Srivastava et al. [16] applied micrometer-sized SiC, Si_3N_4 and Al_2O_3 particles as reinforcement to Ni based composite. The superior wear resistance exhibited a Si_3N_4 reinforced composite, but there was no significant variation in the friction coefficient for all three composites. Jaworska et al. [6] analyzed the possibility of application by SHS synthesized Ti_3SiC_2 powders as the binding phase for PCD. The authors found that SiC and Ti_3SiC_2 could be sintered by the high-temperature high-pressure method to obtain compacts of the highest hardness of all the analyzed sintering methods. J. Yang et al. investigated a novel SiC_{nf}/SiC composite with nano-fibers that is characterized with the maximum flexural strength of 678,2 MPa and the fracture toughness of 8,33 MPa m$^{1/2}$ [18].

Nowadays, SiC ceramic is successfully implemented in production of such elements as bearings, nozzles, pistons, and different sliding elements, but there is a few of information about the implementation of SiC ceramic as the burnishing element. Steel of high hardness for balls or rolls are the most common material used in the slide burnishing, but the steel material has the limitations in application for a burnishing element. The adhesive joints and surface deterioration may occurred if the burnishing process is realized with steel burnishing tool-end on steel workpiece.

In this paper, the effect of the implementation of SiC ceramic ball as the burnishing element is presented. The burnishing end of the SiC material characterized high hardness and wear resistance, but the resistance to the fracture toughness resistance is several times smaller than that of steel. This is the limitation of the application of SiC ceramics for specific products. The aim of this study is to examine the possibility of the implementation of SiC ceramic as a burnishing element and the range of technological parameters at which slide burnishing with the SiC ceramic tool is effective. In this paper, the impact analyses of the burnishing technology parameters on selected surface texture parameters are demonstrated.

2. Experimental details

2.1. Specimens, tool, material, and technological parameters

The material subjected to burnishing process was 42CrMo4 steels. The diameter of the specimen (shaft) was 35 mm. The hardness of the steel after heat treatment was 40 HRC. The surface was formed by a precise turning to a roughness less than Sa 1,2 μm. The burnishing technique was used to finish the surface. The special DB-3 burnishing tool was applied and the SiC ceramic sphere was mounted in the toolholder. The mechanical properties of steel samples and the ceramic spheres of SiC are listed in Table 1.

Table 1. Properties of 42CrMo4 steel and SiC ceramic [2, 19]

Material	Density	Hardness	Coefficient of thermal expansion α	Thermal conductivity	Max temperature of operating	Young modulus	Resistance of fracture toughness
unit	g/cm³	HRC/ HV	x 10⁻⁶/K	W/mK	°C	GPa	MPa m$^{1/2}$
42CrMo4	7,86	40 HRC	12	58	120	200	25
SiC	3,12	2800 HV (30GPa)	3	100	1400	450	4

The SEM image of SiC ceramic used for the burnishing element is presented in Fig. 1.
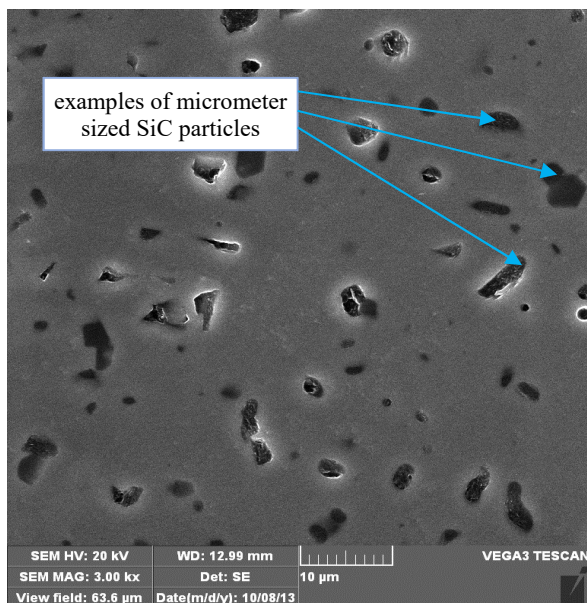
Fig. 1. The SEM image of SiC ceramic (3000x) taken by the VEGA 3 scanning microscope

The burnishing process was performed using a universal lathe type LZ360 (Fig. 2).
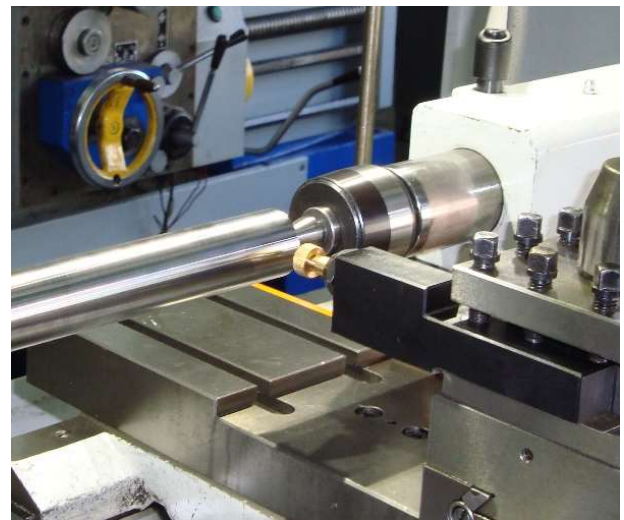
Fig. 2. Photo of the burnishing process

The examined technological parameters were the burnishing force P [N] and the feed f [mm/rev]. The burnishing force P range was 20-200 N with intervals of 20 N, feed f was in the range of 0,025-0,32 mm/rev in nine steps. The rotational speed n stayed constant and was equal to 300 rpm. There were three repetitions of each series. The SiC ceramic ball was 6.35 mm in diameter.

2.2. Evaluation procedure of the effect of the technological parameters on the surface texture

To assess whether the technological parameters of the burnishing process influence the surface texture, the analysis of variance was used. The influence of each technological parameter was analyzed separately. Analysis of the burnishing force effect was carried out for four levels of 20, 80, 140 and 200 N. The other technological parameters stayed constant, the feed was equal to 0,04 mm/rev and the rotational speed was 300 rpm. To examine the influence of the feed, the four levels analyze was used too. The feed values were 0,025; 0,063; 0,16 and 0,32 mm/rev and the constant parameters were as follows the burnishing force was equal to 80 N and the rotational speed was 300 rpm. Fifteen parameters of surface texture were chosen in Table 2 that were the output parameters of the slide burnishing process in these analyzes.

Table 2. Description of selected 3D surface texture parameters

| Parameter	Description
Sp [µm]	Maximum height of peaks
Sv [µm]	Maximum depth of valleys
Sz [µm]	Maximum height of the surface
SHTp [µm]	Surface section height difference corresponding to 20-80% of the material ratio
St [µm]	Total height of the surface
Sa [µm]	Arithmetical mean deviation of the surface
Sq [µm]	Root mean square deviation of the surface
Ssk	Skewness of the surface
Sku	Kurtosis of the surface
Smr [%]	Areal material ratio
Spk [µm]	Reduced peak height
Sk [µm]	Core depth
Svk [µm]	Reduced valley depth
Sa1 [mm^3/cm^2]	Peaks volume
Sa2 [mm^3/cm^2]	Void volume

All series were measured with the Talysurf CCI Lite white-light interferometer. The area of the measured surfaces was 0,8 mm x 0,8 mm. The repetition of measurements was equal to 3.

Surface texture parameters were calculated using the TalyMap Software.

The analysis of variance is one of many other procedures supporting the selection of significant input parameters of a new process (new tool). The scheme of the overall relation between input and output parameters is presented in Fig. 3.
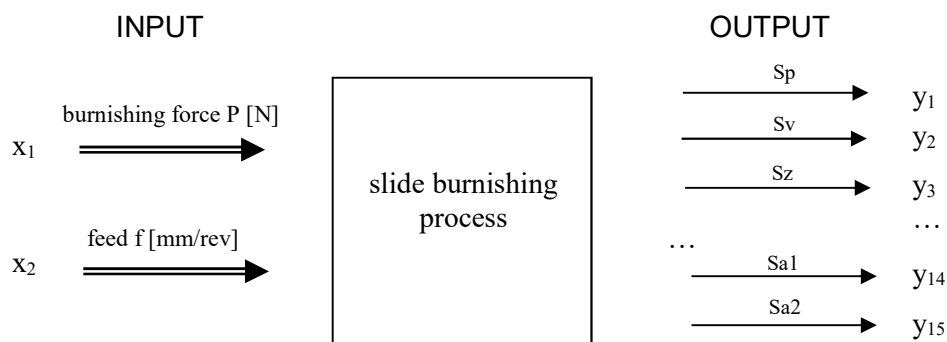

Fig. 3. Scheme of the parameters selected for the input x_i and output y_i of the slide burnishing process

The hypothesis that there was no effect of the input technological parameter on the output parameter was analyzed.

Generally, the variance is calculated for selected groups and in this case they are connected with the levels of the technological parameters. The variances

that were obtained between groups and inside groups were compared, and finally the specific test coefficient F_t was calculated.

The test value F_t was calculated using the formula [11]:

$$F_t = \frac{\sum_{i=1}^{p} n_i \cdot (\bar{y}_i - \bar{y})^2 \cdot (n - p)}{\left[\sum_{i=1}^{p} \sum_{j=1}^{q} (y_{ij} - \bar{y})^2 - \sum_{i=1}^{p} n_i (\bar{y}_i - \bar{y})^2\right] \cdot (p - 1)}$$

The test coefficient F_t was compared to the critical value F_{cr} found in the Fisher-Snedecor table for the importance level α of 0,05.

Confirmation or cancelation the hypothesis is based on the comparison of the values of F_t and F_{cr}. If $F_t \geq F_{cr}$, the assumed hypothesis should be cancelled, which means that the input parameter evidently influenced the output parameter. Otherwise, if $F_t < F_{cr}$, the hypothesis is confirmed and there was no effect of the input parameter on the output parameter in the investigated range.

Additionally, the average values of surface texture parameters were compared between series and to zero series (after precise turning).

The SiC ceramic spheres were examined after the burnishing process to review the wear in the contact zone. Photos of the contact zone of the SiC ball were taken with the optical microscope Neophot2.

3. Results and discussion

In Fig. 4 a view of the exampled surface after precise turning is presented. The periodic anisotropic deterministic surface was created with regular traces after the turning process.
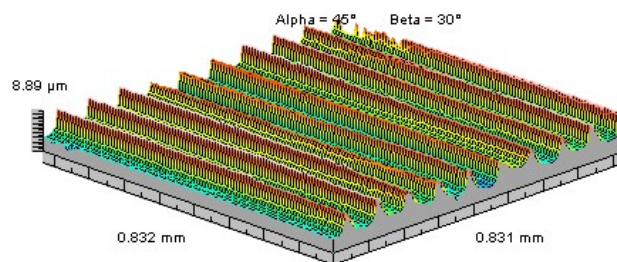

Fig. 4. The isometric view of the surface after precise turning

Figure 5 presents views of burnished surfaces using the tool with the SiC ceramic sphere in the range of burnishing force $P_i = 20 – 200$ N.
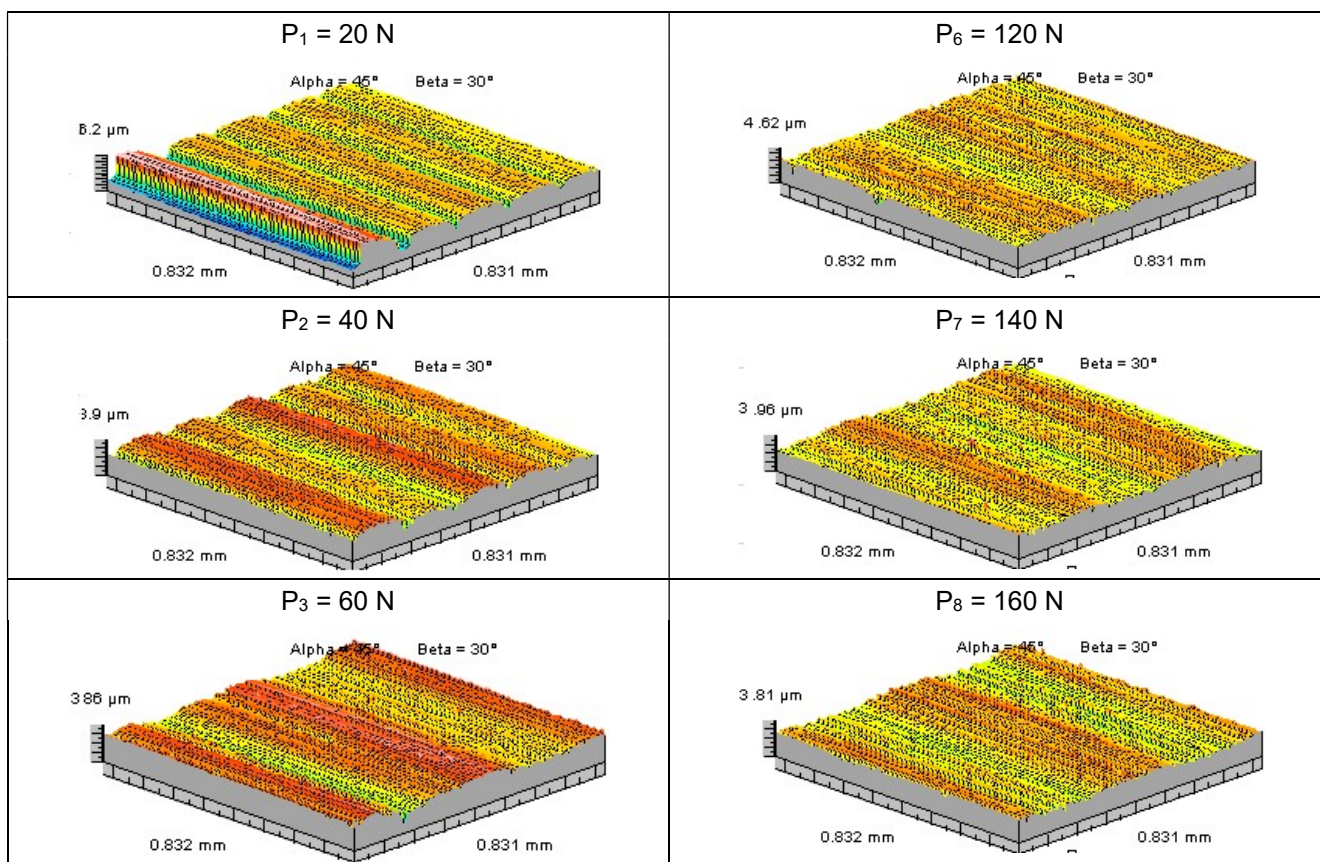

Fig. 5. Isometric views of surfaces burnished by the tool with SiC ceramic sphere in the range of burnishing force $P_i = 20 – 200$ N
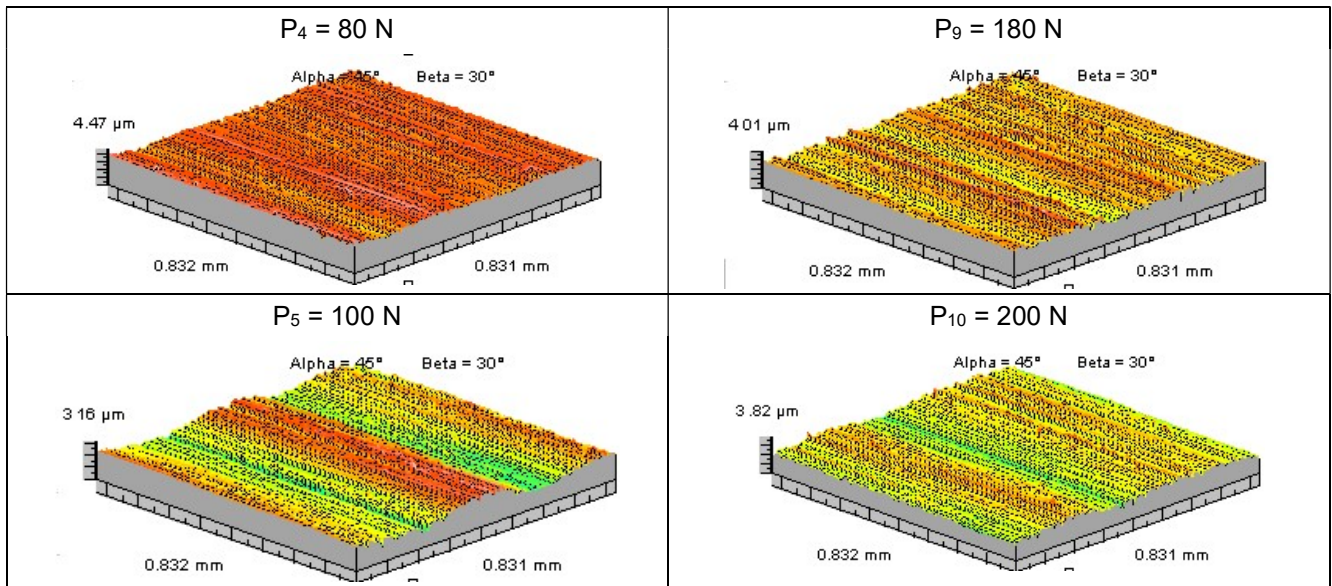
Fig. 5 (cont.). Isometric views of surfaces burnished by the tool with SiC ceramic sphere in the range of burnishing force $P_i = 20 - 200$ N

The analyses of the views of the surfaces and the surface texture parameters (Table 3) demonstrated that the slide burnishing with the SiC ceramic could be a useful method to process the surface. It can be observed that at low burnishing force P_i in the range of 20-60 N valleys formed in precise turning were still on the surface, but the peaks were strongly flatten. At the burnishing force P equal to 80 N, the surface was the smoothest of all examined. As a result of burnishing, most of the surface height parameters decreased. The average values of the surface texture parameters for each surface burnished with SiC ceramic at the burnishing force P_i in the range of 20-200 N and the relevant – without burnishing – are presented in Table 3.

Table 3. The average values of surface texture parameters for each surface burnished with SiC ceramic at the burnishing force P_i in the range of 20-200 N

Parameter	Average value of surface texture parameters at burnishing force P_i [N]										
	20	40	60	80	100	120	140	160	180	200	turned
Sp [µm]	2,16	2,87	1,25	**1,14**	1,42	3,88	1,39	1,38	2,79	1,60	5,99
Sv [µm]	3,54	3,80	3,45	**2,09**	2,18	2,57	2,49	2,28	2,40	2,88	3,94
Sz [µm]	5,07	6,65	4,49	**3,22**	3,58	6,44	3,88	3,66	5,20	4,75	9,93
SHTp [µm]	0,76	0,63	0,61	0,43	0,50	0,43	0,48	0,54	**0,41**	0,52	2,50
St [µm]	5,07	6,67	4,71	**3,22**	3,60	6,44	3,88	3,66	5,20	4,75	9,93
Sa [µm]	0,45	0,34	0,29	0,23	0,25	0,25	0,23	0,25	**0,20**	0,25	1,19
Sq [µm]	0,65	0,46	0,36	0,30	0,31	**0,28**	0,30	0,31	0,26	0,32	1,47
Ssk	**-1,14**	-1,30	-0,76	-0,70	-0,54	-0,58	-0,56	-0,27	-0,36	-0,59	0,93
Sku	4,75	5,78	5,16	4,13	3,76	4,96	4,20	**3,11**	5,95	3,90	2,86
Smr [%]	45,03	4,10	28,17	25,37	11,83	**0,03**	8,47	13,92	7,32	1,70	1,28
Spk [µm]	0,32	0,19	**0,17**	0,24	0,21	0,20	0,19	0,21	0,23	0,24	2,90
Sk [µm]	0,79	0,90	0,92	0,72	0,77	0,65	0,75	0,83	**0,62**	0,76	2,37
Svk [µm]	0,96	0,89	0,46	0,39	0,40	0,44	0,39	**0,30**	0,32	0,42	0,43
Sa1 [mm³/cm²]	33,85	6,93	**5,87**	12,39	9,06	7,72	7,57	8,74	10,53	8,22	376,67
Sa2 [mm³/cm²]	102,30	70,50	25,93	21,43	24,17	28,60	21,17	**16,23**	19,00	29,77	11,86

Most of the surface texture parameters analyzed decreased after the burnishing process with a force in the range of 20 to 200 N. The height parameters Sz and St decreased from 32 to 67%, but this was mainly due to the flattening of the peaks during burnishing. It confirmed a superior decrease in the maximum height of the summits Sp which was in the range of 35-80% compared to a decrease in Sv of 3-46% depending on the burnishing force value used. The mean amplitude parameters showed smaller values of approximately 62-83% for Sa parameter and 55-82% for Sq parameter. A similar tend was observed for the surface

section height difference SHTp and the average decrease was approximately 75% (the range of 69-83%). Quite different changes were obtained in the case of the Smr parameter that corresponds to the material ratio. The values of the Smr decrease was about 97%, but the increase was even of 3417% compared to turned surfaces. The Smr parameter values showed odd performance with increasing burnishing force and compared to changes in other measured surface texture parameters. Skewness of all burnished surfaces became negative (Ssk in the range from -1,14 to -0,27) and the decrease was significant of 125% on average compared to non-burnished samples. The surface kurtosis after burnishing increased in all series, but the range of values was quite wide. The increase in Sku ranged from 8 to 108%. The changes in Sk family parameters were very interesting for analyzing the effect of the increasing force on the surface geometry. Parameters corresponded to the summits of the surfaces Spk and Sa1 decreased with increasing force, and the change in values was significant 92% and 94% on average, respectively. The scatter of values changes was rather narrow 88-94% of Spk and 91-98% of Sa1. The decrease in peaks height and volumes proved that the plastic deformation of the summits was successful. As a result of burnishing, the core depth Sk was smaller than that of turned surfaces of about 66% on average. Values of the Svk parameter with the increase in burnishing force increasing to 60 N were greater than those of the turned surfaces (even 123%), but then from the burnishing force of 80 N the Svk parameter was usually lower and oscillated around 0,4 μm for higher burnishing forces. The maximum decrease was 30% of the Svk parameter. Taking into account the changes of void volumes Sa2 of the burnishing surfaces, we can observe a great increase ranging from 36-762% although the reduced valley depth decreased at higher burnishing forces. This was because a new surface geometry was created during the burnishing process with higher force. The burnishing tool had different geometry than the turning one, and the burnishing sphere left the shallow and smooth traces on the surface instead of deep and sharp after the turning process.

To analyze the effect of the burnishing force on the surface texture parameters, four levels of P_i were selected: minimum $P_1 = 20$ N, $P_2 = 80$ N as the most height parameters reached their minimum, $P_3 = 140$ N and maximum $P_4 = 200$ N. The critical value F_{cr} for 4 levels, 3 repetitions and importance level of 0,05 amounted to 4,06 (Fisher-Snedecor statistics). Using the analysis of variance procedure, it was found that the burnishing force P in the range of 20-200 N had an effect on 11 of the 15 texture parameters analyzed. The burnishing force influenced the surface texture parameters from different groups: height Sp, Sv, Sz, St, mean Sa, Sq, connected with the material ratio SHTp, Smr, skewness Ssk, and from Sk family: Svk and Sa2. The graphs of the relationship between the increase in burnishing force P and the selected texture parameters on which the effect was significant are presented in Fig. 6.
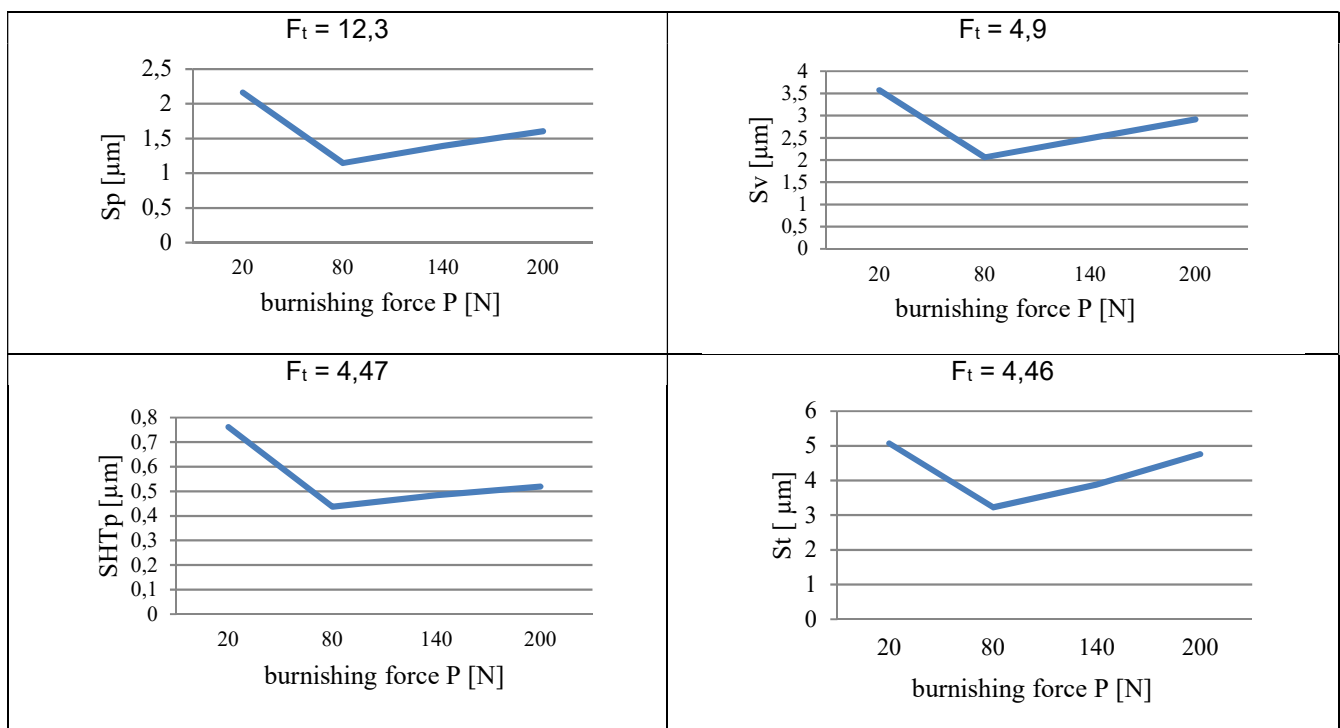

Fig. 6. Relations between the burnishing force P and the selected texture parameters
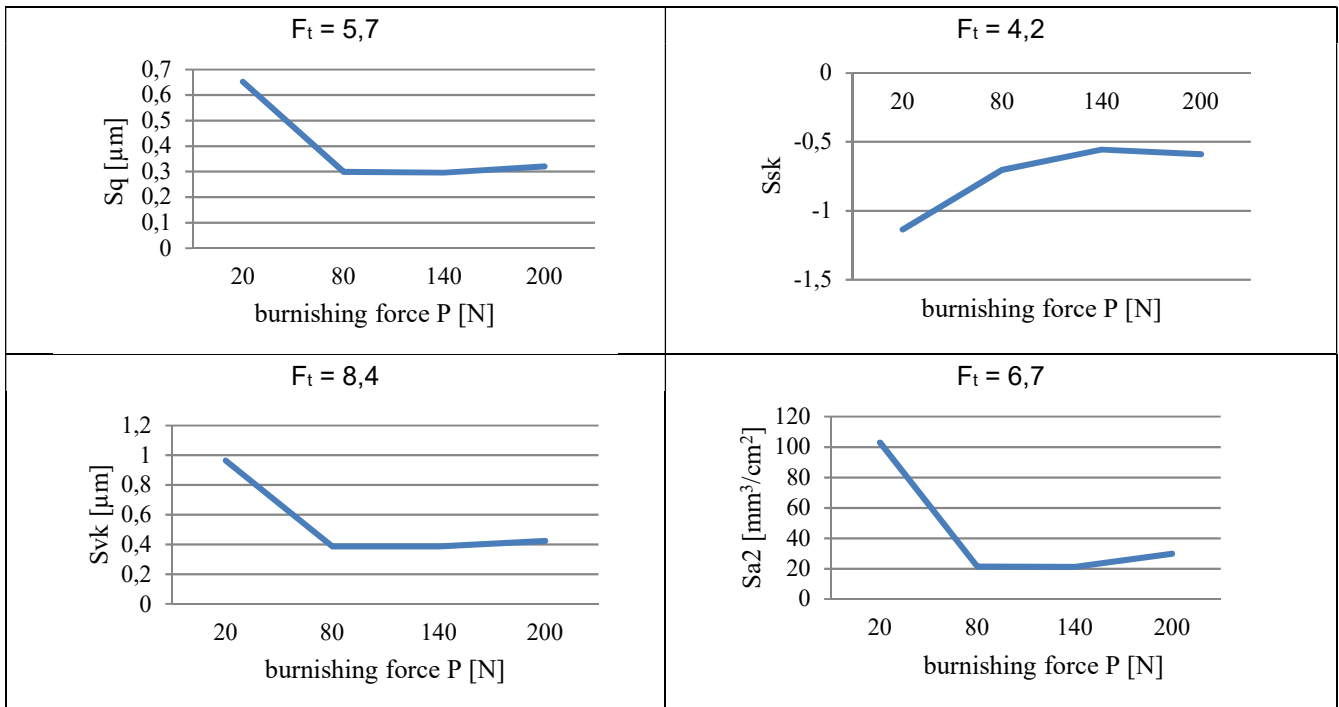
Fig. 6 (cont.). Relations between the burnishing force P and the selected texture parameters

Analyzing the curves, the extreme points can be observed. Minimum values of most surface texture parameters were obtained for a burnishing force of 80 N. The exception was the maximum value of the Ssk parameter when the force was equal to 140 N and for the whole range of force values the skewness remained negative. Significant changes in the surface texture parameters values of the burnished surfaces were obtained when the burnishing force was in the range of 20 to 80 N. Most of the parameters decreased at least by 36% (St) with increasing force to 80 N. Generally, height parameters decreased by about 40%, mean parameters decreased by 55% on average, and the greatest decrease was observed in the void volume of 80%. With the increase of the burnishing force over 80 N values of texture parameters started to enlarge but this growth was not so big, mostly it was about a few percent. Exceptions were the total height of the surface

St and, as a consequence, the maximum height of summits and depth of valleys. At the maximum burnishing force 200 N, they reached almost the same values that were obtained at 20 N. That denoted that there was no need to increase the burnishing force to over 200 N. Comparing results obtained with the SiC burnishing tool to the outcome of the burnishing process with typical steel tool, one may conclude that the quality of the burnished surface after processing with the SiC ceramic sphere is much better than obtained by steel burnishing element [4]. Additionally, taking into account the good tribological performance of the SiC element [1, 5], the new material tool could be a good alternative to the steel.

The influence of feed on surface texture parameters was also analyzed. Fig. 7 presents views of burnished surfaces using the tool with a SiC ceramic sphere with feed f_i in the range of 0,025-0,32 mm/rev.
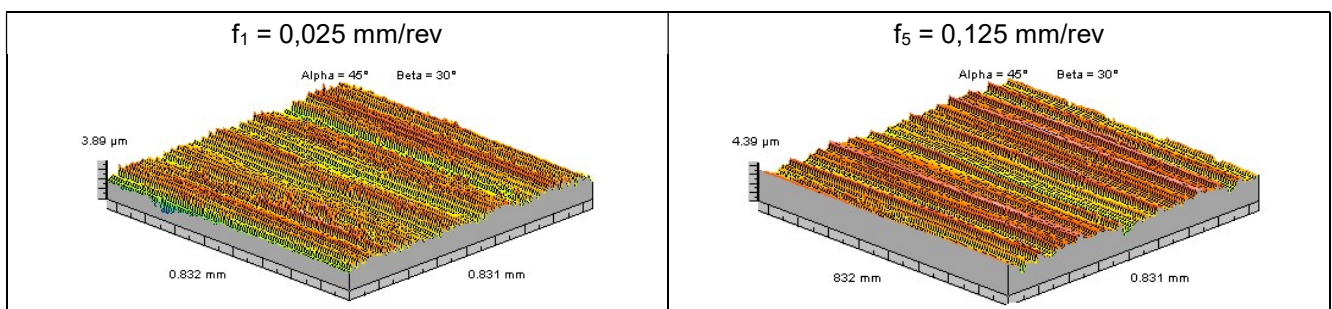
Fig. 7. Isometric views of surfaces burnished by the tool with a ceramic sphere of SiC in the feed range $f_i = 0,025 – 0,32$ mm/rev
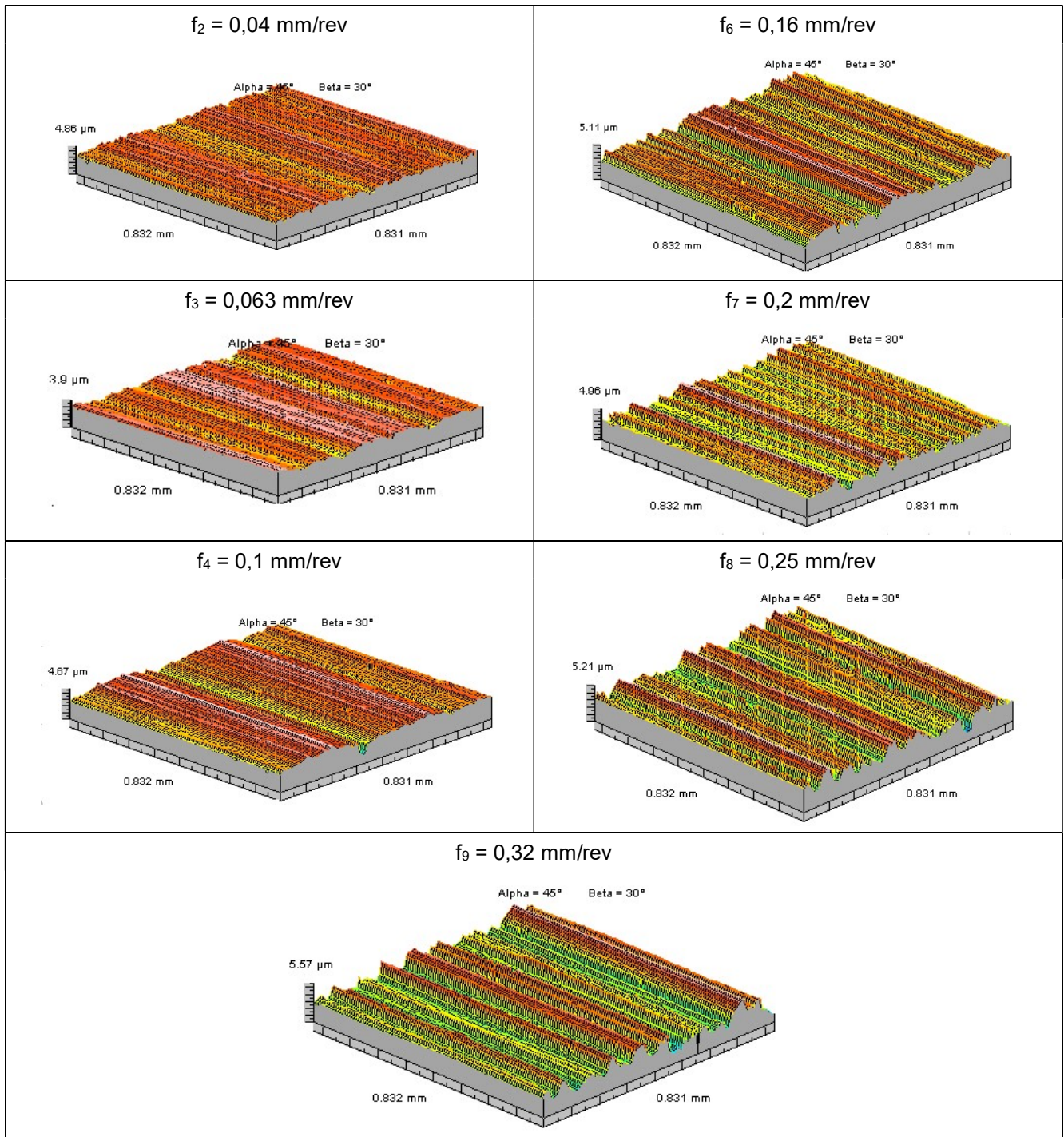
Fig. 7 (cont.). Isometric views of surfaces burnished by the tool with a ceramic sphere of SiC in the feed range f_i = 0,025 – 0,32 mm/rev

The one directional lay of the surfaces was obtained after slide burnishing with a SiC ceramic sphere in the examined range of feed from 0,025 to 0,32 mm/rev. Clear traces of the burnishing sphere pass were visible on the processing surfaces starting from the feed of 0,125 mm/rev. This is typical because with increasing feed, the traces of machining are more observable because of greater distance between them.

With increasing feed, the height of surface texture increased but was lower compared to that after turning (Fig. 4).

In Table 4 the average values of surface texture parameters after the burnishing with SiC ceramic with the feed in the range of 0,025-0,32 mm/rev and the relevant values – from the surface without the burnishing are presented.

Table 4. The average values of surface texture parameters for surfaces burnished with SiC ceramic at feed in the range of 0,025-0,32 mm/rev

Parameter	Average value of surface texture parameters at feed f_i [mm/rev]									
	0,025	0,04	0,063	0,1	0,125	0,16	0,2	0,25	0,32	turned
Sp [μm]	1,42	1,40	**1,16**	1,27	1,49	1,69	1,83	2,14	2,85	5,99
Sv [μm]	**1,84**	2,68	2,85	2,88	2,74	2,94	2,86	3,38	2,79	3,94
Sz [μm]	**2,95**	4,08	4,02	3,70	3,92	4,52	4,63	5,31	5,65	9,93
SHTp [μm]	0,59	0,55	**0,46**	0,54	0,65	0,82	1,02	1,16	1,39	2,50
St [μm]	**3,26**	4,08	4,02	4,15	4,24	4,62	4,69	5,52	5,65	9,93
Sa [μm]	0,28	0,26	**0,24**	0,29	0,32	0,40	0,47	0,58	0,63	1,19
Sq [μm]	0,34	0,33	**0,33**	0,39	0,42	0,51	0,59	0,74	0,77	1,47
Ssk	0,09	-0,44	**-1,20**	-0,75	-0,33	-0,23	0,09	-0,16	0,26	0,93
Sku	2,80	3,62	5,71	5,24	3,69	3,21	2,85	3,01	**2,46**	2,86
Smr [%]	12,60	11,85	18,87	23,70	11,67	9,52	9,35	6,58	2,46	1,28
Spk [μm]	0,30	0,23	**0,18**	0,36	0,40	0,44	0,56	0,65	0,73	2,90
Sk [μm]	0,89	0,82	**0,64**	0,83	0,96	1,27	1,45	1,78	1,88	2,37
Svk [μm]	**0,28**	0,39	0,59	0,72	0,60	0,63	0,53	0,73	0,67	0,43
Sa1 [mm³/cm²]	17,87	10,21	**7,15**	16,50	21,47	23,87	37,60	39,10	62,10	376,67
Sa2 [mm³/cm²]	**12,85**	25,97	48,13	41,63	35,30	31,30	24,33	43,33	22,06	11,86

Most of the surface texture parameters analyzed decreased due to the burnishing process. Eight out of fifteen parameters analyzed got their minimum with a feed of 0,063 mm/rev. There were mainly height but related with summit parameters. Six parameters reached minimum values at the lowest feed of 0,025 mm/rev. That parameters were associated with height of surface and valley dimensions created during the burnishing process. Compared to turning surfaces, the decrease in mean parameters was in the range of 47-80% (Sa and Sq). Similar changes were found in relation to height parameters such as Sp, Sz, St, and SHTp, but the decrease in the Sv values was smaller and varied from 14 to 53%. The parameter Svk related to the surface valley but to reduced depth presented both the increase and decrease compared to Svk of the turned surfaces. The changes in surface texture created during slide burnishing in such a feed range were more evident when one looked at the void volume Sa2 of the processing surfaces. The volume of the void increased in a very wide range of 8% to more than 300% although the maximum depth of the valleys declined at all feeds in the set. It is connected with changes in the skewness and kurtosis of the surfaces. Although the value of the Ssk parameter decreased in the range of 72-230% some of them remained positive. Sku values were usually larger than that after turning even over 100%, but there were some that slightly decreased. The reduced summit heights and summit volumes decreased significantly by at least 75% to almost 100% as a result of flattening the peaks and due to the shape of the burnishing SiC sphere. Core depths were lower than after turning at the whole range of burnishing feed. The values of the Smr parameter increased considerably and the changes were in a large range of 92-1751%.

The analysis of variance was used to analyze the effect of the feed on the surface texture parameters in the burnishing process. As for the burnishing force, four levels of feed f_i were selected: minimum $f_1 = 0,025$ mm/rev, $f_2 = 0,063$ mm/rev because the most of the surface texture parameters reached their minimum, $f_3 = 0,16$ mm/rev and maximum $f_4 = 0,32$ mm/rev. There were 3 repetitions at each level and the critical value F_{cr} was equal to 4,06. It was found that the feed f in the range of 0,025-0,32 mm/rev had influenced 14 of the 15 texture parameters of the surface studied. Statistically, it was not revealed that the feed affected only Sa2 from Sk family. The graphs of the relationship between increasing feed f and selected texture parameters on which the effect were significant are shown in Fig. 8.

From all graphs presented in Fig. 8 only the values of the Sz parameter showed continuous growth with increasing feed. Usually, the minimum parameters values were obtained at 0,063 mm/rev and in the case of kurtosis of the surface, the maximum point was reached. Increasing the feed from 0,025 mm/rev to 0,063 mm/rev resulted in a decrease in the maximum height of the summits of 18% and also in the reduced summit height over 40%. Similar tendency was observed in surface parameters connected with core depth. The smallest decrease was obtained for the mean parameter Sa of 14%. From an economic reason it is more profitable to process at higher velocity, but according to quality assurance standards the surface characteristics should qualify the client's demands. A beneficial result was obtained of the surface

skewness because the Ssk value decreased considerably to negative -1,2, whereas kurtosis of the surface increased over twice. A further increase in feed greater than 0,063 mm/rev caused surface deterioration and the values of all the parameters analyzed except the surface kurtosis increased even several times.
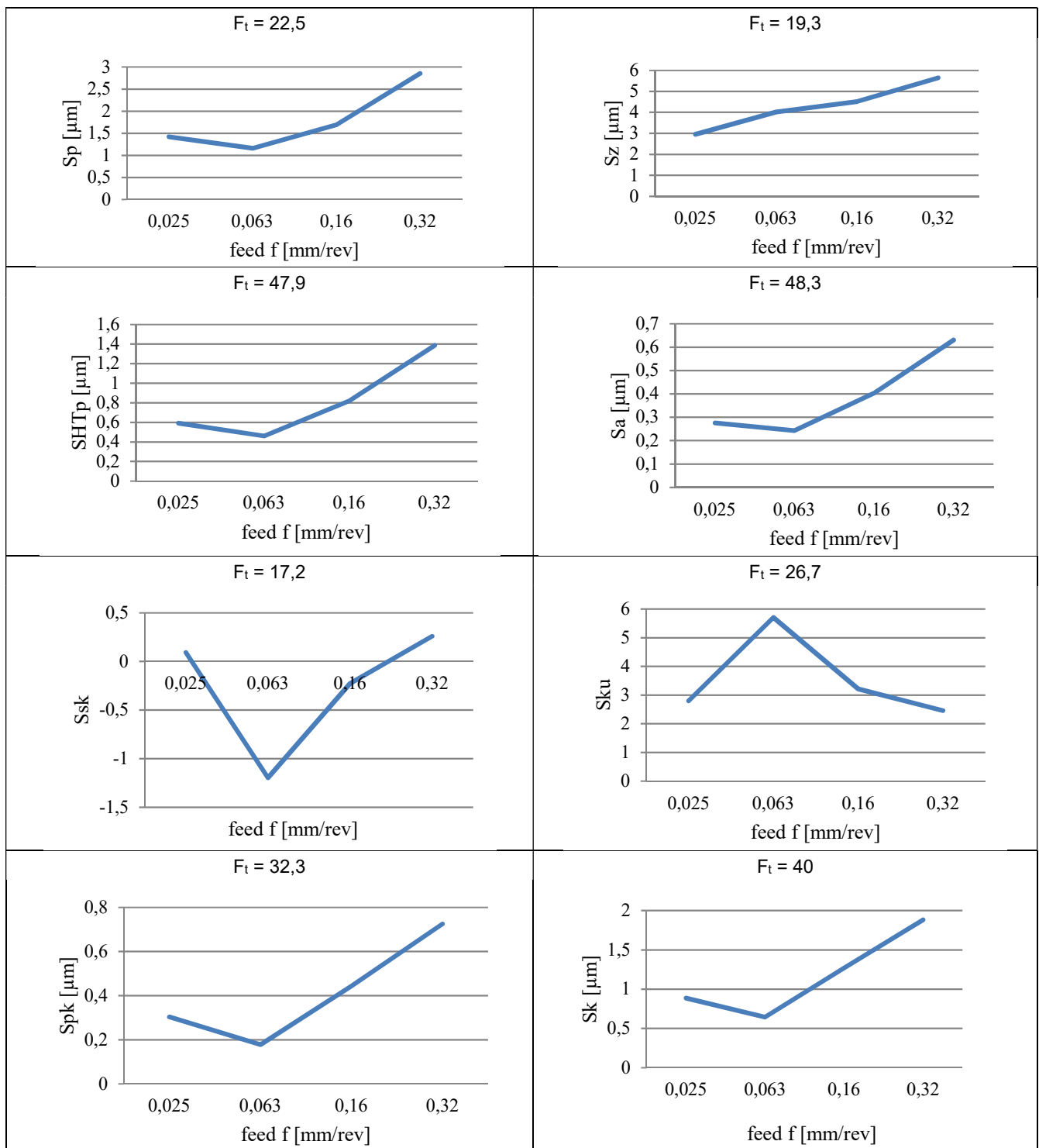
Fig. 8. Relationship between the feed f and the selected texture parameters

In order to find the maximum force P (limitation burnishing force) for the slide burnishing process with SiC ceramic in this application, a further increase in P was realized. During burnishing at P equal to 220 N, the dark abrasive wear debris from the SiC element were observed and the process was stopped. The surface of the burnishing element was subjected to observation. The contact zone of the SiC ball is presented in Fig. 9.

Fig. 9. Photos (x200) of the contact zone of the SiC ball before (left) and after the slide burnishing with P = 220 N (right)

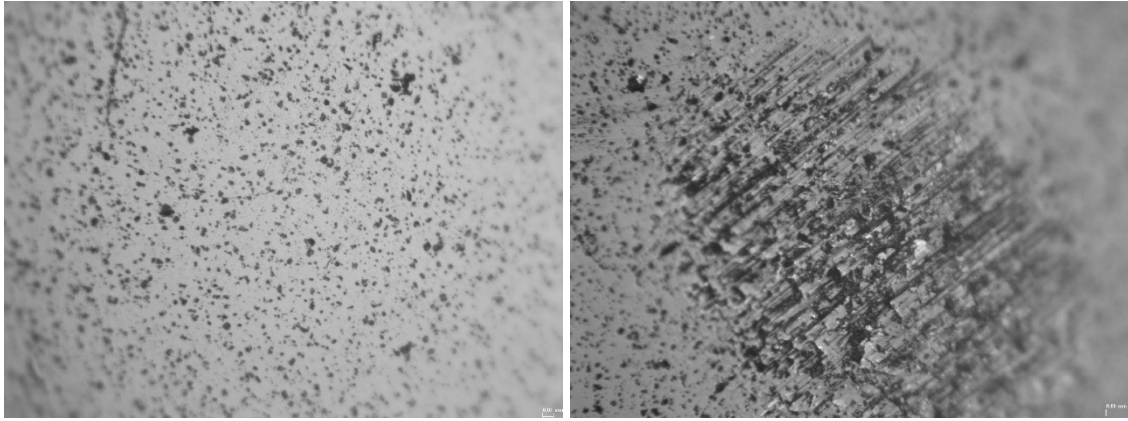There are visible scratches in the contact zone of the SiC ceramic ball after burnishing process with force P of 220 N. The ball surface was interrupted where abrasive wear occurred. This was caused because of the low resistance of fracture toughness as a consequence of the low shear resistance. During slide burnishing between two elements: working ending and processed workpiece, the force system was constituted. Then the roughness deformation took place due to the simultaneous action of normal and shear forces. Because the hardness of the workpiece was much lower, the changes in the surface roughness and performance concern the processed steel, but at 220 N of burnishing force, the abrasive wear occurred on the SiC ceramic tool end. It means that the value of the burnishing force of 220 N for the slide burnishing process is too high in this application. Further detailed examination of the tool life with SiC ceramic is needed.

4. Conclusions

The opportunity of using SiC ceramic as a burnishing tool was examined. It was discovered that the burnishing force and feed influenced the most analyzed surface texture parameters. The ranges of selected technological parameters at which effective processing is possible were found. For slide burnishing the surface of 42CrMo4 steel with SiC sintered ceramic ball of 6,35 mm in diameter, the burnishing force P should not exceed 200 N. The best results in smoothing the surface were achieved at 80 N of burnishing force and 0,063 mm/rev of feed. The values of the amplitude parameters Sa and Sq were five times smaller after slide burnishing at P equal to 80 N compared to the non-burnished surface. Height parameters decreased at least several times, Sp five times, St three times, Sv almost two times, and some parameters such as reduced summit height declined over twelve times. It confirms that there is a potential in the application of SiC ceramic as tool material in the burnishing process.

References

[1] Bulikowska B., Gałda L. 2015. "The effect of surface roughness on the tribological properties of sliding elements in material assembly SiC-42CrMo4". *TRIBOLOGIA*, XLVI(4): 21-31.

[2] Dobrzański A. L. 2008. *Non-metallic engineering materials*. Gliwice: Publishing house of Silesian University of Technology.

[3] El-Tayeb N.S.M., Low K.O., Brevern P.V. 2009. "On the surface and tribological characteristics of burnished cylindrical Al-6061". *Tribology International* 42: 320-326.

[4] Gałda L. 2014. Slide burnishing with ceramic material. In *Contemporary problems in the technology of burnishing,* 143-154. Publishing house of Gdańsk University of Technology.

[5] Gałda L. 2016. "Selected factors effecting on wear resistance of sliding pairs". *BUSES – technology, operations, transport systems* 17: 861-865.

[6] Jaworska L., Sobierski L., Twardowska A., Królicka D. 2005. „Preparation of materials based on Ti-Si-C system using high temperature-high pressure method". *Journal of Materials Processing Technology* 162-163: 184-189.

[7] Jaworska L., Szutkowska M., Morgiel M., Sobierski L., Lis J. 2001. „Ti3SiC2 as a bonding phase in diamond composites". *Journal of Materials Science Letters* 20: 1783-1786.

[8] Jianxin D., Lili L., Mingwei D. 2007. „Erosion wear behaviours of SiC/(W,Ti)C laminated ceramic nozzles in dry sand blasting processes". *Materials Science & Engineering* A 444: 120-129.

[9] Konefał K., Korzyński M., Byczkowska Z., Korzyńska K. 2013. „Improved corrosion resistance of stainless steel X6CrNiMoTi17-12-2 by slide diamond burnishing". *Journal of Materials Processing Technology* 213: 1997-2004.

[10] Korzyński M. 2009. "A model of smoothing slide ball-burnishing and an analysis of the parameter interaction". *Journal of Materials Processing Technology* 209: 625-633.

[11] Korzyński M. 2013. *Experiment design*. Warszawa: Scientific publishing house PWN.

[12] Korzyński M., Lubas J., Świrad S., Dudek K. 2011. „Surface layer characteristics due to sidle diamond burnishing with a cylindrical-ended tool". *Journal of Materials Processing Technology* 211: 84-94.

[13] Liu S., Zeng Y.-P., Jiang D. 2009. "Fabrication and characterization of cordierite-bonded porous SiC ceramics". *Ceramics International* 35: 597-602.

[14] Przybylski W. 1987. *Burnishing technology*. Warszawa: Science Publishing House.

[15] Radziejewska J., Skrzypek S.J. 2009. „Microstructure and residual stresses in surface layer of simultaneously laser alloyed and burnished steel". *Journal of Materials Processing Technology* 209: 2047-2056.

[16] Srivastava M., Grips V.K.W., Rajam K.S. 2008. "Influence of SiC, Si$_3$N$_4$ and Al$_2$O$_3$ particles on the structure and properties of electrodeposited Ni". *Materials Letters* 62: 3487-3489.

[17] Świrad S. 2011. "The surface texture analysis after sliding burnishing with cylindrical elements". *Wear* 271: 576-581.

[18] Yang J., Ma R., Zhu M., Xiong Y., Shi J., Li X., Li H., Che J. 2022. "Microstructure and mechanical properties of hot-pressed SiC nanofiber reinforced SiC composites". *Ceramics International (available online)*.

[19] https://www.ceramit.pl/uploads/PDFy/w%C5%82asno%C5%9Bci_materia%C5%82%C3%B3w_ceramicznych.pdf (28th Feb. 2022)

Afonso Mkaka[1], Anna Burduk[2]

IMPLEMENTATION OF THE INTEGRATED LEAN SIX SIGMA PHILOSOPHY IN AN ANGOLAN MANUFACTURING COMPANY – A CASE STUDY

WDROŻENIE ZINTEGROWANEJ FILOZOFII LEAN SIX SIGMA W ANGOLSKIEJ FIRMIE PRODUKCYJNEJ – STUDIUM PRZYPADKU

Abstract

Today, manufacturing companies strive to find the stability between satisfying their customers by producing in accordance with their expectations (quantity and quality) and keeping leading positions when it comes to competitiveness on their markets. This paper aims to compare two very well-known philosophies in the manufacturing industry: Lean Manufacturing (LM) and Six Sigma (6S). The integration of these two philosophies solves the insufficiency that the absence of one of them causes, considering that Six Sigma is based on statistical tools that focus on measuring and reducing variations in processes and achieving goals set by the customers' requirements. Lean Manufacturing focuses mainly on the value added for a client, for example,by eliminating all kinds of waste from processes what leads to the reduction of time and cost of the process. Lean Six Sigma combines the features of both methods, which means that it meets the client's requirements based on statistical knowledge and the process flow control, but simultaneously in addition to that, it reduces the time and cost of the processes. As a result, it gives manufacturing companies the possibility of having loyal and satisfied customers and who provide companies with new customers. This paper has a greater goal of persuading the Angolan manufacturing industries to implement the Integrated Lean Six Sigma (IL6S) into their production and management processes.

Keywords: quality control, Lean Six Sigma, Lean Manufacturing, production system efficiency

Streszczenie

Dziś firmy produkcyjne dążą do znalezienia stabilności pomiędzy satysfakcją swoich klientów poprzez produkcję zgodną z ich oczekiwaniami (ilość i jakość) a utrzymaniem czołowej pozycji, jeśli chodzi o konkurencyjność na swoich rynkach. Niniejszy artykuł ma na celu porównanie dwóch bardzo dobrze znanych filozofii w przemyśle wytwórczym: Lean Manufacturing (LM) i Six Sigma (6S). Integracja tych dwóch filozofii rozwiązuje problem braku jednej z nich, biorąc pod uwagę, że Six Sigma opiera się na narzędziach statystycznych, które koncentrują się na pomiarze i redukcji zmienności procesów oraz osiąganiu celów wyznaczonych przez wymagania klientów. Lean Manufacturing skupia się głównie na wartości dodanej dla klienta, na przykład poprzez eliminację wszelkiego rodzaju marnotrawstwa z procesów, co prowadzi do skrócenia czasu i kosztów procesu. Lean Six Sigma łączy w sobie cechy obu metod, co oznacza, że spełnia wymagania klienta w oparciu o wiedzę statystyczną i kontrolę przebiegu procesów, ale jednocześnie dodatkowo skraca czas i koszt procesów. W efekcie daje to firmom produkcyjnym możliwość posiadania lojalnych i zadowolonych klientów oraz zapewnia firmom nowych klientów. Większym celem tego artykułu jest przekonanie angolskiego przemysłu wytwórczego do wdrożenia zintegrowanej metody Lean Six Sigma (IL6S) w procesach produkcji i zarządzania.

Słowa kluczowe: kontrola jakości, Lean Six Sigma, Lean Manufacturing, wydajność systemu produkcyjnego

1. Introduction

Both Lean Management and Six Sigma concepts are designed to ensure customer satisfaction. Over the last two decades, it has been possible to achieve significant improvements through both methodologies in cost, quality and time by focusing on the process performance. Six Sigma focuses on reducing variations and improving the process through problem--solving approaches using statistical tools. In comparison, Lean Manufacturing is primarily concerned with eliminating waste and improving the flow [1]. The purpose of the Lean concept is the optimal use of available resources, reducing inventory and shortening a production cycle. A flexible approach to the organization of production in the case of the Lean concept favors a quick response to fluctuations in customer orders [2]. In order to understand the importance of combining both methods better, Table 1

---

lists the limitations of each and the strategic importance of integrating them into one philosophy.

Both approaches to the business improvement evolved independently until it was recognized that they could coexist and make each other stronger. This is because Lean alone cannot obtain stable processes, and Six Sigma alone will not eliminate all losses. This fundamental statement has given rise to a new, integrated approach – Lean Six Sigma (IL6S).

Table 1. Comparison between Lean manufacturing and Six Sigma [2]

Variable	Lean	Six Sigma
Strengths	Remove waste	No defects
	Reduce lead time	Save money
	Cycle time reduction	Uniform process output
	Work-in-progress reduction	Defect reduction
	Shorten delivery time	Culture change
	Space saving	Customer satisfaction
	Less equipment needed	Detailed statistical analysis for improvements
	Driven for efficiency	Driven for excellence
	Improve flow in processes	Reduce variation and improve processes
	Visual workplace and clean environment	Structured problem-solving methodology
Weaknesses	Statistical or system analysis not valued	System interaction is not considered because processes are improved independently
	Process incapability and instability	Lack of specific speed tools
	Lean does not link quality and advanced mathematical tools to diagnose process improvement	Six Sigma does not question existing methods of operation and if it adds value, as long as it does, it does not produce variation
	No focus on reducing variation and maintaining uniform process output	No focus on process improvement throughout an entire value stream
	Does not concentrate on dramatic improvements through innovation	Lack of the importance of visual workplace and clean work environment

The impressive results achieved by the companies such as Toyota, General Electric, Motorola, and many others and accomplished by using either one of them have inspired many other companies to follow their example. As a result, most companies have either a Lean or Six Sigma system as an approach for the effectiveness of services and/or products [1]. However, using just one of them alone instead of integrating them into one has limitations [4], [7], [8]:

- Six Sigma will eliminate defects. However, it will not address the issue how to optimize the process flow;
- Lean principles exclude the advanced statistical tools often required to achieve the process capabilities needed to accomplish the company's goals.

Therefore, this paper aims to describe the advantages of implementing the IL6S for better efficiency in achieving the world-class GE in manufacturing companies by focusing on zero defects, zero loss, zero accidents mindset and the total engagement of all employees in a company.

2. Lean 6 Sigma applications

As it was mentioned, IL6S is a philosophy created by Lean Manufacturing and Six Sigma, and it is definitely the only philosophy that joins Lean Manufacturing and Six Sigma tools and principles in order to optimize and continuously improve the quality of equipment, the process flow and the people who run the machines using differerent methds and tools. The implemented IL6S helps manufacturing companies to improve their services to the world-class levels. The general algorithm of solving problems with the use of IL6S tools is presented in fig. 1.

The IL6S is a transversal revolution of the industry and all the processes that come along with it. Its usage in assembly processes has its fundamental bases considering safety, waste elimination, optimization of processes and quality control [8], [10].

The IL6S tools go through reducing variations in processes and by setting standards. In general, these are the bases for the assembly processes, ensuring that the applied processes are safe for those working in them as well as for the end-users. Therefore, it is

crucial to ensure that the quality control system and its processes meet the customers' requirements.
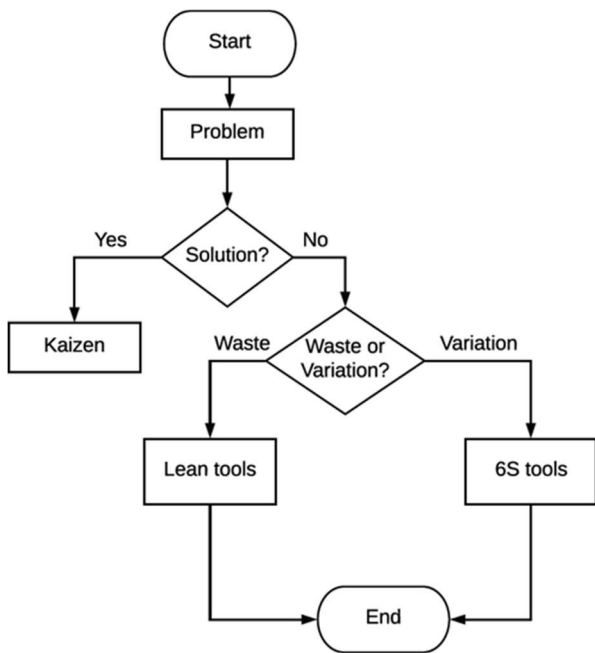

Fig. 1. IL6S approach to solving problems

Comparing the traditional and Lean management is accuracy when comes to achieving goals. Even when pursuing the same strategy, a manager who uses IL6S approaches will always outperform a competitor with a traditional managerial approach. Companies using IL6S philosophy relentlessly focus on delivering more value to their customers than competitors. Develop their people and taking the waste out of every daily process is done for the customer's benefit. Table 2 presents a comparison of the traditional management and the management based on IL6Sigma.

Table 2. Traditional management vs IL6Sigma [1], [9], [11]

Traditional	IL6S
Lack of Zero Loss Mentality	Zero Loss Mentality in Place
Only Managers and Engineers know the plant and business performance	100% of the Plant employess know the plant and business performance
Only Managers and Engineers are capable to solve problems	Core team is capable to tackle losses
Mainly Seniority is awarded	Contribution, Participation and Performance of any employee is rewarded
Average results are pursued	World Class results are pursued
Results are obtained through a lot of muscle power.	Everything is achieved based on methods, processes and systems
There are a lot of crises	Everything is under control
Competitors reach/surpass them	Always above competitors

Companies using the IL6S approach know what they have to deliver in precise details in a manufacturing branch. They set targets and strive to become the best internally and externally by looking for better ways to provide their services and products to customers. That is why, these companies become more efficient on timing, zero loss, zero defect and 100% engagement of its employees, just as shown in fig. 2.
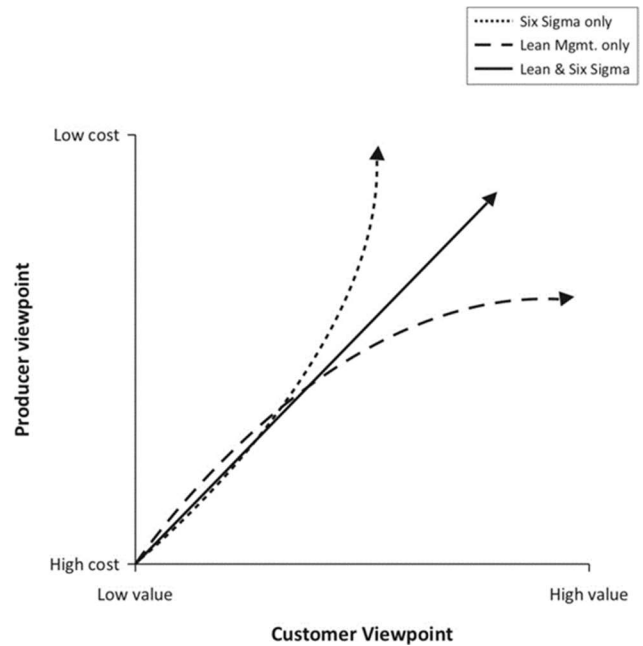

Fig. 2. Advantages for enterpises using Six Sigma, Lean and IL6S tools [1]

The application of IL6S in practice allows to achieve shorter production time, better quality and significantly lower the costs compared to the traditional approach because [1], [2], [12], [13], [14]:
- It is the only method that is strictly focused on people, machines and methods; it builds a career path and ownership;
- Its production and planning is focused on the customer's needs only;
- It focuses on high quality products and on cutting off over-production;
- Safety comes first, zero accident and zero loss mindset;
- Full ownership and engagement of people regardless of their primary positions;
- It is driven by long-term and short-term goals;
- It is focused on competence skills, an internal development and continuous learning process of its employees; it builds capabilities;
- Working in order with IL6S, employees do not spend time in the office they do gemba, what means that they work at the site, at the working place with the operators; it a builds career path;

- It liminates defects, downtimes, stops through the ownership of equipment and the process flow becomes sustainable:
- The results are reviewed or present activities are discussed with managers and all the employees/operators.

As described, both Lean Manufacturing and Six Sigma are critical methods for manufacturing companies. Combining these methods into one, including Total Productive Maintenance (TPM), High Performance Work System (HPWS), for the continuous improvement of people's technical knowledge and soft skills leads to better effectiveness of companies' outcomes and, most importantly, the satisfaction of the customers is guaranteed. A Diagram of IL6Sigma construction is shown in fig. 3.
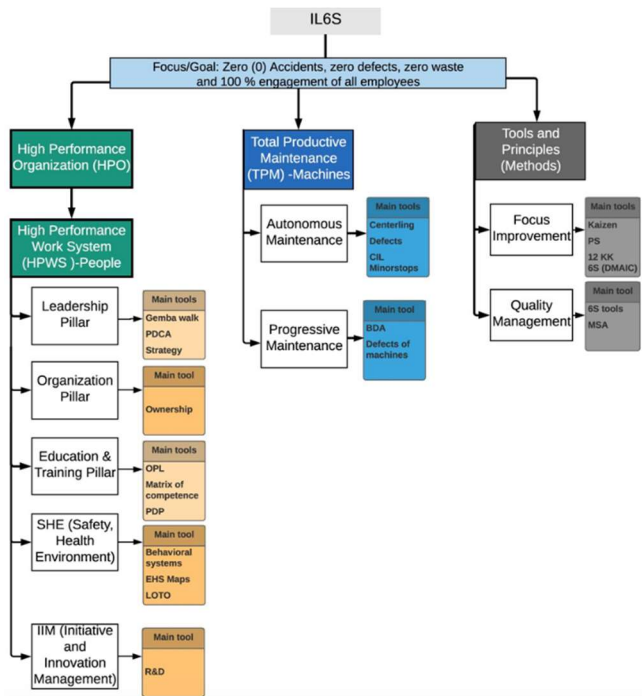

Fig. 3. Diagram of IL6Sigma construction

An integrated Lean Six Sigma pillar is a center of excellence that progressively develops a set of activities, systems, tools, and methodologies in order to build the required capability and to achieve the company's core values and goals. It is a structural element that needs to work in combination with other pillars to support the achievement of the planned goals by engaging 100% of all the employees.

Through the TPM approach, the methodology developed in Japan to improve the equipment efficiency and other results by re-educating the operators and getting their full involvement, workers [3]:

- Act as a plant owner due to the responsibilities every one holds, and the open management system;

- Develop generally either professionally or out of it;
- Feel helpful and proud to work for the company because they see their ideas being implemented at the plant;
- Are unique and important;
- Working better as teams rather than in solos;
- Teach and learn from the others.

Some of the main tools used in IL6Sigma result from the combination of Lean and Six Sigma techniques in order to improve business results by pinpointing the goals set and customer satisfaction are shown in fig. 4.
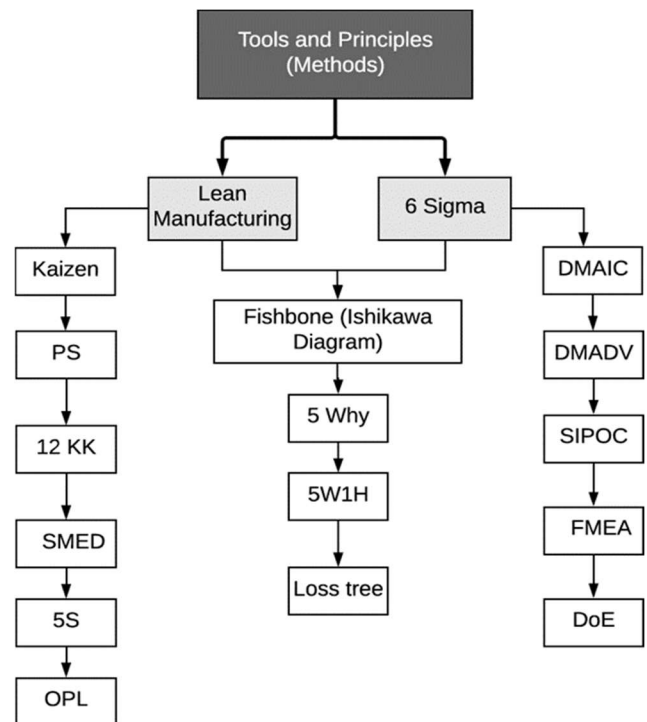

Fig. 4. IL6S tools

Three working stations where defected products were detected at the Quality control (QC) station and for which the reason is unknown are shown below. This is the exact moment where Problem Solving (PS) tools are applied.

3. Contribuition to the development of the industry in Angola

Angola is recovering from a post-war period that was followed by an economic crisis caused by the drop in the price of oil on the international market and, very recently, the collateral effects of COVID-19 which, on the one hand, left the economy totally vulnerable and weakened but, on the other hand, opened an opportunity for the process of economical reinvention and diversification as well as for the implementation

of reforms in the strategic sectors and improvements in the business environment.

At this moment, Angola is going through a very crucial moment as there is an accelerated growth of the industrial sector, considering the fact that industry is the a determining factor for the development and evolution of Angola aimed at promoting and fostering national production. However, in order for this growing number of industries in the most varied sectors to meet expectations, to match the competitiveness with the industries in neighbouring countries, SADC – Southern African Development Community, ZLCLA – Free Zone of African Continental Trade and industries in other continents, it is very important to standardize and conform national production to the world's highest standards of quality and efficiency.

With the standardization of the Industrial Activity in Angola (by the Ministry of Industry and Commerce), Angola will not only increase the level of competitiveness or improve the quality of products and services provided by the already installed and future industries, as it will also help the Ministry of Industry and Commerce coordinate it in an easy and orderly way. It is because the industry standardization will help to reduce waste, occupational accidents and increase the quality of skills of the employees in the industrial sector through the application of the IL6S philosophy.

This is an ongoing process, similar to what happened in Japan in the post-war period. Angola is designing sustainable, efficient and effective goals in order to organize the industrial sector through the IL6S philosophy.

The Ministry of Industry and Commerce (MINDCOM), which is a public sector specialized to define and implement policies and strategies in order to standardize and meet the national and international customer requirements by using ISO, IFS and national norms. Its been a challenge since 2020 when the country started a general diagnosis to get to know the processes andpolicies used in the different industries installed in Angola in 1975-2020. Therefore, it is possible to standardize it. Considering the benefits of the IL6S Philopphy, the Angolan government is looking forward to implementing it.

4. Case study

The implementation of the selected tools of IL6Sigma will be presented in a company producing steel products in Angola. The project aimed at optimising a chosen production process according to the criteria:
- production time,
- resources utilisation and
- inventory levels.

The obtained results will allow quick elimination of broadly defined waste in the analysed process, which has a negative impact on the production capacity and company's financial condition. In order to reach the project's objective, LM techniques were used, namely Value Stream Mapping (VSM) and Single Minute Exchange Of Die (SMED).

The implementation of the assumed goals took place in four stages. The first stage consisted of building a production line model for individual products and checking the production capacity. The model was used to test the planned variants of solutions. The existing technology of the performance of the current machines and stations and the plan of a layout were used to build the model. The ProModel modelling and simulation software was used to build the model. The model from stage 1 was used to compare the results from the other stages of the project.

The second project stage consisted in conducting the analysis of existing problems in the two chosen processes and indentifying the sources of waste within the enterprise. The VSM method was applied, enabling to scrutinise holistically the production system in the search for losses. The general present state map is presented in fig. 5.

Organisational changes were proposed. The introduction of them should shorten the lead time by 50% and minimise work-in-process inventory. Such a result was achieved through changing the existing production scheduling system to a kanban-controlled system, and by introducing supermarkets, what consequently decreased the storage area and allowed the removal of storage – switching station.

Additionally, an altered operating principle of the assembly cell, shifting to a continuous flow cell was proposed. A detailed analysis of fitter's activities led to their modification so that a single employer will carry out as much activities as possible without having to change the instrument. That solution decreased production cycles, enabled the reduction of employees as well as the elimination of redundant movements and redundant parts transport.

Subsequently, theinformation flow within the enterprise was subjected to an analysis. Anassembly cell was proposed as a process peacemaker, and the assumption that schedulling will be done at that cell was made. Consequently, the company is capable of processing a client's order within one day, not instantly of course, but the order will await the completion in the tasks-in-process queue.
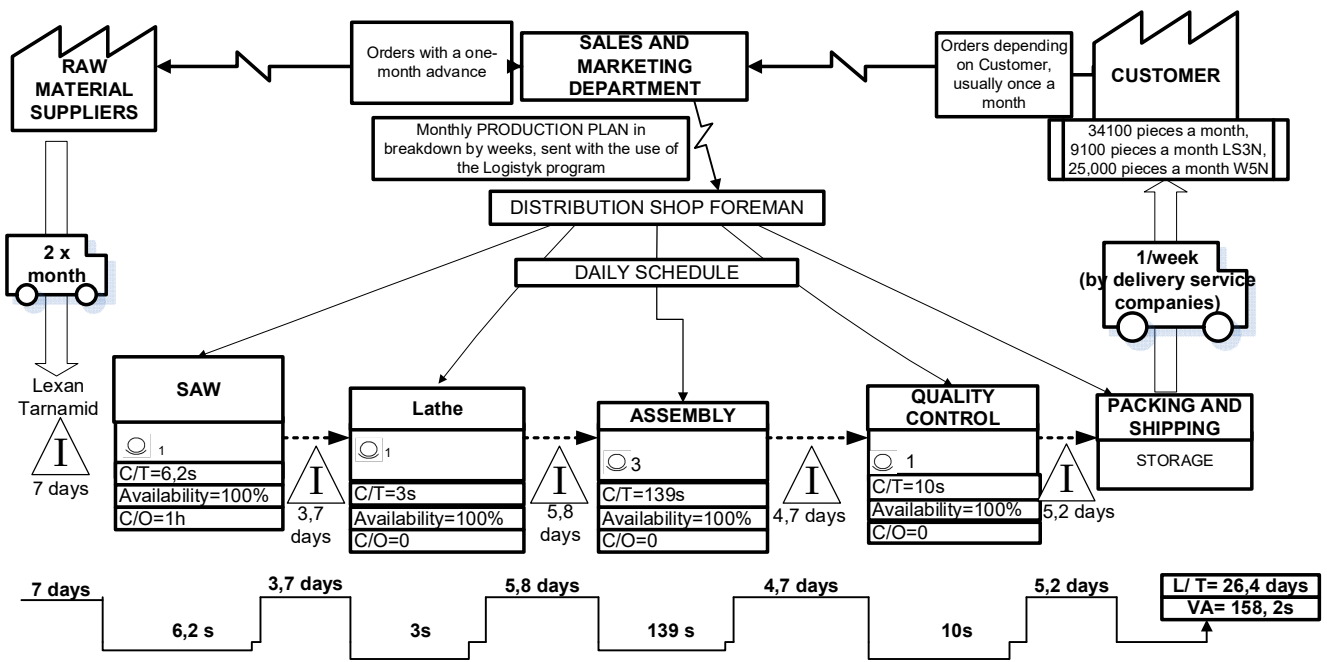
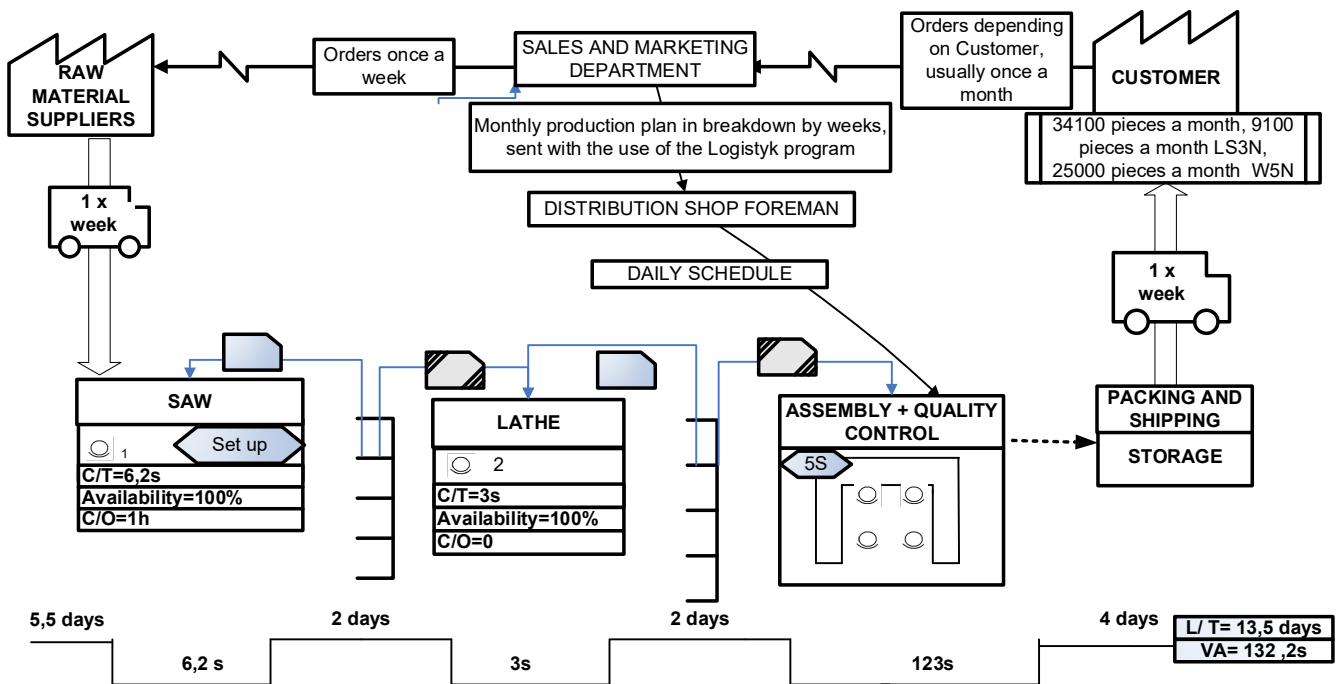Fig. 5. Production process map – current state

Fig. 6. Future state map for the analysed process

In the third stage of the project, in order to eliminate the bottlenecks, organizational changes were suggested including introducing the third shift for the selected workstations, employing new workers or purchasing other instruments and equipment, depending on the expected investment costs. A new distribution of operations between workstations was introduced and the quality inspection so far performed in the main production line was relocated. The optimized U shaped production line is shown in fig. 7.
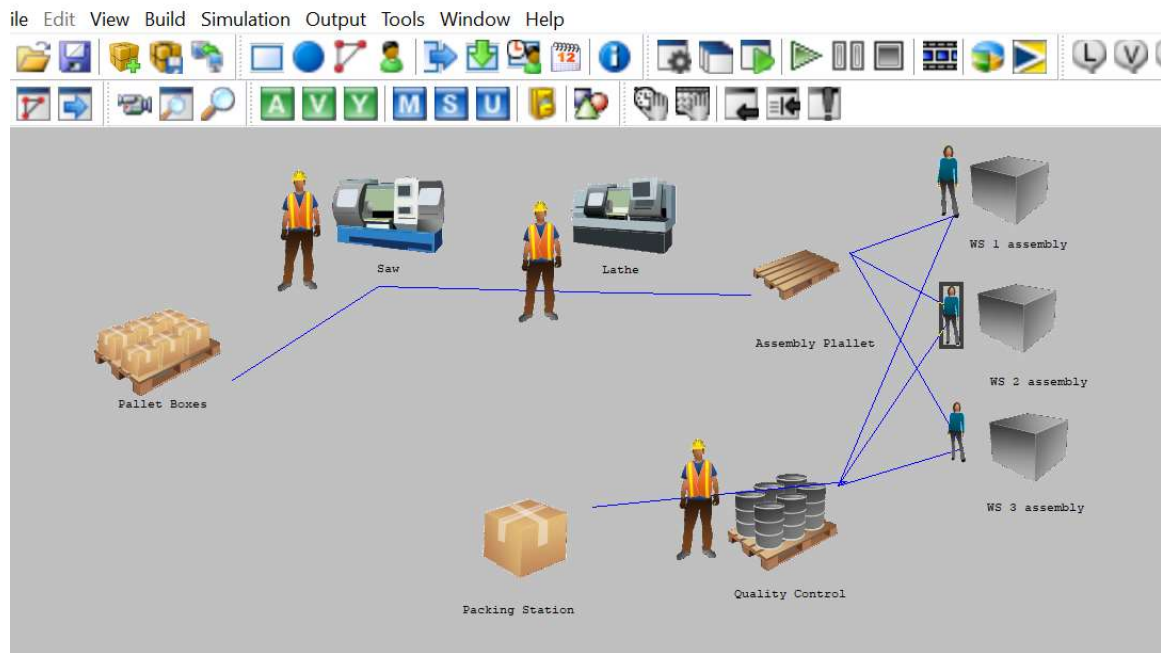
Fig. 7. Optimized U shaped production line

The project's fourth stage was to use one of the Lean manufacturing methods - SMED (Single Minute Exchange Of Die) focused on the waste reduction in manufacturing processes and to provide a rapid and efficient conversion and optimization. In this specific case study, by using SMED, it was possible to optimize the production time, the distance in-between the production stations and the time spent by each employee at every station, cutting off the wasted time and making it more productive in order to maximize the results. Individual steps of the SMED Method carried out in the project are shown in fig. 8.
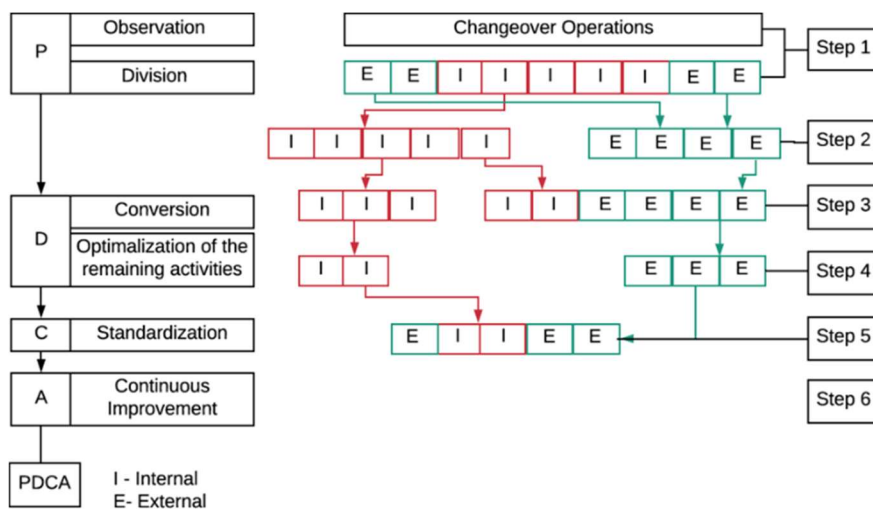

Fig. 8. Steps of the SMED method carried out in the project

The productivity of the selected workstations before and after the changes is shown in figure 9.

To summarise, applying lean methods such as VSM, SMED method and modelling and simulation tools provides enterprises with tangible benefits. In the current market situation, cost-cutting becomes ever-more difficult. The best practice is to seek economies at the source of their origin, i.e., eliminating waste. The presented process optimizing methods allow to achieve a considerable efficiency improvement be-cause the proposed changes render the enterprise capable of producing-to-order by utilizing the pro-duction resources and labor to the maximum extent.
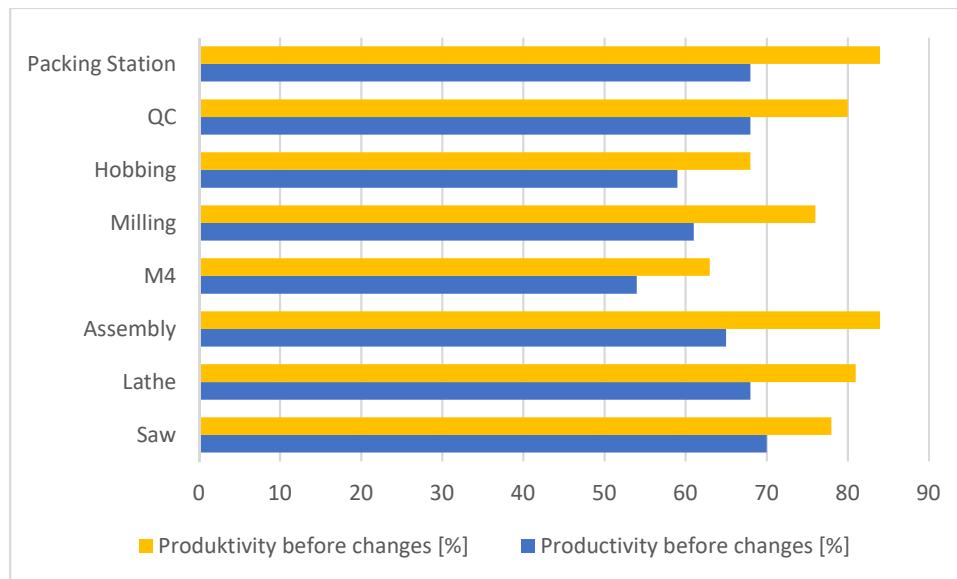
Fig. 9. The productivity of the selected workstations before
and after the changes

5. Conclusion

The philosophy IL6S provides a better management and more effective result achievement for the manufacturing companies. As companies look forward to reducing costs, accidents, defects and they aim to produce on time and with high quality by reducing batch sizes, changing setup times and have a more effective flow of systems, looking forward to satisfying the requirements and/or needs of their customers, the IL6S is a perfect philosophy to usebecause it focuses exclusively on achieving zero (0) accidents, zero (0) defects, zero (0) waste and 100% involvement of every and each of the employees in order to provide products and/or services on time to the customer with higher quality and lower costs.

Through this philosophy, the problems of the companies are handled timely and efficiently, considering the fact, that, every individual in the organization is able to highlight problems, ask for help whenever is needed and he/she is focused on fixing the problems in his/her area. Thanks to IL6S, manufacturing companies have well-planned, detailed and deployed targets. Based on this philosophy manufacturing companies develop a mindset of a highly professional organization that takes losses and defects as personal challenges and works to eliminate them by fixing the root causes.

Integrated Lean Six Sigma improves the GE of manufacturing companies to the world-class levels, up to 75–85% of outcomes, and a total guarantee of satisfaction of their customers, stakeholders and all users of their products/services.

References

[1] Arnheiter, E. D., Maleyeff, J. The integration of lean management and Six Sigma. The TQM Magazine, 17(1), (2005).

[2] George M.L. Lean Six Sigma: Combining Six Sigma Quality with Lean Speed, The McGraw-Hill Companies, (2002).

[3] Rathilall, R., Singh, S. A Lean Six Sigma framework to enhance the competitiveness in selected automotive component manufacturing organisations. South African Journal of Economic and Management Ssciences, 21(1), pp. 1-13, (2018).

[4] Eckes G. (2011). Six Sigma jako trwały element kultury organizacji, MT Biznes, Warszawa.

[5] Marchwiński, John Shook, Alexis Schro-eder. Wrocław : Lean Enterprise Institute Polska, cop. 2010. pag. [86].)

[6] Alhuraish, I., Robledo, C., Kobi, A. A comparative exploration of lean manufacturing and six sigma in terms of their critical success factors. Journal of Cleaner Production, vol.164, pp.325-337, (2017).

[7] Salah S., Rahim A., Carretero J.A. The integration of Six Sigma and lean management. International Journal of Lean Six Sigma (2010).

[8] Stadnicka, D., Stępień, P. Zastosowanie wybranych metod Lean Manufacturing do doskonalenia produkcji palet transportowych. Technologia i Automatyzacja Montażu, (3), pp. 46-52, (2012)

[9] Pepper M., spedding P.J, Trevor A. The evolution of lean Six Sigma. International Journal of Quality & Reliability Management, (2010).

[10] Antosz, K., Kużdżał, E. Doskonalenie procesu przezbrajania maszyn montażowych z wykorzystaniem metody SMED. Technologia i Automatyzacja Montażu, (1), pp. 49-53, (2015).

[11] Antony J., Snee R., Hoerl R. Lean Six Sigma: yesterday, today and tomorrow. International Journal of Quality & Reliability Management, (2017).

[12] Drohomeretski E., Gouvea da Costa S. E., Pinheiro de Lima E., Garbuio, P. A. D. R. Lean, Six Sigma and Lean Six Sigma: an analysis based on operations strategy. International Journal of Production Research, 52(3), pp. 804-824, (2014).

[13] Sarman S., Soediantono D. Literature Review of Lean Six Sigma (LSS) Implementation and Recommendations for Implementation in the Defense Industries. Journal of Industrial Engineering & Management Research, 3(2), pp. 24-34, (2022).

[14] Yadav V., Gahlot P., Kaswan M. S., Rathi R., Singh M. Sustainable Green Lean Six Sigma Methodology and Application Status: A Perspective Review. Recent Trends in Industrial and Production Engineering, pp. 251-266, (2022).